Origin and pathways of pro- and retrograde fluids, PTt paths and fluid-mineral equilibria from Alpine veins of the Central Alps: Case studies of the Fibbia and Amsteg areas.

Tjerk Cornelis Heijboer

Basel, September 2006

Origin and pathways of pro- and retrograde fluids, PTt paths and fluid-mineral equilibria from Alpine veins of the Central Alps: Case studies of the Fibbia and Amsteg areas.

Inauguraldissertation

zur
Erlangung der Würde eines Doktors der Philosophie
vorgelegt der
Philosophisch-Naturwissenschaftlichen Fakultät
der Universität Basel

von

Tjerk Cornelis Heijboer

aus Zwolle (die Niederlande)

Basel, September 2006

Genehmigt von der Philosophisch-Naturwissenschaftlichen Fakulät auf Antrag von:

Prof. J. Mullis
(Dissertationsleiter/Fakultätsverantwortliche)

Prof C. de Capitani
(Korreferent)

Prof. T. Vennemann
(External expert)

Basel, den 19. September 2006   ———————————————

Prof. Dr. Hans-Jakob Wirz

Dekan der Philosophisch-

Naturwissenschaftlichen Fakultät

Acknowledgements

When I started this PhD I was in a state of not knowing that I did not know, how the thesis would look like in the end. Supposedly it would be a bit like my diploma thesis, which I found at the time slightly disorganised and going a bit into several directions and only later did I like to look at it again. However the topic and the approach of my PhD was completely different, the situation here in Basel was completely different than in Utrecht and that and a dose of time led to a change in how I worked here. Also the very positive atmosphere and relations with other PhD students was, I think, very important in changing my attitude to science, and to life in general. In addition to this I am very happy with the advent of some internet communities which made me more aware of the situation in the world today and the events that preceded them. In any case before I start blathering about all of those less important things I want to thank all whom I had the pleasure of meeting, getting to know, to work with and who have contributed not only to my work but also to my life here in Basel. At the end I hope to have attained the level of knowing that there is so much to know that I will probably have forgotten about it by the time that I really need it.

To be a bit more specific and giving credit where credit is due, I want to thank Prof. Josef Mullis for initiating this project, for his continuous support, introduction into microthermometry and generally into the now broad field of research in fluid inclusions, Prof. Christian de Capitani for introducing me into state of the art thermodynamic modelling particularly for fluid-rock systems and generally providing interesting view points and Prof. Torsten Vennemann for introducing me to the field of stable isotope geochemistry, teaching me the techniques necessary for carrying out this research and giving helpful advice about science.

Those people that helped out in the field need also to be mentioned. Without the rich heritage of crystal seekers in Switzerland a lot of samples would still be somewhere cemented in the Alps: Bruno Schaub, Carlo Peterposten are specially thanked for providing some of the samples, for making it possible that we could collect samples and kindly giving the opportunity to stay in their cabin. In addition B. Frei and F. Keller from the NEAT and

"Be calm in arguing;
for fierceness makes error a fault,
and truth discourtesy"

G. Herbert 1593-1633

Contents

List of Figures

List of Tables

Chapter 1

Abstract

In order to constrain the conditions of and processes related to vein formation and the origins of mineralising fluids, field work, multiple geochemical methods applied to whole rocks, minerals, and fluid inclusions, as well as thermodynamic modeling on these vein-wall rock systems have been carried out. The focus of this study was on vein and fissure systems from two particular areas in the external parts of the Central Alps: the Fibbia area in the southern Gotthard massif and the NEAT-Cable tunnel (Amsteg) in the northern Aar massif. The observations and results are divided into three chapters.

The first chapter focusses on fluid-rock interactions around five vein types found in the Fibbia area. Fluid-rock interactions were not visible and measurable in the case of $V_{1a,b}$ and V_5 veins, very minor for V_3-V_4 veins, and significant for V_2 veins. The host rock and mineral alteration near V_2 is documented geochemically and compared with the geochemistry of the different fluid populations, that were measured with LA-ICPMS and crush leach analyses. The host rock near V_2 veins indicates silica depletion and a relative enrichment in K, Na, and Al. During the early stages of V_2 opening, biotite and quartz were leached from the host rock, while during later stages pores formed by earlier leaching were refilled with biotite, albite, quartz, albite, muscovite, and with hematite and chlorite during V_3 and V_4 vein formation. The alteration is mainly iso-chemical and shows a segregation of material from the host rock to the vein. Nevertheless, minor external input of some components (CO_2, SiO_2) may also have occurred. The fluids in these five veins contain Na, K, Cl and minor Ca, Li, Mg, Fe, Cu, Rb, Sr, Pb, Ba, Cs, Zn, As, Br, and SO_4^{2-}. Thermodynamic speciation calculations on the Na and K concentrations and ratios in the fluids in equilibrium with a rock of granitic composition using a modified version of THERIAK yield an approximate comparison to the measured fluid chemistries up to 1 molal Cl concentrations. The Na-K concentrations and ratios are not related to the total anion concentration in the fluid. Fe-Mg-Ca concentrations in the modelled fluids are lower than the analysed concentrations. This is mainly related to possible over-saturation of Ca, Fe, Mg or to the lack of Ca, Fe, and Mg species in the database used.

The second chapter concerns the origins and flow paths of pro- and retrograde fluids in the Fibbia area. V_{1a} veins are pre-Alpine and V_{1b} veins are prograde Alpine older than 37 Ma. V_2-V_5 veins formed between 20–13 Ma during Alpine retrograde metamorphic conditions at temperatures from 420 to ≤ 200 °C and fluid pressures of 4 to ≤ 1 kbar. Vein formation was characterized by varying tectonic conditions: unknown for V_{1a} veins and related to S_1 formation for V_{1b} veins, V_2 formed during near-vertical extension and V_3-V_5 formed during horizontal NE-SW extension. The V_1 and V_2 vein fluids contain up to 7 mol% CO_2 and 1 mol% NaCl. Later retrograde fluids from V_3 and V_4 veins are CO_2 depleted and contain up to 2 mol% NaCl. V_5 fluids are CO_2 free and have a salinity lower than 0.6 mol%. Hydrogen isotope measurements on fluids and minerals from V_1-V_4 veins

give evidence supporting a metamorphic origin. In contrast, for V_5 veins hydrogen isotope analyses support a meteoric origin. δD values less than -130 ‰ for V_5 fluids and hydrous minerals indicate that the meteoric fluids originated from a high altitude mountainous area (≥ 3000m) of 15–10 My. Stable isotope measurements on minerals from host-rock and veins and fluid inclusions shows that the scales of fluid flow are constrained to 1–10 m for V_{1b}-V_4 and were ≥ 8 km for V_5, as the overburden during meteoric fluid flow in V_5 was at least 8 km. Middle Miocene orogen-parallel extension was important for facilitating localized meteoric fluid ciruclation along large-scale V_5 fracture systems. Before V_5 veins formed, meteoric fluid influence was not observable in the studied areas.

The third chapter focusses on Alpine fissures from the Amsteg area (northern Aar massif) and the differences in vein formation that are observed between V_2 veins from the Fibbia area and the Amsteg area. The Alpine fissures in the Amsteg area formed between 19–14 Ma at temperatures between 350–250 °C and pressures between 3.5–2.5 kbar by sub-vertical extension and SE-NW compression, with little fluid-rock interaction. All three fluid populations are of the H_2O-NaCl type and contain up to 5 wt% NaCl eq. The mineralisation is similar to the V_2 veins from the Fibbia area, although pyrrhotine and pyrite are common accessory minerals. Small amounts of REE-containing carbonates were observed as well. Hydrogen and oxygen stable isotope measurements on fluid inclusions and vein minerals (quartz) indicate that the mineralising fluids were mainly metamorphic. The change in mineralisation in the veins as well as slight salinity decreases of later vein forming fluids suggests that fluids from lower temperatures flowed through the veins systems.

Chapter 2

Introduction

2.1   Introduction to studying fluids in the earth's crust

Fluids are important phases that facilitate many natural processes above, at, and beneath the earth's surface. In the earth's crust fluids occupy spaces inside and between the solid phases: in hydrous minerals, in fluid inclusions and in the inherently and secondary formed pore structure. Fluids can vary considerably in physical properties as well as in chemical constituents. In some cases they may behave like liquids, in other cases like gases and at ultra-high pressure and temperature as a melt. The most common volatile components of fluids are H_2O, CO_2, and CH_4 with additional presence of N_2, SO_2, and H_2S. In addition, solid phases can be dissolved in fluids to different amounts. Aqueous fluids commonly have the highest concentrations of dissolved species because of the di-polar nature of the H_2O molecule. Even within one particular geodynamic setting the chemical and physical characteristics of fluids change significantly in space and time. The chemical composition and density of fluids, and changes in these properties are partly explained by the ability of fluids to flow and to interact with the surrounding rocks, partly by the differences in bulk chemistry of the rocks with which the fluids came into contact and partly by the origins of the fluids.

The fluid characteristics in the earth's crust and mantle are studied by different methods. The properties of paleofluids can be studied by analyzing the physical and chemical characteristics of small pockets of fluid trapped in minerals i.e. fluid inclusions. One can obtain direct information about the properties of the fluids that were present at a particular time in the rock. Alternatively, the approximate chemistry of the fluid that was present in the rock can be constrained by studying the mineralogical, geochemical or stable isotopic changes of rocks due to the presence or passing of fluids. In addition, this approach may yield information on amount, the processes and scales of fluid flow. In this study both methods are used, but the focus is on applying different analytical methods to fluid inclusions. Using geochemical methods on fluid inclusions provides constraints on the origins and flow paths of mineralising fluids and may furthermore be used to compare the chemistry of the fluids with the mineralisation and alteration of host rocks.

Basic constraints on the origin of fluids are based on the type of mineralisation that the fluid produced, its relationship with the host rock and the bulk compositions of fluid inclusions (e.g. Mullis et al., 1994). Additional inferences can be made from the electrolyte geochemistry of the fluids (e.g. Banks et al., 1991) and stable isotope analyses of minerals and fluids. The most common electrolytes used for this purpose are Cl, Br, and I, because these ions are considered to be conservative in aqueous solutions and their concentrations are modified only passively by fluid rock interactions. In addition the H, C and O stable isotope compositions of minerals and associated fluids (Mullis et al., 1994; Sharp et al., 2005) yield reliable constraints on temperature of mineralisation, the amount

of equilibration with the host rock and their origin.

However, the origins of vein forming fluids cannot always be traced solely by using a single chemical or mineralogical parameter, as the chemical components of fluids and associated mineralisations may have various origins. CO_2 may be derived from decarbonatisation reactions, whereas the inherited Cl/Br ratio of the fluid may be magmatic, sedimentary or sea-water derived. Oxygen isotope compositions of mineralisations may be equilibrated with the host rock, whereas those for hydrogen may retain a meteoric composition that is not in equilibrium with the host rock. This indicates that various chemical characteristics of the fluids contain distinct pieces of information on the origin or migration history of the fluids. Only in some cases do these characteristics point to one ultimate source.

Orogenic fluids, i.e. fluids occurring in the crust during orogenesis, can originate from metamorphic reactions or can have a magmatic, pre-metamorphic or meteoric origin. Metamorphic exchange reactions can give fluids a composition characteristic of "metamorphic" equilibrated fluids (Nesbitt and Muehlenbachs, 1995), however Yardley (1997) links the concept of metamorphic fluid to be at least partly the product of metamorphic devolatisation reactions. In this study we differentiate "metamorphic fluids" into isotopically or chemically equilibrated metamorphic fluids and fluids derived from metamorphic devolatization reactions. Equilibrated fluids can have a pre-metamorphic origin, while devolatization reactions release volatiles that were previously bound to a mineral structure, i.e. producing "new" fluids.

2.2 Tectonometamorphic evolution of the Central Alps

The Central Alps were affected by Cretaceous and Tertiary orogenesis. During the Cretaceous the Austroalpine nappes thrusted over the Southern Penninic units in an active continental margin setting. During the late Cretaceous a phase of extension resulted in a series of normal faults in the upper tectonic levels and exhumation of the Austroalpine units before Tertiary orogenesis. The early Tertiary (65–50 Ma) is marked by thrusting in the Austroalpine units and early subduction stages of the Briançonnais domain, which culminates in complete subduction at 50 Ma, together with large parts of the North Penninic Bündnerschiefer. At about 50 Ma the southern tip of the European plate started to be subducted, which continues until present day. Between 50 and 35 Ma the upper tectonic nappes (Suretta, Tambo (Briançonnais) and Adula-Cima-Lunga (European)) formed. At later stages, nappe stacking was also characterised by the progressive exhumation of the Tambo, Suretta and Adula nappes from (ultra)-high-pressure conditions. This was finished at around 32 Ma. This period is characterised by heating and magma generation evidenced by, for example, the Bergell intrusion between 32 and 30 Ma. According to

Schmid et al. (1996) the Penninic Basal Thrust was active at around 40 Ma detaching the Helvetic sediments from the Gotthard massif. Subsequently, the earliest slivers of the Gotthard "massif" were detached from the European crust, which is also related to the formation of the lower penninic nappes. A penetrative cleavage formed in the Gotthard "massif" between 37 and 30 Ma during the D_2 stage. Between 30 and 23 Ma the Lepontine area cooled from 600 °C to $\sim 400°C$ in the South-West near the Simplon fault zone and to approximately 200 °C near the Bergell area (Schlunegger and Willett, 1999), indicating a westward shift of the area of maximum cooling towards the Simplon fault zone. During this period two phases of re-folding of the nappes occurred (D_3 and D_4 (Maxelon, 2004, and references therein)). After these events the Lepontine area was geometrically divided into the Tosa/Simplon and the Ticino anticlinal culminations. Maxelon (2004) indicates that the D_4 phase in the Southern Steep Belt is probably older than the D_4 phase in the Northern Steep Belt although direct radiometric dates are lacking. Maxelon and Mancktelow (2005) propose that the Chièra synform, which affected the Northern Steep Belt during backfolding is a feature of D_3 deformation rather than of D_4 or later. Schmid et al. (1996) show that the Chièra synform formed at around 23 Ma but exact time constraints are lacking. During this period the structurally highest slivers of the Aar massif formed and the geometry of the "Gotthard massif" evolved further towards its present geometry. Between 19 Ma to present further thrusting in the Molasse basin as well as in the Southern Alps increased the width of the orogen. In the Central Alps this period is marked by uplift and erosion, particularly at the Tosa-Simplon culmination slightly to the east of the Simplon Fault Zone. According to Grasemann and Mancktelow (1993) the Simplon Shear Zone was most active between 18 and 15 Ma and later evolved into the brittle Rhône-Simplon Line with a paleo-stress regime consistent with NW-SE shortening and SW-NE extension (Grosjean et al., 2004). The uplift of the Aar massif became also more pronounced in this period. Michalski and Soom (1990) showed that cooling in the Aar and Gotthard massifs started in the East at around 25 Ma and moved subsequently to the South-West, where latest apatite cooling ages are of Late Pliocene/Early Pleistocene age.

2.3 Vein formation studies in the Central Alps

The many years of research in the Alps also include studies on mineralised fractures and veins. As the Alps are very complex in their architecture and history, veins that formed during the Alpine orogenesis may have been formed by the interplay of different processes and consequently can have a variety of characteristics (compare e.g. Mullis, 1976; Burkhard and Kerrich, 1990; Diamond, 1990; Mullis et al., 1994; Henry et al., 1996; Mullis, 1996; Marshall et al., 1998). In addition, metasomatic effects of fluid flow may

also be apparent from shear-zones (e.g. Keller, 2004) or lithological boundaries. Veins in the External Helvetic Nappes are predominantly brittle features within brittle deforming lithology, whereas in the more internal parts they are linked to ductile deformation of the host rock. Often their original geometries are obscured by later deformation phases and folding. To determine what their mode of formation is and whether fluid flow occurred during mineralisation, it is necessary to establish their relative time of formation i.e. their linking to certain deformation phases (Henry et al., 1996).

"Alpine fissures" can be generally described as partly mineralised cavities, that formed during Alpine orogenesis and in which crystals generally precipitated from domantly aqueous fluids in their natural shapes. Mullis et al. (1994); Mullis (1995, 1996) link their formation to late European-Apulian continent-continent collision, which causes crustal thickening in the Central Alps. As "Alpine fissures" can occur in different shapes, different orientations with respect to the main foliation, in different spatial arrangements and with more or less pronounced alteration features, different formation mechanisms can be envisaged. In addition, Mullis et al. (1994) and Mullis (1995) showed that mineralising fluids from Alpine fissures can have a wide range of compositions and compositional evolution and that the type of mineralisation depends on the fluid as well as on the host-lithology. Generally, the composition of fluids found in Alpine fissures are related to metamorphic grade and to the type of host-rock present. As Alpine fissures generally are thought to post-date the main-foliation event they can be used as a relative time marker. In addition the occurrence of datable vein minerals makes veins possible absolute time markers. However, particularly in the Lepontine Area of the Central Alps, several phases of refolding of the main foliation and secondary foliation formation makes it difficult to establish temporal relations, from known datasets. Several radiometric studies, however, show that at least late stages of mineralisation occurred between 20 and 10 Ma (e.g. Sharp et al., 2005), which constrains their opening to Neo-Alpine time.

2.4 Problem statement and focus of research

Commonly Alpine fissure formation occurred after the main Alpine deformation, during neo-Alpine retrograde conditions. However, the sequence and the stress regimes prevailing during their formation has not been widely studied (see Mullis et al., 1994; Mullis, 1995). Furthermore, the relation between deformation events and Alpine fissure formation is not always clear and has not been studied in this part of the Central Alps. Integrating this information with common geochemical methods and also determining additional information on earlier and later vein forming events can provide a more complete picture of how fluid-regimes evolved over time, particularly during the retrograde stages. In this study a complete structural and geochemical study of veins and their structural setting from two

areas in the Central Alps (the Fibbia area and Amsteg areas) has been undertaken.

Mineralisation of previously open fractures can be caused by locally derived fluids or alternatively, by externally derived metamorphic fluids (e.g. Henry et al., 1996). The latter case is not always directly noticeable from the vein size or geometry, but must be determined by geochemical means. In addition, the type of mineralisation that develops in a vein is determined by the host rock mineralogy and the mechanisms by which fluid-rock interaction occurred. Particularly in cases where external fluids were derived from rocks that were chemically very different from infiltrated rocks, fluids have a great potential to alter the host rock and leave a chemically distinct mineralisation in the veins (large scale advection). However also at "near" equilibrium conditions different processes can induce chemical changes in host rocks (e.g. diffusional exchange between veins and host rock in response to small chemical potential gradients). The structural and geochemical results from the veins found in the two areas are used to asses the importance of externally derived fluids and to determine what the most likely sources are for material that was newly mineralised. On this basis conceptual models are derived of the type of fluid regimes present at the time of mineralisation. Equilibrium thermodynamic modelling was used to determine the types of fluids present in the different vein types and to predict the change in composition with changes in temperature and pressure.

Fluids from veins and faults associated with retrograde metamorphic conditions can be surface-derived and can be of meteoric origin, such as in the Namche Barwa region, Himalaya (Craw et al., 2005), in the Southern Alps, New-Zealand (Jenkin et al., 1994; Upton et al., 1995), in the Ruby Mountains, Nevada, USA (Fricke et al., 1992) and in British Columbia, Canada (Nesbitt and Muehlenbachs, 1995), or of marine origin, such as in the Pyrenees, France (Wickham and Taylor, 1985). Dissolved silica necessary for quartz precipitation can originate from the host rock (Wangen and Munz, 2004) even when fluids originated from other areas (Munz et al., 1995). Similarly, the silica could also have been transported from external sources, where silicates were dissolved (Fisher and Brantley, 1992; Bons, 2001). Recently, Mullis et al. (2001) (see also appendix A) and Sharp et al. (2005) showed that in the Central Alps meteoric fluids were able to penetrate to depths of about 10 km. Sharp et al. (2005) did not provide more details on the mechanisms of this flow or on the spatial extent of pathways that facilitated this downward flow, but proposed that increased pervasive meteoric infiltration could result in increased cooling of the Central Alps and consequently the downward migration of the brittle-ductile transition in the crust. However, when meteoric fluid infiltration is only confined to certain structures, the effect on crustal scale cooling patterns is limited. Mullis et al. (2001) proposed that meteoric fluid infiltration occurred at a topographic high in the Southern Penninic nappes and that this led to a large scale fluid flow system along episodically open fracture systems.

This resulted, according to Mullis et al. (2001), in fluid escape and quartz precipitation during upward flow to the surface. In this thesis the author addresses the modes of meteoric fluid influx in greater detail to gain more understanding of the importance of meteoric fluids in the earth's crust during the evolved stages of exhumation in the Central Alps.

The preceding questions can also be applied to vein systems from other locations in the Alps and other mountain belts as veining is very widespread. For comparison, vein formation and mineralisation was studied in meta-sedimentary rocks from lower metamorphic grades in the Amsteg area of the northern Aar massif. In this way parallels and distinctions between the Fibbia area and the Gotthard massif can be drawn.

2.5   Layout of the thesis

1. Chapter 3 is concerned with the documentation of the macroscopic pathways and the PTt-paths and fluid-mineral equilibria from Alpine veins in the Fibbia area. It is divided in a section describing the five vein types in the Fibbia granite, a section on the petrography and geochemistry of wall-rocks and veins, a section characterising the different fluid inclusion populations from the different vein types (using conventional microthermometry, LA-ICPMS and crush-leach analyses) and a section in which these results are combined, PT-conditions of vein formation are established and constraints from thermodynamic modelling are implemented.

2. In chapter 4 geochemical results of fluid inclusions from chapter 3 are inter-linked to stable isotope results in order to constrain the origins and the scale of fluid flow in the veins from the Fibbia area. Conceptual models of fluid flow patterns in the five vein types are further explained.

3. Chapter 5 is a combination study of fluid origins, mineralisations and vein formation; i.e. a combination of both chapters 3 and 4, but for the Amsteg area. The ultimate goal is to compare the vein formation conditions in two lithologies (meta-granite in the Fibbia area and meta-sedimentary in Aar massif).

4. Appendix A contains a closely related work, concerning late Alpine fractures in the northern Penninic area. It is an extended abstract which details some of the previous research on fluid-flow models which are important for understanding chapter 4.

5. Appendix B and C are results from Raman-analyses of fluid inclusions and the method to convert measured intensities from LA-ICPMS to fluid inclusion compositions.

Chapter 3

Characterisation of fluid rock interaction and mass transport in successive veining events from the Fibbia meta-granite of the Gotthard Massif, Switzerland.[‡]

Abstract

The physicochemical characteristics of Alpine vein formation and associated fluids in the Fibbia granite (Gotthard massif) were investigated using an analytical and thermodynamic approach in order to identify the PT-conditions of vein formation, to quantify the amounts of alteration of the surrounding rocks and the mass transfer and fluid flow mechanisms around the veins. Five veining events are associated with prograde and different retrograde stages of Alpine metamorphism. V_{1a} and V_{1b} veins are massive quartz veins without any alteration zones, which formed during pre-Alpine and prograde Alpine metamorphic conditions, respectively. The lack of wall-rock alteration around these veins precludes a local origin of the mineralised quartz. Significant wall-rock alteration was observed around V_2 veins and is characterised by up to 20 wt% SiO_2 loss and a relative gain of Al, K and Na. Biotite and quartz were dissolved in the alteration zones by CO_2-enriched aqueous saline fluids, from which typical Alpine fissure minerals precipitated in the open fissures and in the pore spaces of the alteration zones.

Nearly no alteration is observed along V_3 and V_4 mineralised fractures, where phengite and hematite (V_3) and chlorite (V_4) precipitated from volatile-free aqueous salt-enriched fluids. V_3 and V_4 minerals also developed in some of the still open V_2 veins. Massive V_5 quartz veins are found in chemically unaltered host-rocks and were precipitated from NaCl-depleted fluids. Chemical analyses using LA-ICPMS and crush-leach techniques of the different fluid inclusion populations indicate that the electrolyte composition of the vein forming fluids is mainly Na-K-Ca-Li-Cl with trace amounts of Mg, Fe, Mn, Sr, Ba, Cu, Zn, Pb, As, and minor anions of Br and SO_4^{2-}. Changes in fluid compositions during mineralisation are mainly related to changes in CO_2 content and salinity. The PT-conditions of fluid trapping range from up to 440 °C and 4 kbar for V_1, 420 °C and 3.0 kbar for V_2 to 180 °C and 1 kbar for early V_5 veins, indicating a fluid pressure change from near lithostatic for the V_{1b} and V_2 veins to near hydrostatic for the early V_5 veins. V_{1b} veins probably formed from dehydration reactions in underlying rocks either from deep seated fluid migration or multiple hydrofracturing events. V_2 veins have opened as extensional fractures after the gneissic foliation developed during early exhumation of the Gotthard massif. V_3 to V_5 are related to later stages of exhumation, where σ_3 is horizontal, SE-NW directed. V_5 veins are formed as a consequence of several phases of cataclastic deformation and during ongoing SE-NW extension and further uplift in the middle to the late Miocene. These veins acted as major flow paths for externally derived fluids before and during mineralisation.

3.1 Introduction

Metamorphic veins in the earth's crust commonly form as a consequence of the presence of mineralising fluids in cavities or fractures and are often associated with mineralogical and chemical alteration of the host rock. The physical and chemical conditions and mechanisms of metamorphic vein opening and subsequent mineralisation vary significantly (Oliver, 1996; Oliver and Bons, 2001). Different fluid sources, mechanisms for mass transfer and fluid flow can be inferred by applying structural, petrological, geochemical and thermodynamical approaches to the vein-host rock system. The parameters and mechanisms, which are important for vein formation, in turn also play an important role for understanding the paleo-hydrology of the earth's crust (e.g. Etheridge et al., 1983; Walther and Wood, 1986; Thompson and Connolly, 1992; Oliver, 1996; Ord and Oliver, 1997; Connolly and Podladchikov, 2004; Ague, 2004).

In the internal parts of the Central Alps several aspects of Alpine veins and fissures have been characterised: vein structure and the evolution of vein geometries (Ramsay, 1980; Ramsey and Huber, 1987; Pennacchioni, 2005), bulk fluid chemistry based on fluid inclusions and Raman spectroscopy from vein minerals (e.g. Poty et al., 1974; Mercolli, 1979; Luckscheiter and Morteani, 1980; Mercolli et al., 1987; Diamond, 1990; Mullis et al., 1994; Mullis, 1996), stable isotope compositions of fluids from veins and vein minerals (e.g. Hoefs and Stalder, 1977; Marquer and Burkhard, 1992; Mullis et al., 1994; Henry et al., 1996; Lucchini, 2002; Sharp et al., 2005) and fluid chemistry based on crush leach extraction and laser induced breakdown spectroscopy (Poty et al., 1974; Yardley et al., 1993; Mullis et al., 1994; Mullis, 1996; Marshall et al., 1998; Fabre, 2000; Fabre et al., 2002).

These studies have mainly focussed on veining events during peak to early retrograde metamorphic conditions: the conditions at which fluid flow and fluid-rock interactions are most common and pronounced (Yardley, 1997). Few of these studies were aimed at investigating the complete evolution of different veining events during prograde and retrograde metamorphic conditions in the Alpine orogenic phase (e.g. Mullis et al., 1994; Mullis, 1996; Marshall et al., 1998). However, preliminary results of Mullis et al. (2001) showed that meteoric fluids were able to penetrate the upper crust of the internal parts of the Central Alps during late retrograde conditions as was expected by Marquer and Burkhard (1992). This implies a transition from a metamorphic to a meteoric fluid dominated regime, which is associated to different vein formation mechanisms and fluid flow patterns.

In this study the structural, petrological, geochemical and fluid evolution of Alpine veins are investigated with the aim to characterise the *PTXt*-evolution of vein formation during metamorphism and to constrain the mechanisms of mass transfer and fluid flow in the

Fibbia area of the southern Gotthard massif. In addition, thermodynamic calculations are used to further constrain the *PT*-conditions and the mass transfer mechanisms for vein formation.

3.2 Geological background and previous research

The Gotthard massif is the southernmost part of the external Alpine Massifs (Helvetic nappes, Aar and Gotthard massif). It consists of a poly-metamorphic basement with a sedimentary cover. It is bordered to the south by the Penninic thrust front and is separated from the Aar-massif in the North by the Tavetch Massif and the Urseren zone. During Alpine orogenesis the southern Gotthard area was metamorphosed to upper green-schist facies at $T = 500$ °C and P ∼4 kbar (Frey et al., 1980). The peak meso-Alpine metamorphic event is estimated at around 37 Ma (Deutsch and Steiger, 1985).

The studied area is situated at the southern border of the Gotthard massif (Fig. 3.1a). The late Carboniferous Fibbia granite is surrounded by late Ordovician granitoids, migmatic gneisses, and pre-Ordovician meta-sedimentary gneisses (e.g. Hafner, 1958; Mercolli et al., 1994) (Fig. 3.1b). Near the boundaries with the Scoresia gneiss, 1-10 meter sized amphibolite blocks are intercalated within the meta-granite. Biotite-rich 1-20 meter long pre-Alpine lamprophyres containing up to 30 wt% FeO, crosscut the Fibbia granite steeply at different outcrops. Marquer (1990) showed that the Fibbia granite has been partly overprinted by a gneissic foliation and shear-zones (S_1 during Alpine orogenesis). In the southern part of the Gotthard massif, the S_1 foliation was re-oriented to the north west (S_1: 060/40 NW) during the Chièra synform formation (backfolding) at around 23 Ma (Schmid et al., 1996; Maxelon and Mancktelow, 2005).

According to the fluid zone map of Mullis (1995) early fissure fluids in the Aar- and northern Gotthard massif are generally characterised by $\geq$ 90 mol% H_2O (H_2O zone). Early retrograde fissure fluids from the southern part of the Gotthard massif and Penninic nappes contain $\geq$ 10 mol% CO_2 (CO_2 zone). The Fibbia area is located slightly to the North of the boundary between the H_2O and the CO_2 zone. Three different saline aqueous fluid inclusion populations were distinguished in Alpine fissures from the Fibbia granite (Mullis, 1995). The earliest fluid inclusion population is characterised by 6.9 mol% CO_2 and 1.3 mol% NaCl equivalent, whereas the two later fluid inclusion populations are CO_2-poor NaCl-bearing fluids. Molar K/Na ratios of the earliest fluid inclusion population was 0.156 (Mullis et al., 1994). This ratio implies, a fluid trapping and early quartz formation temperature of approximately 420 °C (Poty et al., 1974).

The timing of exhumation of the southern Gotthard massif was constrained by K/Ar and Rb/Sr on mica and amphibole and fission-track data on zircons and apatite by Pürdy
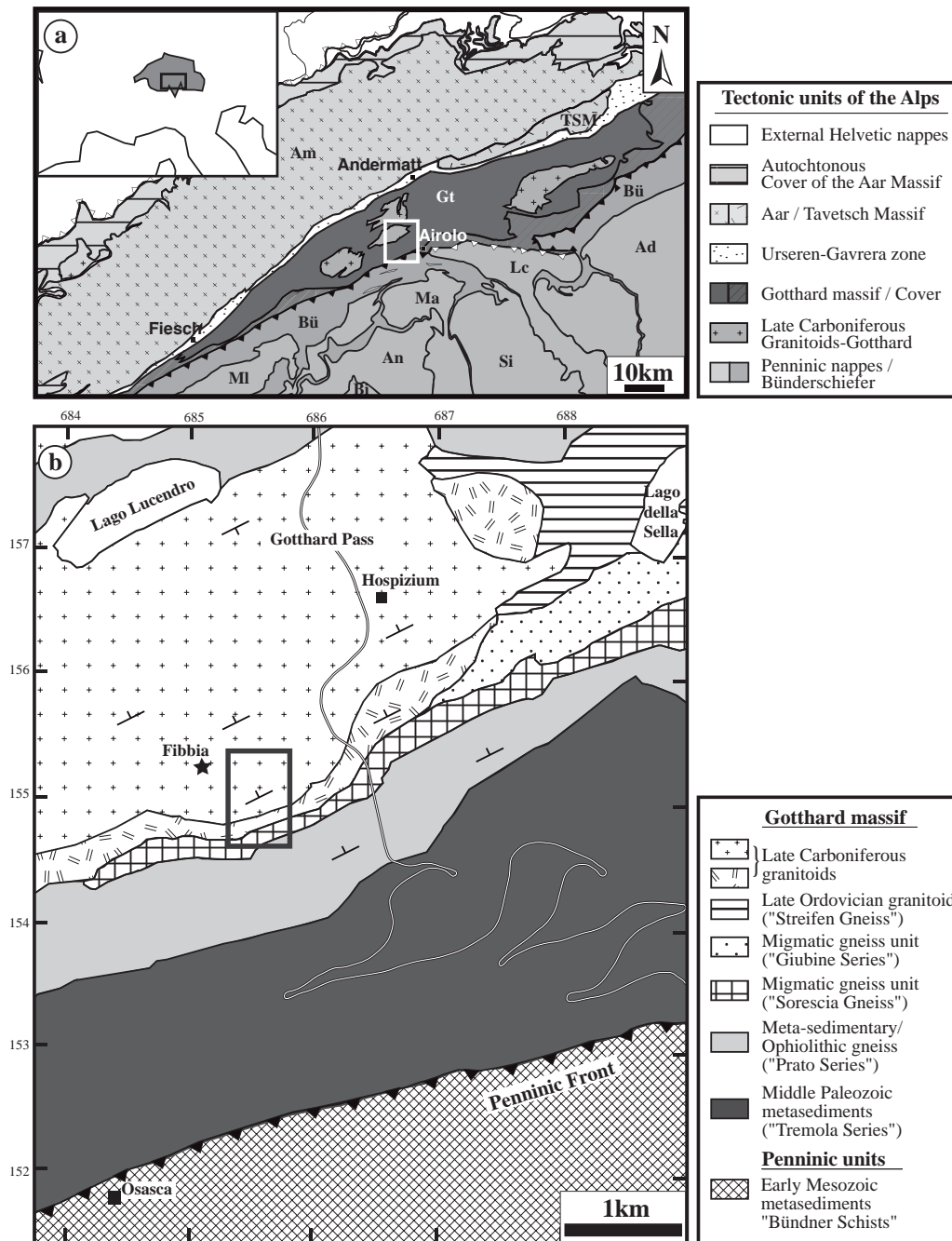
Fig. 3.1: a) Tectonic map of a part of the External and Central Swiss Alps after Spicher (1980). The white box indicates the map section in b). b) Geological map of the Fibbia area with the different lithological units of the Gotthard massif and the adjacent Penninic metasediments. A detailed study of mineralised fractures and veins was made in the area indicated by the black box. The general orientation of the S_1 foliation is shown. Lithological distinctions are based on Mercolli et al. (1994) and Hafner et al. (1975). For abbreviations see chapter 4.

and Stalder (1973), Wagner et al. (1977), Peretti et al. (1981) and Michalski and Soom (1990). Their data indicate that the Fibbia area was exhumed at a rate of $\sim$ 0.3-1 mm/yr during the past 35 Myrs (Michalski and Soom, 1990). "Alpine fissures" opened according to Mullis (1996) and Sharp et al. (2005) at approximately 20 Ma and the main quartz growth stages in the Alpine fissures took place at around 19 to 14 Ma.

3.3 Analytical techniques and thermodynamic modeling methods

All five vein types were sampled for unaltered host rock, altered rock and when possible, vein material, to obtain an indication of the average amount of mass-transfer from the alteration zones to the veins. Whole rock geochemical analyses were done on the granitic gneisses. From a representative sample of approximately 1 kg powdered sample 300 mg sample was taken. Major elements were measured using fused glass beads containing a mixture of this 300 mg sample material and 4700 mg lithium-tetra-borate. All analyses were performed at the University of Basel on a Siemens SRS3000 wavelength dispersive sequential X-ray spectrometer with a Rh end window tube (4kV) and calibrated with internal standards. The results were collected using the Bruker AXS Spectraplus program. In addition about 7 gram material from the same rock was used in Hg-porosimetry at the university of Fribourg to obtain the porosity and density of rock samples.

Mineral compositions were determined using electron microprobe spot-analyses at the University of Basel. A JEOL JXA-8600 microprobe with three different WDS spectrometers and Voyager software by Noran instruments. Analyses were conducted using a focused electron beam with single spot analyses. Acceleration voltage was 15 kV, beam current 10 nA and counting times between 10 and 20 seconds. Standards used for calibration are well characterised natural materials. For raw data processing the PROZA/ZAF correction method was applied and all Fe was assumed to be 2+ except in the case of hematite.

Fluid inclusion studies were done on a Chaixmeca heating-freezing stage, designed to work in the range of -160 °C to 600 °C (Poty et al., 1976). The stage is mounted on a Leitz cross-polarized light microscope. The heating-freezing stage was calibrated as described by Mullis et al. (1994). Uncertainties in measurements from -60 °C to 30 °C are $\pm$ 0.1 °C and above +100 °C the uncertainty is $\pm$1 °C.

Microthermometric measurements were performed on double-polished (0.2-0.5 mm thick) sections of quartz. Where two phase CO_2 was visible within the fluid inclusions at room temperature, CO_2 melting (T_m CO_2), clathrate dissociation (T_d) and CO_2 homogenisation (T_h CO_2) were measured together with ice melting (T_m ice) and bulk fluid inclusion homogenisation (T_h). In the presence of two-phase CO_2-bearing fluid inclusions, salinity was calculated in wt% NaCl equivalent. From the dissociation temperature of clathrate,

using Equation 1 of Diamond (1992). Salinity of aqueous fluid inclusions without volatiles was calculated with the equation of Potter and Clynne (1978). Densities of the total fluid inclusions were calculated using the programs BULK and DENSITY from the FLU-IDS software package by Bakker (2003). Fluid inclusions from the same fluid inclusion populations as measured by microthermometry were analysed by Raman spectroscopy to determine the presence of volatiles that were not detectable by microthermometry (CO_2, CH_4, H_2S, N_2, H_2 and SO_4). A Dilor Labram Raman spectrometer connected to a Olympus BX40 microscope using a Innova 90C Ar-laser with wavelength of 488 nm was used at the ETH, Zürich. Analyses were done using 50 and 100x lenses, which give laser spot-sizes of 8–16 μm. Calibration was done on a silicon-melt piece to standardise the laser beam at a frequency-shift of 0 cm^{-1}. The duration of analyses was two times 300 seconds. Analyses were conducted at room temperature on the vapour bubble present within the fluid inclusions. Analyses were not used for quantification of the minor volatile amounts, as no fluid standards were available for calibration of the Raman spectroscope.

Laser ablations ICPMS spot analyses of fluid inclusions were done to establish the cation concentration in the fluids. 10 to 20 fluid inclusions with a width-depth ratio of 0.7–1.3 and a size of 10 to 100 μm from a single fluid inclusion population were chosen for analyses. The setup used is a Excimer 193 nm ArF laser (Lambda Physik, Germany) combined with special beam energy homogenisation optics linked to an Elan 6100 quadrupole ICP-mass spectrometer at the ETH, Zürich (see Günther et al., 1998; Heinrich et al., 2003). The laser output-energy was set to 130mJ and the pulse frequency of 10Hz was used for controlled ablation of the fluid inclusions hosted in quartz. Different pit-sizes at the same laser settings were obtained by using different apertures for the laser-beam. External standardisation of the elements was done using NIST-glass standard SRM-610. Up to 40 elements were analysed, for which the following isotopes gave steady signals: ^{7}Li, ^{9}Be, ^{23}Na, ^{25}Mg, ^{39}K, ^{42}Ca, ^{49}Ti, ^{55}Mn, ^{66}Zn, ^{75}As, ^{85}Rb, ^{88}Sr, ^{133}Cs, ^{137}Ba, ^{208}Pb. The Na concentration of the measured standard was then used to transform the measured intensities to relative element concentrations. The average salinity of a fluid inclusion population was used for interpolation of the salinity of the fluid inclusions that were not measured by microthermometry (see also appendix C). The NaCl concentrations in the fluid inclusions (wt%, eq) was subsequently used to recalculate the other cations measured to "real" concentrations in ppm (Heinrich et al., 2003). The detection limits were calculated for each element in each fluid inclusion individually using three standard deviations of the background signal divided by its sensitivity.

To compare the results obtained from LA-ICPMS, bulk crush leach analyses were performed on approximately 1 gram of different generations of vein quartz. Crush leach analyses were performed in Leeds, using techniques described by Bottrell et al. (1988) and

Banks and Yardley (1992). The following elements were analysed: Li, Mg, Na, K, Ca, Mn, Fe, Cu, Rb, Sr, Cl, Br and SO_4. Cations from acidified $LaCl_3$ leachates were analysed by FES (Flame Emission Spectroscopy) /ICPAES (Ion coupled Plasma Atomic Emission Spectroscopy) and anions from double distilled water leachates by Ion Chromatography. Detection limits are: for cation analyses ≤ 1 ppb, for Cl^- and SO_4^{2-} 5 ppb, and for Br^- 0.5 ppb. According to Yardley et al. (1993), the following are considered to be likely sources for uncertainty in the analyses: contamination in the laboratory, contamination of the solution by solid impurities in the sample or the presence of different fluid inclusion populations in the crushed samples. To preclude contamination by heterogeneous fluids as much as possible samples were carefully selected and prepared to contain only one fluid inclusion population and little to no daughter minerals or mineral inclusions. In the case of the samples of V_3 to V_5 veins some impurities might be present, as in thick-sections along growth zones and fractures accidental solid inclusions of chlorite and white mica were sometimes observed. The analysed concentrations were converted to quantitative molal concentrations by employing the equation described by Banks et al. (2002) and Gleeson (2003). The average salinities of the fluid inclusion populations based on T_m ice or T_d of clathrate, were used in this recalculation procedure.

Quartz, chlorite, biotite and hematite from the five vein types were manually separated for oxygen stable isotope thermometry on mineral pairs. Oxygen was extracted by letting F_2 react with the sample material during laser ablation. The oxygen was then separated from other residual gases and expanded into the mass spectrometer. Reference oxygen gas was used for comparison. The sample gas was transferred into the bellows of a dual inlet mass spectrometer using 13X molecular sieves to adsorb the oxygen. The precision was estimated using two quartz standards measured before and after each series of samples (reproducibility was generally better than 0.1‰). This method is similar to that described by Rumble and Hoering (1994) and Kasemann et al. (2001).

The Domino/Theriak package (de Capitani and Brown, 1987) extended to include aqueous solutions were used to perform thermodynamic calculations of fluid-mineral equilibria in the CNKFMASH system using bulk rock chemistries. These programs allow the prediction of 1) equilibrium phase assemblages, 2) the concentrations of dissolved species in fluids in equilibrium with these mineral assemblages, and 3) the characteristics of the minerals and fluids during the initial stages of vein formation. The predicted parameters are subsequently evaluated and compared to the actual observed mineral assemblages, fluid chemistries and vein formation conditions. Using this approach, the extend of equilibration between vein-system and host rock and the minimum amount of mass transfer from external sources can be inferred.

The software used is a modified version of Theriak, which is able to calculate speciations

of aqueous fluid in equilibrium with a stable phase assemblage, calculated by the Theriak routine. Calculations were done with an updated version of the Berman (1988) thermodynamic database for minerals and fluids[*] and aqueous species using the "prons98" database from SUPCRT (Johnson et al., 1992). The following solid solution models were applied in the modeling: For chlorite a calibrated complex ideal solid-solution of Hunziker (2003), for white mica the non-ideal (Ms, Pa, Fe-Cel, Mg-Cel) mixing model of Keller et al. (2005), for feldspars the ternary-non ideal (Kfs,Ab,An) solution model of Fuhrman and Lindsley (1988) and for biotite an ideal binary (Fe,Mg) site mixing model. Speciation calculations were done using a simple Davies type (extended-Debye-Huckel) equation for calculating the activity coefficients of charged dissolved species. This equation allows speciation calculations to Cl concentrations of ~ 1 molal, with increasing in-accuracy towards higher salinities. The salinities of the measured fluids were between 1 and 2 molal and can therefore be approximated with this method. At higher ionic strengths the routine becomes unstable and the activities of the species deviate considerably from measured values.

3.4   Results

Vein structure

Five different vein types were distinguished on the basis of their orientation and relative age from V_1 to V_5 (Fig. 3.3). V_1 is separated into V_{1a} and V_{1b} as these veins show a similar mineralogy, but are very different in size and have a different orientation. V_{1a} veins are SW-NE oriented and dip sub-parallel to the S_1 foliation to the northwest (Fig. 3.3a) and were probably re-oriented during the development of the S_1 foliation. V_{1a} veins mainly consist of white milky quartz with minor K-feldspar and biotite and are up to 40 m long and up to 1 m wide. Occasionally zones of 5–10 cm large transparent parts made up of quartz can be observed within these veins. This transparent quartz is often cut by sets of healed fractures of up to 10 cm in length with the main orientation SE-NW. V_{1b} veins are largely made up of quartz, also have transparent zones with parallel healed fractures, but are only up to 2 m long and 0.4 m wide. They are commonly oriented SW-NE and dip to the SE, perpendicular to the S_1 foliation and the V_{1a} veins. In addition, 5–10 cm large cavities can be found in V_1 veins (similar as in Mullis et al., 1994). These cavities are usually irregularly shaped, without preferred orientation and partly filled with minerals typical of V_2 veins.

V_2 includes the typical "Alpine fissures". In this study, the more schematic designation V_2 is used because these veins can be distinguished into three sub-types based on their structure. However they commonly have a similar size (0.5 to 1 m long, and 0.1 to 0.3

---

[*]http://titan.minpet.unibas.ch/minpet/theriak/prog140205/TheriakData_140205 (jun92.bs)
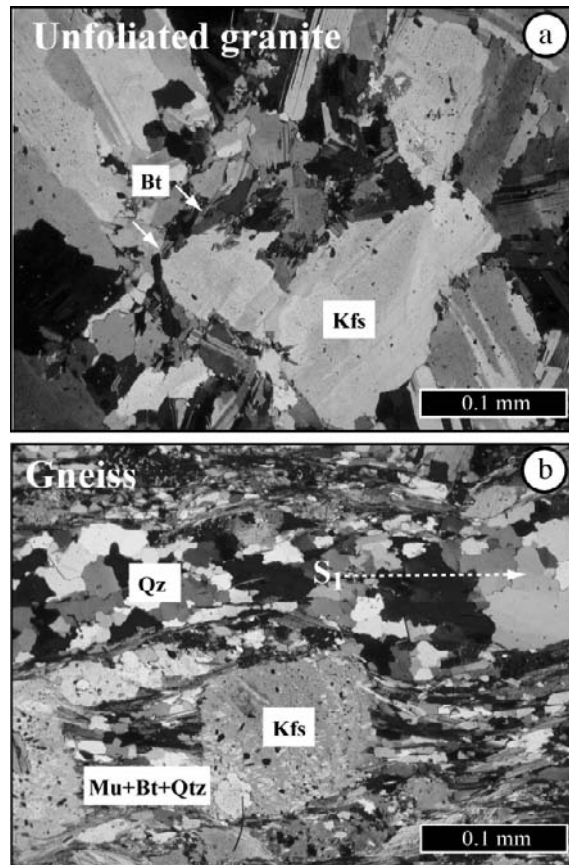
Figure 3.2: Petrographical characteristics of host rock. a) un-foliated granite with mainly K-feldspar and albite and minor biotite at the grain boundaries. b) gneissic foliation with mica-rich ribbons and partially muscovitised, stretched K-feldspar clasts.

m wide), alteration and vein mineralogy. The V_2 structure is mainly determined by pre-existing lithological in-homogeneities and their relation to the main stress orientation. The first sub-type of V_2 veins is characterised by fractures overprinting the massive quartz-filled boudin-necks, which formed as a consequence of internal boudinage during S_1 formation. The second sub-type overprint the pre-Alpine and prograde Alpine V_1 quartz-filled veins. The third sub-type V_2 veins are arranged in en-echelon geometry that formed in response to small movements on weak sub-vertical, biotite-rich lamprophyres. The planes parallel to opening of the V_2 veins are near-perpendicular to the S_1 foliation (Fig. 3.3b).

V_3 veins are small (0.1–1 m long, 1–5 mm wide), NW-SE trending phengite-hematite veins, that cut the S_1 foliation perpendicularly (Fig. 3.3c). V_4 veins are similar in orientation to V_3 veins. They are slightly younger, up to several meters in length and filled solely with chlorite (Fig. 3.4d). There is no indication that shearing took place on the vein surfaces, implying that the veins formed as mode-I fractures or joints.

V_5 veins follow the orientation of V_3 and V_4 veins (Fig. 3.3e), but are 10–100 m long and 0.1–1 m wide. V_5 veins were opened and filled mainly with quartz after at least two events of cataclastic deformation, forming two chlorite-muscovite-quartz gouges. The first fault gouge (gouge$_I$) is dark green containing fragments of the granitic host-rock, whereas
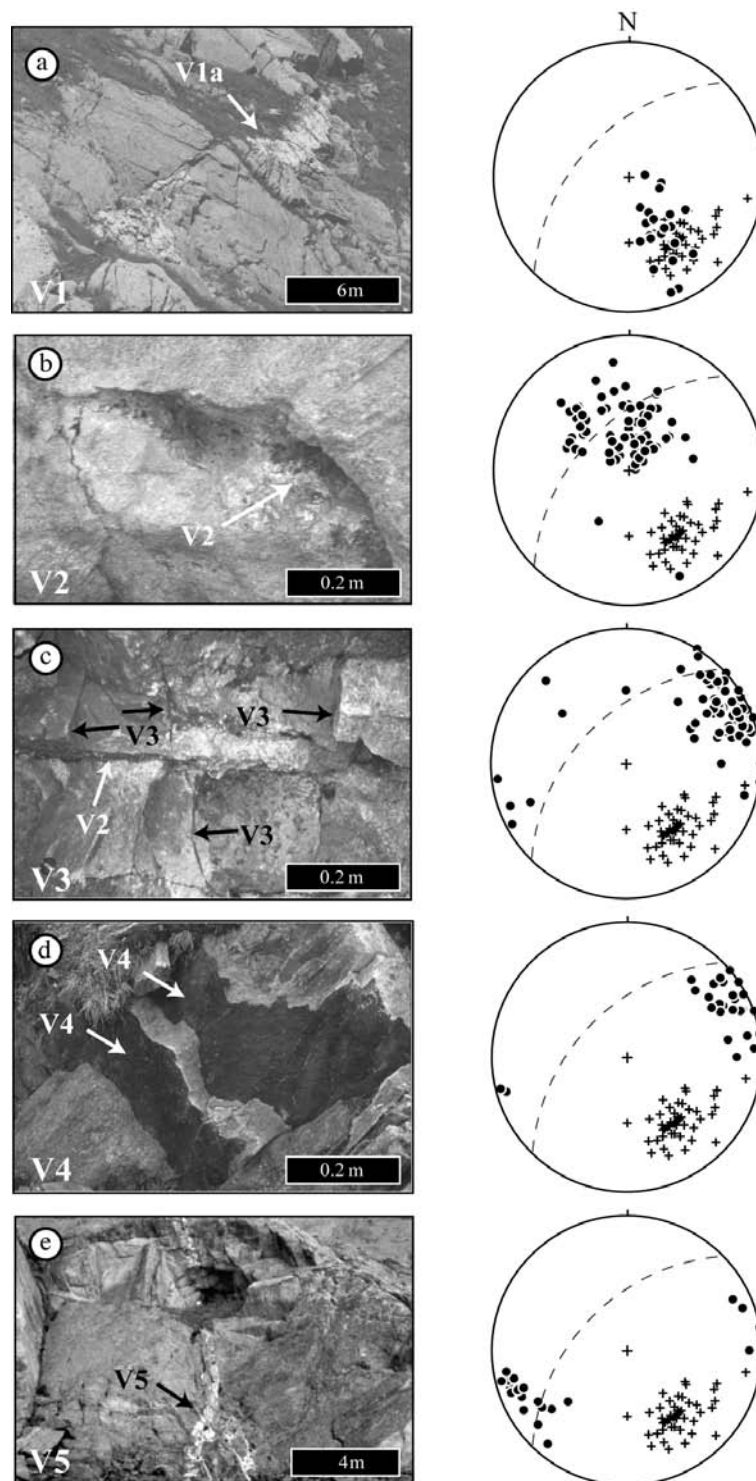
Fig. 3.3: The five vein types (V_1-V_5) and the stereographic projections of the orientations on Schmid-nets, lower hemisphere. Dots represent poles to planes of the fracture or vein surfaces, crosses represent poles to the S_1 foliation. The average of the S_1 orientation is plotted as a great circle.

gouge$_{II}$ and gouge$_{III}$ contain fragments of the first darker green chloritic gouge and of the granitic host-rock. The host rock and chloritic gouges are in turn repeatedly cut by fractures formed during the V$_5$ vein opening and which are partially to totally filled with needle and split-growth quartz. Vein filling is symmetric around both fracture walls. Vein filling quartz often halts near the median line of the fracture leaving a millimeter spaced opening or in some cases spherical cavities.

Host rock petrography

In this study mineral abbreviations are used after Kretz (1983) with extensions for the habits of vein quartz (see Fig. 3.5). The Fibbia granite consists of approximately 30 vol% quartz, 30 vol% albite, 30 vol% K-feldspar, 5 vol% biotite, 5 vol% muscovite, and minor apatite, zircon, titanite and occasionally tourmaline. The host rock does not contain iron- or titanium-bearing oxides. In undeformed rocks, K-feldspars show primary magmatic twinning. Biotite and muscovite are newly crystallised at the grain boundaries of feldspar clasts (Fig. 3.2a). Occasionally biotite (Table 3.1) is directly retrograded to chlorite and muscovite, especially near the V$_5$ veins. Muscovite can form stringers between K-feldspar grains, replacing feldspars. In more gneissic granites, banded dynamically recrystallised quartz and elongated partly replaced feldspars are often observed.

Vein petrography

The five stages of mineralisation are shown in Figure 3.4 and summarised in Figure 3.5. The V$_1$ vein microstructure is characterised by recrystallised fine-grained quartz and up to 1 cm large quartz clasts. Large quartz clasts show undulatory extinction together with sub-grains, which have the same size as the finer matrix (Fig. 3.4a). The larger quartz grains have been indented by smaller high angle strain-free quartz grains. Small quartz grains often indent into larger neighbouring grains, while grain boundaries of fine recrystallised quartz are sometimes straightened healed fractures can be confined to single grains, but often cross-cut them. Alteration of the host rock is not observable near the vein-hostrock interface or further away from the veins.

V$_2$ veins are filled with newly crystallised euhedral minerals including quartz crystals showing a transition habit between prismatic habit to Tessin habit quartz. (Fig. 3.4b). Host rocks are altered up to 15 cm around V$_2$ veins. The same minerals that crystallised in the veins also crystallised in the mm-sized, partially re-filled pores of the alteration zones. The boundary of the altered zones and the fissures is characterised by fractured and altered host-rock minerals.
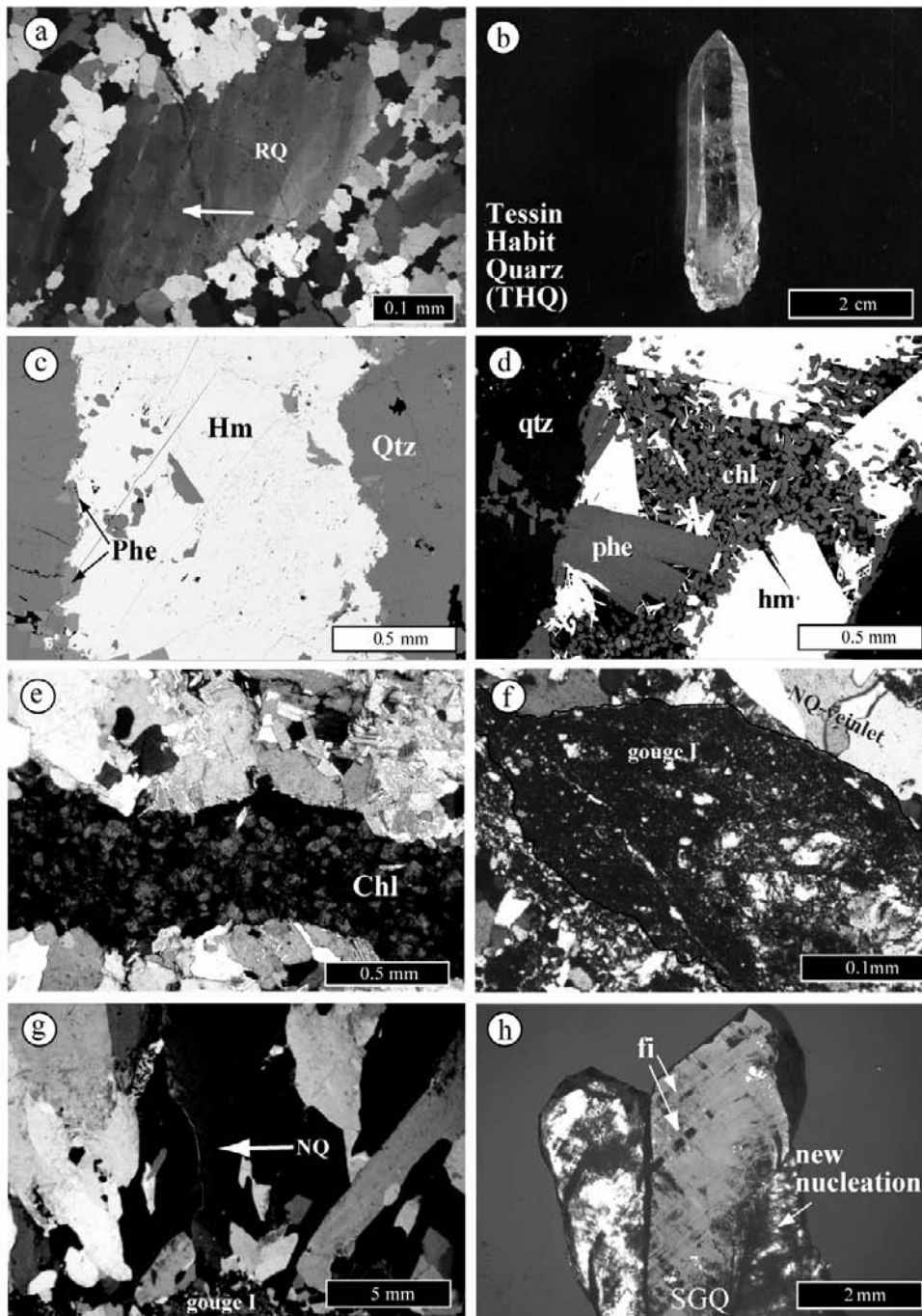
Fig. 3.4: Micrographs of vein microstructures: a) Dynamically recrystallized quartz from V_1 veins (RQ). b) V_2 vein quartz: the habit is a transition between "Tessin-habit" quartz (THQ) and normal prismatic quartz (PQ). c) V_3 veins with first phengite crystallisation preceding growth of fracture filling hematite. d) V_3 vein with open spaces filled with wormy chlorite during V_4 vein formation. e) V_4 veins filled with "wormy" chlorite. f) V_5 chlorite-muscovite-quartz gouge preceding the formation of quartz veins. g) $V_{5.1}$: coarse grained "needle-like" quartz (NQ) growing on fine-grained fault gouge. h) $V_{5.2}$: nucleation of new quartz crystals on growth zones of split-growth quartz (SGQ).

sample	Mu 209 (HR)		TH4(HR)		Mu 209 (V3)		TH4(HR)		mu 209 (V3)		TH4 (V4)	
minerals	biotite		biotite		phengite		phengite		clinochlore		clinochlore	
Nr. analysis	5		4		7		3		12		6	
	Mean value	St dev	Mean value	St dev	Mean value	St dev	Mean value	St dev	Mean value	St dev	Mean value	St dev
SiO_2	38.14	0.72	37.57	1.19	48.96	0.59	46.99	2.54	27.63	0.67	27.99	0.37
TiO_2	2.47	0.14	2.22	0.26	0.63	0.17	0.73	0.10	0.03	0.04	0.05	0.06
Al_2O_3	15.03	0.12	14.86	0.34	27.37	0.86	27.44	1.14	17.81	0.53	18.10	0.21
FeO	19.08	0.31	19.59	0.40	6.83	0.23	7.10	0.26	20.32	1.05	21.27	0.29
MnO	0.15	0.09	0.15	0.10	0.03	0.03	0.05	0.04	0.19	0.05	0.19	0.03
MgO	10.28	0.22	9.86	0.12	2.65	0.19	2.13	0.16	19.63	0.93	19.34	0.32
CaO	0.03	0.04	0.07	0.02	0.02	0.02	0.02	0.02	0.04	0.03	0.04	0.02
Na_2O	0.06	0.02	0.09	0.01	0.11	0.02	0.11	0.05	0.01	0.02	0.01	0.01
K_2O	9.55	0.53	9.87	0.33	8.75	1.18	9.75	1.43	0.02	0.02	0.01	0.01
Total	94.79		94.27		95.35		94.32		85.67		87.00	
Stoichiometry based on 24 oxygens									Stoichiometry based on 36 Oxygens			
Si	5.81	0.05	5.79	0.07	6.68	0.09	6.54	0.11	5.74	0.11	5.76	0.06
Ti (IV)	0.15	0.01	0.13	0.01	0.03	0.01	0.04	0.01	0.01	0.01	0.01	0.01
Al (IV)	2.04	0.04	2.08	0.08	1.29	0.08	1.42	0.11	2.26	0.11	2.24	0.06
Al (VI)	0.66	0.02	0.62	0.07	3.11	0.08	3.08	0.13	2.10	0.07	2.15	0.03
Fe	2.43	0.03	2.52	0.08	0.78	0.03	0.83	0.01	3.53	0.19	3.66	0.06
Mn	0.02	0.01	0.02	0.01	0.00	0.00	0.01	0.01	0.03	0.02	0.03	0.01
Mg	2.33	0.04	2.26	0.02	0.54	0.04	0.44	0.02	6.08	0.26	5.93	0.07
Ca	0.01	0.01	0.01	0.00	0.00	0.00	0.00	0.00	0.01	0.01	0.01	0.01
Na	0.02	0.01	0.03	0.00	0.03	0.01	0.03	0.01	0.00	0.00	0.00	0.00
K	1.86	0.09	1.94	0.11	1.52	0.20	1.74	0.33	0.01	0.01	0.01	0.01
H (12 wt%)	4.07	0.05	4.12	0.08	3.64	0.03	3.72	0.14	16.64	0.13	16.48	0.08
sum IV	8.00	0.00	8.00	0.00	8.00	0.00	8.00	0.00	8.00	0.00	8.00	0.00
sum VI	5.45	0.03	5.44	0.03	4.43	0.06	4.35	0.13	11.71	0.07	11.74	0.05
Mg/(Mg+Fg)	0.49		0.47		0.41		0.35		0.63		0.62	

Table 3.1: Chemical compositions of biotite, phengite and chlorite from host rock, V_3 and V_4 veins, as determined by electron microprobe analyses.

V_3 veins are partially filled first with phengite, which was later overgrown by hematite (Fig. 3.4c). Phengite and hematite grow freely into the open fracture space, but occasionally hematite is internally fractured. The composition of phengite is $K_{1.54}(Fe_{0.78},Mg_{0.54})Al_{4.4}Si_{6.68}O_{20}(OH)_4$ (Table 3.1). Occasionally remnants of biotite and phengite are situated in a matrix of hematite. Early hematite is enriched in Ti (hematite I, Table 3.2). The Ti concentration decreases during hematite growth, and during the latest stages hematite is nearly pure Fe_2O_3 (hematite III, Table 3.2). Phengite and hematite occasionally do not completely fill the fractures. In the case of remaining spaces in the V_3 veins hematite is overgrown by chlorite (Fig. 3.4d; Table 3.1), filling the younger V_4 veins completely (Fig. 3.4e). Chlorite has an average composition of $(Mg_{6.08}Fe_{3.53})Al_{4.36}Si_{5.57}O_{20}(OH)_{16}$ with an Mg/(Mg+Fe) of 0.63.

V_5 vein formation is preceded by two phases of cataclasite formation. The earliest cataclasite is characterised by a fine-grained mixture of white mica, chlorite, quartz and occasionally remnants of albite, K-feldspar and quartz (Fig. 3.4f). The quartz remnants have serrated grain-boundaries bordered by very fine-grained material and display internal fractures filled with the same material. Quartz clasts show undulatory extinction, indicative of a high dislocation density and chlorite and white mica were formed in small pores of the fine grained cataclasite.

sample	mu 209 (V3) hematite I		mu 209 (V3) hematite II		mu 209 (V3) hematite III	
analysis	3		2		2	
	Mean value	St dev	Mean value	St dev	Mean value	St dev
Fe2O3	92.0	0.42	97.04	0.80	98.42	0.01
TiO2	6.31	0.36	2.95	0.06	0.67	0.44
Total	98.34	0.06	100.07	0.76	99.22	0.51
Stoichiometry based on 3 oxygens						
Fe	1.82	0.01	1.92	0.01	1.98	0.01
Ti	0.07	0.01	0.03	0.01	0.01	0.01
sum total	1.89	0.01	1.95	0.01	1.99	0.01

Table 3.2: Chemical compositions of hematite from V_3 veins as determined by electron microprobe analyses. hematite I corresponds to the core of hematite crystals, II to intermediate growth stages, and III to the rim of large hematite crystals and cores of fine grained hematite crystals. The latter are associated to chlorite.
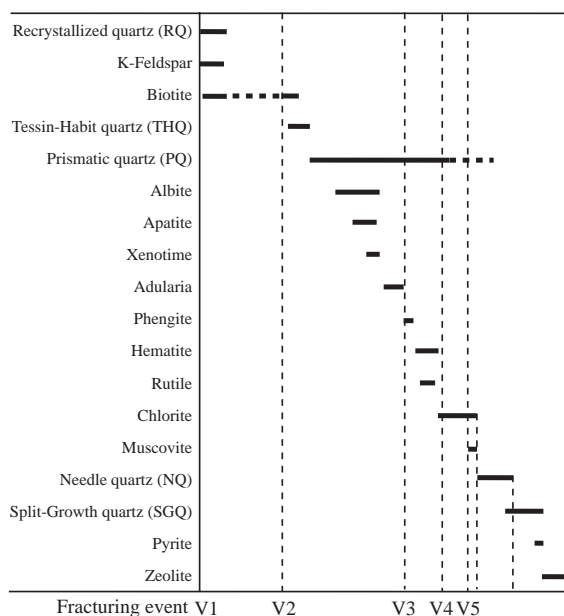
Figure 3.5: The succession of vein minerals from V_1 to V_5.

These cataclasites were subsequently overgrown during further V_5 fracturing events by prismatic "needle-like" habit quartz with a "comb texture" (Fig. 3.4g) followed by "split-growth quartz" or "feathery texture" (Adams, 1920; Dong et al., 1993) (Fig. 3.4h). Split-growth quartz is characterised by repeated growth zones and nucleation of new prismatic quartz on growth zones of the host-quartz, giving the crystal the appearance of a cauliflower. Grigorev (1965) and Mullis and Ramseyer (1999) attribute the nucleation of new crystals to larger amounts of impurities, forming irregularities in the host quartz lattice during fast quartz precipitation. Distinct sets of fluid inclusions perpendicular to the prism and rhomboedral planes of quartz are related to fast incorporation of fluids at sites of irregularities on the surface of the crystal (Fig. 3.4h). During the last growth

stages in the vein, quartz precipitates together with late adularia and zeolite.

Petrographic and geochemical characteristics of the vein-host rock interface
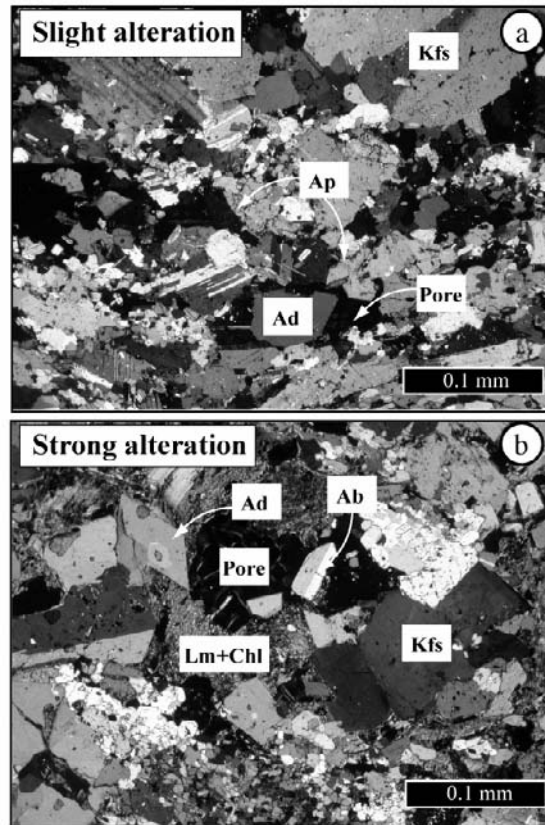
Figure 3.6: a) precipitation of new minerals in pores of slightly altered gneiss. b) Similar to a) but nearer to the vein interface, where the host rock was more strongly altered.

Petrography (Fig. 3.6), whole rock geochemistry (Fig. 3.7, Table 3.3), porosity and density measurements (Fig. 3.8 a,b, Table 3.3) of the vein-host rock interface were performed to determine the amounts of alteration that occurred during vein formation.

No host rock alteration could be observed near V_1 veins. The width of host rock alteration zone of V_2 veins increases from 0 cm at the vein tip to 15 cm at the center of the vein. Two individual veins may have different maximum alteration zone widths. At about 5–10 cm from the fissures small pore spaces are visible in bt-ms-rich zones. These are partly refilled with new biotite, albite, quartz, apatite and adularia (Fig. 3.6a,b). The pore-size and the size of new crystals increases towards the vein interface. The S_1 foliation is progressively destroyed due to pore formation and fracturing, indicating that the S_1 foliation formed before the host rock alteration. Old primary twinned albite is progressively replaced by new twin-free albite and feldspars are progressively altered to white mica. Chlorite and Fe-rich carbonate, which was subsequently oxidised to limonite are the last minerals to crystallise in the pores (Fig. 3.6b). In some cases a 0.2–0.5 cm wide bleached zone could
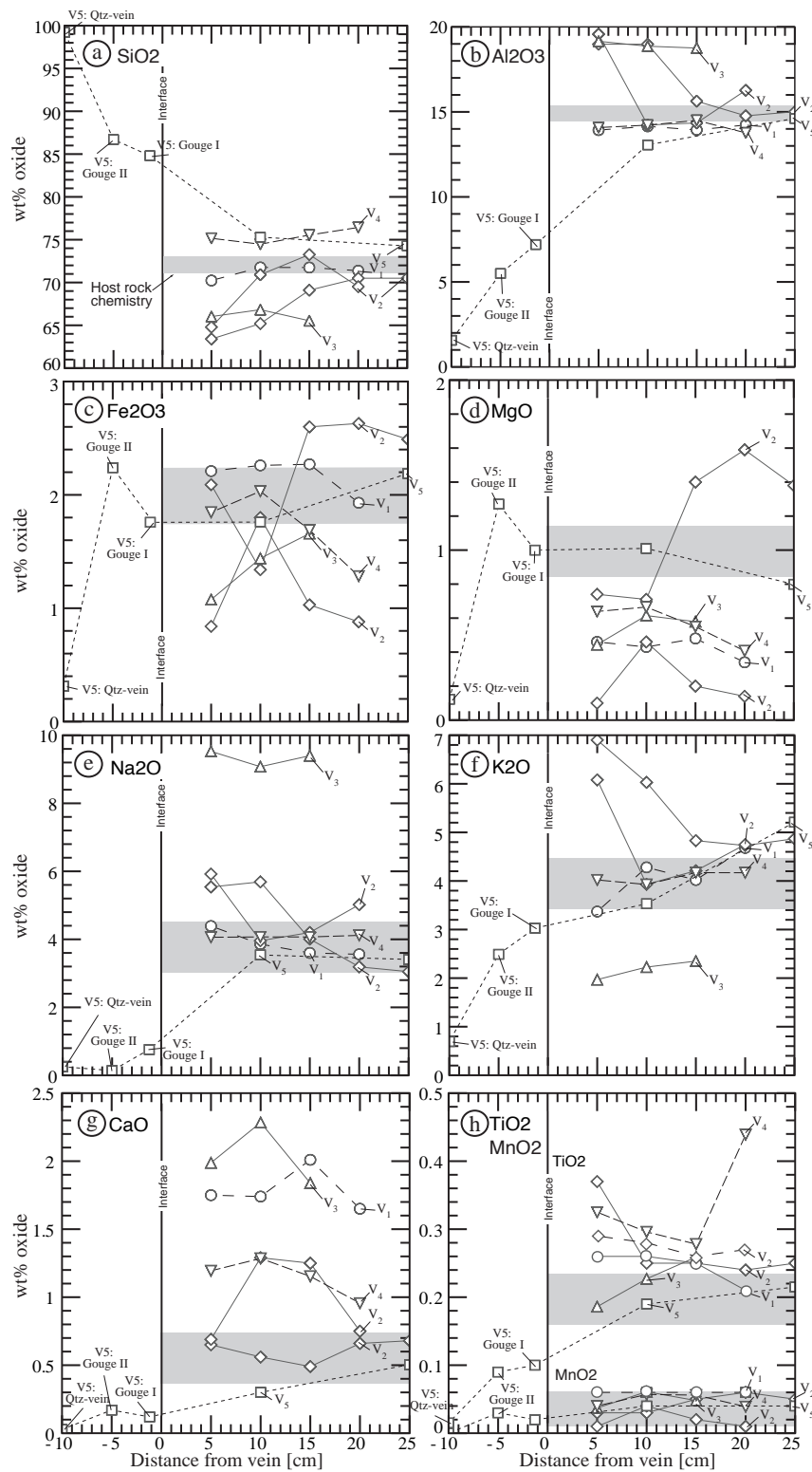
Fig. 3.7: a-h) Changes in major oxide chemistry of the host rock towards the interface with the V_1 to V_4 veins and the fault gouge of V_5 veins. Grey fields signify average of four host granite analyses. Note differences in vertical scale.

| Vein type | Th. Nr | Sample | distance | APD(A) | Density | | Porosity | Bulk Chemistry | | | | | | | | | total |
					BD	ASD		SiO2	Al2O3	Fe2O3t	MnO	MgO	CaO	Na2O	K2O	TiO2	
Hostrock	Th.3	average of 4	x	0.0112	2.55	2.64	3.32	72.03	14.95	2.08	0.03	1.08	0.30	3.77	4.09	0.19	98.52
		stdev	x	0.0077	0.02	0.04	1.33	0.76	0.23	0.33	0.02	0.15	0.02	0.50	0.41	0.03	
V1	Th.4	Th.4.1	20.0	0.0306	2.55	2.66	4.29	71.38	14.23	1.93	0.06	0.34	1.65	3.56	4.68	0.21	98.03
		Th.4.2	15.0	0.0146	2.58	2.70	4.58	71.75	13.94	2.27	0.06	0.48	2.01	3.60	4.02	0.25	98.38
		Th.4.3	10.0	0.0143	2.55	2.68	4.85	71.76	14.15	2.26	0.06	0.43	1.74	3.86	4.28	0.26	98.80
		Th.4.4	5.0	0.0155	2.54	2.66	4.67	70.23	13.93	2.21	0.06	0.46	1.75	4.39	3.37	0.26	96.66
V2	Th.3	Th.3.13.1	25.0	0.0138	2.58	2.69	4.23	70.50	15.01	2.49	0.05	1.38	0.68	3.05	4.87	0.25	98.28
		Th.3.13.2	20.0	0.0118	2.55	2.65	4.05	70.50	14.77	2.63	0.06	1.59	0.66	3.19	4.73	0.24	98.37
		Th.3.13.3	15.0	0.0151	2.52	2.65	5.08	69.10	15.63	2.60	0.05	1.40	0.49	4.01	4.83	0.25	98.36
		Th.3.13.4	10.0	0.0202	2.44	2.59	5.67	65.20	18.98	1.34	0.03	0.71	0.56	5.69	6.03	0.25	98.79
		Th.3.13.5	5.0	0.0226	2.37	2.53	6.34	63.40	18.98	2.09	0.03	0.74	0.65	5.54	6.90	0.37	98.70
V2	Th.78	Th.78.1	20.0	0.0123	2.53	2.64	4.15	69.51	16.27	0.88	0.01	0.14	0.75	5.02	4.75	0.27	97.59
		Th.78.2	15.0	0.0127	2.50	2.61	4.14	73.26	14.35	1.03	0.02	0.20	1.25	4.20	4.21	0.26	98.79
		Th.78.3	10.0	0.0181	2.50	2.66	6.11	70.91	14.23	1.80	0.04	0.46	1.29	3.96	3.93	0.28	96.90
		Th.78.4	5.0	0.0334	2.29	2.48	7.7	64.79	19.57	0.84	0.01	0.10	0.69	5.92	6.08	0.29	98.30
V3	Th.1	Mu.209.A.1	15.0	0.0118	2.58	2.68	3.48	65.53	18.76	1.659	0.05	0.58	1.84	9.4	2.35	0.26	100.42
		Mu.209.A.2	10.0	0.0103	2.58	2.66	2.99	66.83	18.86	1.44	0.06	0.62	2.28	9.08	2.23	0.23	101.62
		Mu.209.A.4	5.0	0.0093	2.59	2.67	3.03	66.02	19.15	1.076	0.04	0.44	1.99	9.53	1.97	0.19	100.40
V4	Th.78	Th.78.2.1	20.0	0.0125	2.54	2.66	4.58	76.43	13.77	1.283	0.04	0.41	0.96	4.12	4.17	0.44	101.61
		Th.78.2.2	15.0	0.0125	2.55	2.67	4.39	75.54	14.5	1.69	0.06	0.55	1.15	4.07	4.17	0.28	102.01
		Th.78.2.3	10.0	0.0115	2.55	2.67	4.31	74.47	14.22	2.032	0.06	0.67	1.29	4.07	3.93	0.3	101.03
		Th.78.2.4	5.0	0.0131	2.48	2.60	4.64	75.16	14.08	1.846	0.04	0.64	1.19	4.06	4.02	0.33	101.37
V5	Th.8	Th.8Hr	25	0.0182	2.50	2.64	5.64	74.27	14.62	2.189	0.04	0.8	0.5	3.41	5.21	0.22	101.25
		Th.8.31.1	10.0	0.0122	2.55	2.67	4.6	75.30	13.06	1.76	0.04	1.01	0.3	3.54	3.53	0.19	98.73
		Th.8.1.2.1	0.0	0.01	2.56	2.68	4.42	84.80	7.20	1.76	0.02	1.00	0.12	0.77	3.03	0.10	98.80
		Th.8.1.2.2	-5.0	0.0079	2.58	2.67	3.44	86.70	5.49	2.24	0.03	1.27	0.17	0.14	2.49	0.09	98.62
		Th.8.1.2.3	-10.0	0.0063	2.59	2.64	2.02	99.22	1.568	0.312	0	0.12	0.03	0.25	0.69	0.02	102.21

Table 3.3: Whole rock geochemical compositions as measured by X-ray fluorescence and porosity (APD is the average pore diameter (μm)) and density (BD is the bulk density (gr/cm^3), ASD= Apparent Skeletal Density (gr/cm^3) i.e. the density calculated by subtracting the porosity) as measured by Hg-porosimetry.

be observed near V_3 and V_4 veins, but this could not be resolved geochemically. V_5 veins are bordered by fault rock and by host granite. Fault rocks and granites are cut by quartz filled fractures formed during the subsequent veining events. Host-rock minerals are more intensely retrograded in these fractured rocks than in un-fractured host rock.

The composition of the host rock (Table 3.3, Fig. 3.7) (excluding V_5 fault gouge and vein material) shows a relatively large variability particularly for SiO_2, Al_2O_3, Na_2O and K_2O. The host rock compositions near V_1 and V_4 are nearly the same as the average

host rock composition. For the other vein types SiO_2 varies between 62–75 wt%, Al_2O_3 varies between 13–20 wt%, Na_2O between 3–9 wt% and K_2O between 3–7 wt%. For these elements samples 20–25 cm away from the V_2 and V_5 veins have nearly average host rock composition. V_3 at locality Th.1 at 15 cm from the vein has a lower SiO_2 and K_2O and higher Al_2O_3 and Na_2O content than the average host rock. The higher $Na/(Na+K)$ ratio indicates that near V_3 the rock contains more albite and less quartz than the average gneissic host rock. The host rock near V_2 veins at Th.3 and Th.78 shows significant changes in porosity, density and bulk geochemistry compared to the host rock (Fig.3.8a,b, Table 3.3). The whole rock geochemistry indicates that the rock is depleted in SiO_2 near the vein-rock interface. Al_2O_3 increases towards the interface of the vein as do Na_2O and K_2O. Fe_2O_3, MgO and MnO remain relatively constant or decrease slightly. There is an indication of a slight increase in TiO_2 towards the vein. Overall porosity increases from 3 to 4% to up to 8% near the vein interface and the apparent density of the rock decreases from nearly 2.7 gr/cm^3 to 2.5 gr/cm^3 (Fig. 3.8a,b, Table 3.3).

Figure 3.8c,d show the evaluation of the weight gain and loss from the alteration zone. Biotite was nearly completely dissolved near the vein interfaces and the pore spaces were later filled with wormy chlorite. K-feldspars were progressively altered to muscovite near the vein interface but not totally destroyed. The whole rock geochemical differences therefore only represent averages of dissolution and new precipitation and not the compositions, density and porosity of the host rock during each individual mineralisation event. Changing the reference isocon from constant volume to constant Al does not significantly change the observations that: SiO_2, CaO and Fe_2O_3 were depleted, Al_2O_3, Na_2O and K_2O follow both isocons or indicate relative enrichment and TiO_2 and MnO remain fairly constant. The data indicate that approximately 20% of the silica was dissolved from the alteration zones of Th.3 and Th.78.

Fluid inclusion topology

Thirteen fluid inclusion populations could be distinguished based on their microstructural occurrence (see Table 3.4). However four fluid inclusion populations could be correlated with one another based on their T_{hom} and T_m ice, making a total of 9 different fluid inclusion populations (see next section). Their characteristics are summarised below:

V_1 fluid inclusion populations: Fluid inclusions in quartz from V_1 are found in three separate assemblages: as groups in transparent quartz ($V_{1.1}$), in parallel trails cutting through quartz grains ($V_{1.2}$), along grain boundaries and as parallel trails cross-cutting $V_{1.1}$ and $V_{1.2}$ fluid inclusion populations ($V_{1.3}$). Both $V_{1.1}$ and $V_{1.2}$ fluid inclusion populations are characterised by two-phase vapour bubbles and partially decrepitated fluid inclusions
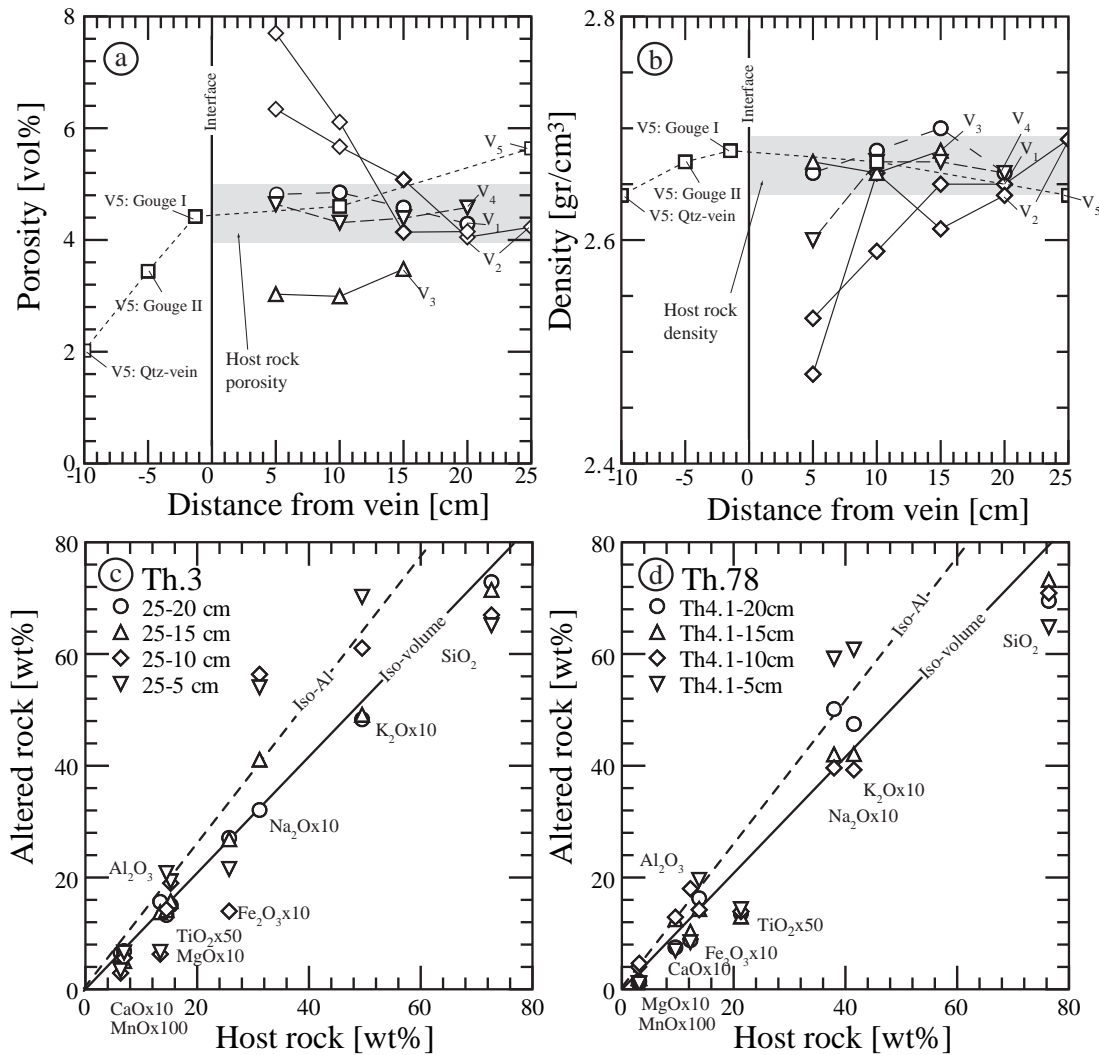
Fig. 3.8: a,b) Porosity and density changes from the host rock to the vein interface for V_1 to V_5 veins. c,d) Isocon diagrams for V_2 veins Th.3 and Th.78 after Grant (1986). Indicated are the chemical data for 20 to 5 cm from the vein and the constant volume isocon and constant Al isocon for localities. In the case of Th.78 reference sample is used from V_4 sample Th.78.2.1.

that have subsequently been re-healed (Fig. 3.9a,b). The $V_{1.3}$ fluid inclusion populations did not contain two-phase vapour bubbles. Fluid inclusions on the grain boundaries were badly healed and did not contain vapour bubbles, making them unsuitable for microthermometry.

V_2 fluid inclusion populations: Early $V_{2.1}$ fluid inclusions are situated in trails that cut early growth stages of the Tessin habit crystals. Fluid inclusions along these trails contain two-phase vapour bubbles (20–25 vol%) and commonly have a negative crystal shape

(Fig. 3.9c). Small phyllosilicates and rutile whiskers are present in most of these fluid inclusions. Later fluid inclusion populations cross-cut the whole quartz or originate from the crystal surface. These contain only one-phase gas bubbles (10–15 vol%) and have well to poorly healed shapes ($V_{2.2}$, $V_{2.3}$) (Fig. 3.9d). $V_{2.4}$ fluid inclusions are associated with accidentally trapped hematite, implying that hematite must have precipitated before the $V_{2.4}$ fluid inclusion populations. The volume of the gas bubble in $V_{2.4}$ fluid inclusions is 5–10 vol%.

V_3 fluid inclusion population: $V_{3.1}$ is defined by irregular shaped fluid inclusions situated in Tessin habit quartz-hematite inter-growths from V_2 veins. These fluid inclusions represent fluids that are associated with hematite formation (Fig. 3.9e) during V_3. The mono-phase gas bubble in the fluid inclusions is about 15 vol% in size. No daughter minerals of hematite were observed inside these fluid inclusions.

V_4 fluid inclusion population: Healed fractures in massive V_1 quartz with accidentally trapped chlorite and irregular shaped fluid inclusions (Fig. 3.9f) are temporarily close to the fluids associated with chlorite growth ($V_{4.1}$). Vapour-bubbles fill 10 vol% of the fluid inclusions.

V_5 fluid inclusion populations: Fluid inclusions in V_5 veins are regular to irregular shaped depending on the morphology of the quartz crystal and their mode of occurrence (Fig. 3.9g,h). Fluid inclusions from needle quartz are commonly poorly healed ($V_{5.1.1, 5.1.2}$). Daughter minerals (Fig. 3.9g) are often present in different amounts inside the fluid inclusions and are characterised by their irregular size and shape. Vapour bubbles in $V_{5.1.1}$ fill about 15 vol% of the fluid inclusions, whereas vapour bubbles in $V_{5.1.2}$ are slightly smaller. Commonly very small fluid inclusions form during the last needle quartz growth stages, which are similar to fluid inclusions related to the early stages of split-growth quartz. Fluid inclusions from split-growth quartz are situated in trails perpendicular to the prism and rhomboedral faces of quartz or in fine healed cracks, which cut parts of the crystals. In split-growth quartz up to 20 different growth zones with fluid inclusions could be distinguished. Fluid inclusion population $V_{5.2.1}$ are from the first growth zone and $V_{5.2.2}$ fluid inclusions are from the tenth growth zone of split-growth quartz. Fluid inclusions in $V_{5.2.1, 5.2.2}$ have 5–10 vol% gas-bubbles. The last growth stages are characterised by fluid inclusions ≤ 3 μm which could not be analysed by microthermometry.

Microthermometry and Raman analyses of fluid inclusions

Results from microthermometry and Raman studies of fluid inclusions from different quartz generations are depicted in Table 3.4, in Figure 3.10 and in appendix B. Figure 3.10 visualizes the evolution of the different fluid inclusion populations from the five
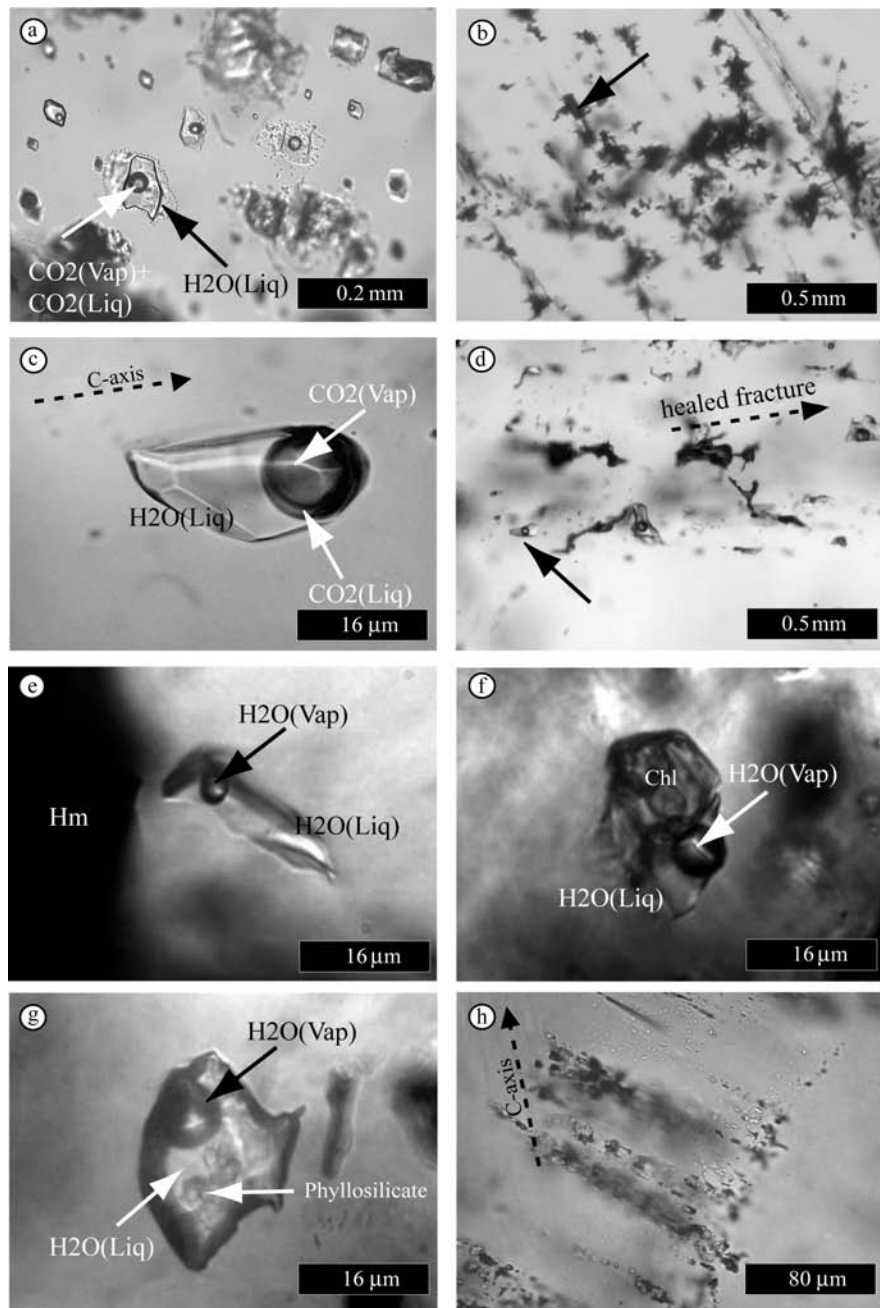
Fig. 3.9: Different fluid inclusion types based on morphology and distribution of fluid inclusions. a) Partially decrepitated, grouped fluid inclusions from V_1 veins. b) Partially decrepitated, three-phase CO_2-bearing fluid inclusions lying in parallel trails from V_1 veins, cutting the grain boundaries. c) Early three-phase CO_2-bearing fluid inclusions formed in THQ(Tessin habit quartz) from V_2 veins. d) Late fluid inclusions along badly healed fractures in THQ. e) Fluid inclusions formed along hematite-late THQ inter-growths in a V_2 vein. f) Two-phase fluid inclusions in trails with accidentally included wormy chlorite. g) Relatively large aqueous fluid inclusions in needle quartz ($V_{5.1}$) with accidental included phyllosilicates. h) Two-phase small and poorly healed fluid inclusions, in trails that are perpendicularly arranged to the rhombohedral faces in late split-growth quartz ($V_{5.2}$).

vein types, based on the melting and homogenisation temperatures.

V_1 *fluid inclusion populations:* Melting temperatures of solid CO_2 at -56.6 to -57.4 °C in $V_{1.2}$ signifies that the two-phase fluid inclusions from V_{1a} veins contain relatively pure CO_2, which is substantiated by Raman analyses. Clathrate dissociation is at +5.8 to +7.9 with for FP $V_{1.2}$ and CO_2 liquid-vapour homogenisation to liquid is nearly critical at +30.0 °C. Salinity based on clathrate dissociation is between 5.4 and 4.4 wt% NaCl equivalent $V_{1.1}$ and $V_{1.2}$ contain 5.5 and 6.7 mol% of CO_2 respectively and about 14 to 1.6 mol% NaCl equivalent and the density ranges between 0.94 and 0.91 gr/cm^3. The fluctuations in density to the change of homogenisation of CO_2 from vapour into liquid. $V_{1.3}$ is a later population attributed to retrograde conditions, depleted in CO_2 and with 2.3 mol% of NaCl equivalent with a slightly lower density of 0.88 gr/cm^3.

V_2 *fluid inclusion populations:* The T_m of CO_2 of $V_{2.1}$ fluids is between -56.9 to -57.7, which implies that the vapour phase is nearly pure CO_2. The salinity based on T_d of clathrate of +7.7 is 4.4 wt% NaCl equivalent. CO_2 liq-vap homogenises to the liquid but in some cases critically. This changes the total inclusion density from 0.84 to 0.87 gr/cm^3, similar to $V_{1.1}$ and $V_{1.2}$. The $V_{2.1}$ fluid inclusion population contains 6.0 to 6.4 mol% CO_2 as $V_{1.1}$ and $V_{1.2}$ and 1.4 mol% NaCl equivalent. This was observed in 3 different vein localities: Th.1, Th.3 and Th.37. $V_{2.2}$ does not show any CO_2 melting, clathrate dissociation or CO_2 homogenisation. Raman observations on these fluid inclusions show two small peaks at 1286 and 1385 cm^{-1}, indicative of small amounts of CO_2. $\leqslant$ 1.0 mol% of CO_2 can be dissolved in water without forming clathrates between -5 and +10 °C. As no clathrate dissociation was observed during or after final ice-melting it is assumed that ice-melting was not influenced by the presence of clathrate and that therefore the salinity of 8.8 wt% NaCl equivalent for $V_{2.2}$, which is based on the ice melting temperature, refers to the "true" salinity (similar to Fabre et al., 2002). The overall density of the fluids (0.93 gr/cm^3) is slightly higher compared to the density of $V_{2.1}$. $V_{2.3}$ is CO_2-free and has a lower salinity (5.6 wt%). It has a density of 0.92 gr/cm^3. $V_{2.4}$ is characterised by a lower salinity of about 5 wt% and a higher density of 0.94 gr/cm^3. The homogenisation temperature decreases from $\sim$ 260 °C for $V_{2.1}$ to as low as 160 °C for $V_{2.4}$.

V_3 *fluid inclusion populations:* Salinity and homogenisation temperatures for $V_{3.1}$ fluid inclusions correspond well to the salinities and homogenisation temperatures of $V_{2.2}$. The $V_{3.1}$ fluid inclusion population was measured at the interface between hematite-quartz inter-growths, while $V_{2.2}$ fluid inclusions were measured in other positions in the quartz. It was not possible to measure this fluid inclusion population in hematite veins as no minerals used for microthermometry precipitated in the V_3 veins.

V_4 *fluid inclusion populations:* The $V_{4.1}$ fluid inclusion population has similar fluid inclu-

sion characteristics (T_m and T_h and gas-bubble size) as $V_{2.3}$ fluid inclusion population, which were measured in fractures cutting V_2 Tessin habit quartz. They have similar salinity (6.0 wt%), density (0.93) and a mean homogenisation temperature of 210 °C.

V_5 fluid inclusion populations: The early fluid inclusion populations from needle quartz in V_5 veins have a homogenisation temperature of 255 °C, higher than the $V_{2.2}$ and $V_{2.3}$ fluid inclusion populations but have very low salinity of 0.8 mol% and no volatiles are present.
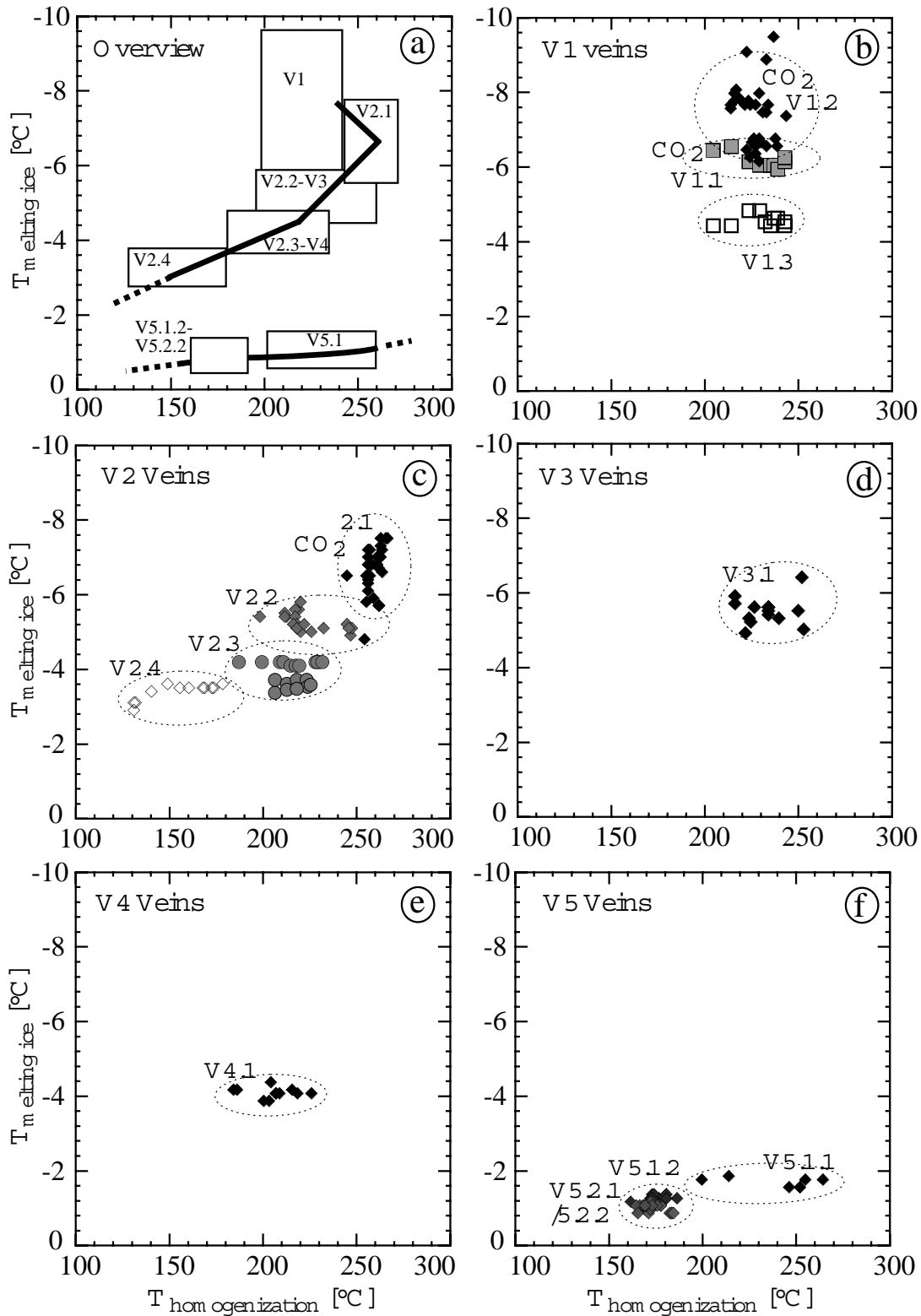
Fig. 3.10: Homogenisation temperature (T_h) against melting temperatures of ice (T_m). a) Composite diagram of all investigated fluid inclusion populations from all the vein types and. b-f) Evolution of the fluid inclusion within the five separate vein types.

The salinity of fluid assemblages in later split-growth quartz is lower than the earlier populations, down to 0.5 mol% and the homogenisation temperature decreases to 178 °C.

Fluid evolution of the five vein types: Considering the earliest fluid inclusion populations of each vein type, melting and homogenisation temperatures decreased during fluid evolution (Fig. 3.10a). Only a marked density controlled increase of T_h for V_2 and V_5 veins is given. The CO_2 concentration increases from the first to the second vein type and decreases during subsequent vein evolution. In V_4 vein fluids are CO_2 free. The similar evolution of T_m, T_h and CO_2 content is documented by the retrograde V_2 fluid evolution, as already shown by Mullis et al. (1994) in other places in the Central Alps. In contrast, the T_h of prograde V_{1a} veins remain more or less constant, whereas T_m and the CO_2-content decrease during progressive evolution. As already expected $V_{3.1}$ vein fluids correspond to vein fluid $V_{2.2}$, and $V_{4.1}$ vein fluids to $V_{2.3}$ fluids. Similar behaviour is documented by the V_5 vein fluids, where T_h and T_m decrease in absence of other volatiles, from the first to the last fluid inclusion population. The salinities of the fluids generally decrease from early V_1 to late V_5 fluid inclusion populations. However between $V_{2.1}$ to $V_{2.2}$ salinity is markedly increased from 4.8 to 8.3 wt% equivalent. The relatively large salinity decrease between the $V_{4.1}$ fluid inclusion population and the $V_{5.1.1}$ fluid inclusion population from 6.5 wt% to 2.5 wt% is indicative of a change in fluid chemistry between the two vein types.

Fig. 3.11: Opposite page: All measured fluid inclusion populations from the five vein sets. Numbers between brackets below the column headings indicate: (1) fluid inclusion population, (2) fissure number, (3) host mineral (RQ = recrystallised quartz, THQ = Tessin habit quartz, PQ = prismatic quartz, NQ = needle quartz, SGQ = split-growth quartz), (4) fluid inclusion type (P = primary, PS = pseudo secondary, S = secondary), (5) number of measured fluid inclusions, (6) volatile type present in fluid inclusions, (7) estimated volume % of bubble, (8) ice melting temperature, (9) melting temperature of solid CO_2, (10) clatrate-dissociation temperature, (11) homogenisation temperatures of CO_2, (12) bulk homogenisation temperature, (13) salinity in wt% NaCl equivalent, (14) mol% of different species within the fluid inclusions, (15) density in gr/cm^3, (16) daughter minerals (rt = rutile, ph=phyllosilicate). The three columns for the different temperatures represent the average, the minimum and maximum value in °C. (V) indicates homogenisation into the vapour phase, (C) indicates critical boiling, (L) indicates homogenisation into the liquid phase.

type	FP (1)	FN (2)	HM (3)	IT (4)	nI (5)	VoT (6)	V% (7)	Tm (ice) (8)	Tm (vol) (9)	Td (clath) (10)	Th (vol) (11)	Th (bulk) (12)	NaCl (13)	CO2 (14)	H2O	NaCl	Density (15)	DM (16)
V1	1	3	RQ	PS	17	CO_2	20	-5.0 -5.2 -4.7	- -	7.7 7.7 8.0	30.0(V) 30(L) 30.0(V)	239(L) 239 239	4.4	5.5	93.1	1.4	0.94	rt
	2	4	RQ	S	41	CO_2	20	-6.3 -6.7 -5.9	-57 -57.4 -56.6	7.2 5.8 7.9	29.4(L) 28.8 30.2	228(L) 215 240	5.4	6.7	91.7	1.6	0.91	none
	3	53	RQ	S	10	H_2O	15	-4.6 -4.8 -4.4	- -	- - -	- - -	223(L) 206 240	7.2	≤1.0	96.7	2.3	0.88	none
V2	1	1	THQ	PS	41	CO_2	20	-6.6 -7.5 -4.8	-56.9 -57 -56.6	7.8 7.6 7.8	30.4(C) 29.8 30.6	257(L) 253 264	4.4	6.4	92.2	1.4	0.84	rt+ph
	3		THQ	PS	20	CO_2	20	-5.6 -5.7 -5.6	-56.8 -56.6 -57.4	8.0 7.9 8.0	30.0(L) 30.0 30.0	260(L) 260 260	4.4	6.0	92.6	1.4	0.87	rt+ph
	37		THQ	PS	5	CO_2	20	-5.8 -5.9 -5.7	-56.7 -56.8 -56.6	7.7 7.7 7.7	30.7(C) 30.6 30.7	260(L) 259 261	4.8	6.0	92.6	1.4	0.86	rt+ph
	2	1	PQ	S	31	H_2O	15	-5.2 -6.0 -4.8	- -	- - -	- - -	238(L) 225 247	8.3	≤1.0	96.3	2.7	0.93	none
	37		PQ	S	11	H_2O	15	-7.1 -7.3 -6.8	- -	- - -	- - -	227(L) 213 240	10.5	≤1.0	95.5	3.5	0.89	rt+ph
	3	1	PQ	S	20	H_2O	15	-3.5 -3.6 -3.2	- -	- - -	- - -	215(L) 212 221	5.6	0.0	98.1	1.9	0.92	none
	3	3	PQ	S	11	H_2O	15	-3.6 -3.7 -3.4	- -	- - -	- - -	216(L) 206 223	5.9	0.0	98.2	1.8	0.92	
	4	1	PQ	S	10	H_2O	5	-3.2 -3.5 -2.8	- -	- - -	- - -	160(L) 149 178	5.1	0.0	98.4	1.6	0.94	none
V3	1	1	PQ	S	20	H_2O	15	-5.3 -6.4 -4.9	- -	- - -	- - -	230(L) 217 251	8.3	≤1.0	96.2	2.7	0.95	none
V4	1	78	PQ	S	16	H_2O	15	-3.9 -4.0 -3.7	- -	- - -	- - -	205(L) 184 226	6.5	0.0	97.0	2.0	0.93	none
V5	11	8	NQ	S	5	H_2O	15	-1.4 -1.6 -1.4	- -	- - -	- - -	255(L) 248 265	2.5	0.0	99.2	0.8	0.87	ph
	12	8	NQ	S	19	H_2O	10	-1.1 -1.2 -1.0	- -	- - -	- - -	178(L) 164 189	2.0	0.0	99.4	0.6	0.90	none
	2_1	8	SGQ	P	15	H_2O	10	-0.8 -1.0 -0.7	- -	- - -	- - -	178(L) 169 187	1.4	0.0	99.5	0.5	0.90	none
	2_2	8	SGQ	P	15	H_2O	10	-0.9 -1.0 -0.8	- -	- - -	- - -	184(L) 179 190	1.6	0.0	99.5	0.5	0.90	none
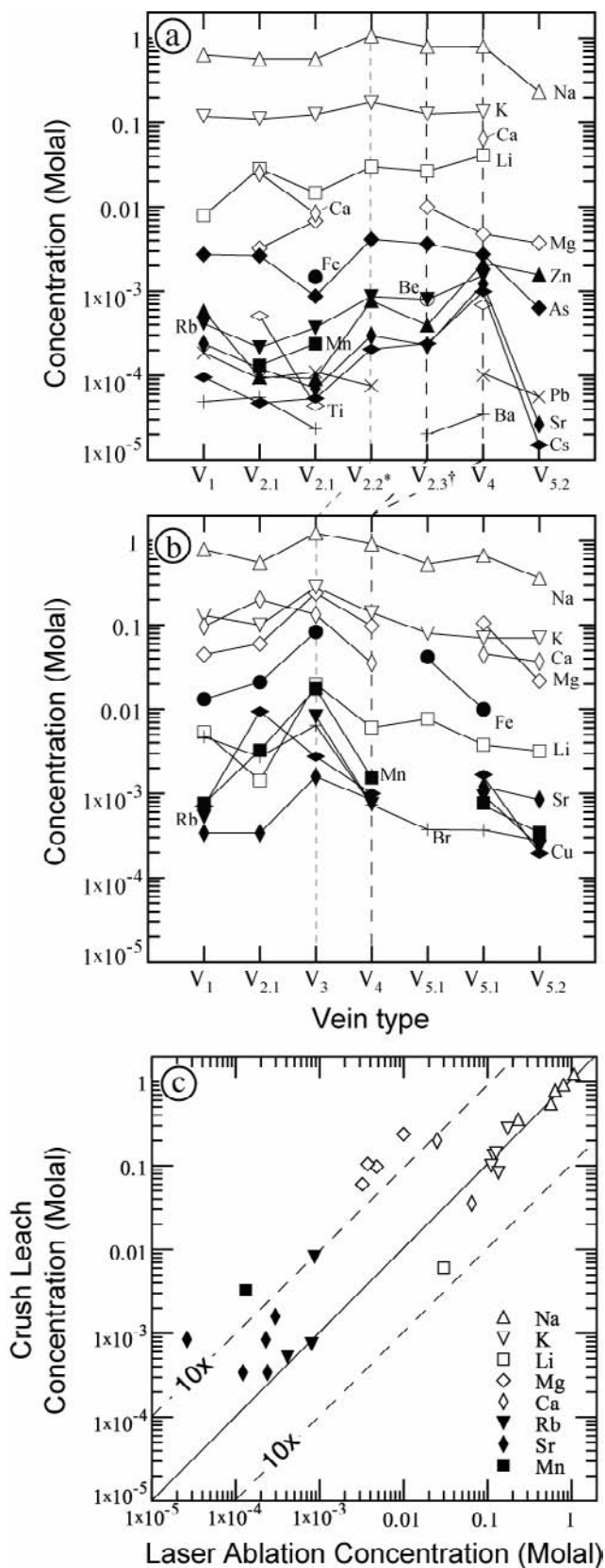
Figure 3.12: Cation and anion compositional evolution of the aqueous vein fluids from all vein types, a) from laser ablation analyses and b) from crush leach analyses. Note Ba in a) has the same symbol as Br in b). c) Comparison of concentrations of dissolved species determined both by LA-ICPMS and crush leach analyses for the same sample material.

Laser ablation-ICPMS and crush leach analyses

Chemical analyses of fluid inclusions by laser ablation and crush leach methods (see Appendix D for raw data) were recalculated from ppm to molal concentrations assuming that Cl^- was the only anion present (Table 3.4a,b). This introduces a small systematic error between laser ablation compared to the crush leach analyses, because in the latter case $SO4^{2-}$ was also measured. The recalculation from ppb to molal concentrations depends critically on the salinity, determined by microthermometry. Errors in measurement of the ice melting or clathrate dissociation have small effects on the molalities of the species. The lowest concentrations that were measured for these fluids range from approximately $1x10^{-6}$ molal for heavy elements like Pb or Ba to 10^{-4} molal for light elements like Li, Be. The results of both analytical methods are shown in Figure 3.12 a - c.

Alkali and earth alkali elements: Na and K are the main components of the measured fluids and are positively correlated for both the crush leach analyses and laser-ablation data. Variations in salinities of the fluid inclusion populations cause the differences in concentrations. Na concentrations range between 0.1 and 1 molal for both the laser ablation and crush leach data. The range of K concentrations is between 0.07 and 0.28 molal for crush leach analyses and is relatively constant for the fluid inclusion populations analysed with laser ablation at 0.11 to 0.17 molal.

For the crush leach analyses, Li was only measured above the detection limit in the sample from V_4 vein fluid. The Li concentration of 0.003 molal for V_4 veins is about 1 order of magnitude lower than the Li concentrations measured by laser ablation, which are between 0.008 and 0.04 molal. The laser ablation analyses also indicate a slight increase in Li concentration from V_2 to V_4, which is probably due to the increase in salinity of the fluids. Na/Li ratios remain fairly constant.

Ca could be measured within samples Th.3.19.1 and Th.78.3. In other samples Ca was below detection limits. Ca was measurable by crush leach analyses in all samples, except sample Th.8.34, which had a very low yield. Ca concentrations range from 0.04 to 0.20 molal for crush leach data and 0.009 to 0.065 molal for laser ablation.

Mg concentrations are at the detection limit in the case of the laser ablation analyses. Mg was detectible in appreciable amounts in some of the fluid inclusions of sample Mu.209.4.1.2. In the case of crush leach data Mg was found above detection limits in all samples, which gave recalculated concentrations of 0.02 to 0.1 molal. Crush leach anal-

a) La-ICPMS

element	Th.4.15.3 V1.2	Mu.209.4.2.5 V2.1	Th.3.19.1 V2.1	Mu.209.4.1.3 V2.2	Mu. 209.4.1.2 V2.3	Th.78.3 V4	Th.8.23.3 V5.2.1
Li	0.0079	0.028	0.015	0.030	0.027	0.041	bd
Be	b.d.	b.d.	0.0015	b.d.	0.0008	b.d.	b.d.
Na	0.64	0.57	0.57	1.07	0.80	0.81	0.23
Mg	b.d.	0.0032	0.0068	0.010	b.d.	0.0048	0.004
K	0.12	0.11	0.12	0.17	0.13	0.14	b.d.
Ca	b.d.	0.025	0.008	b.d.	b.d.	0.065	b.d.
Ti	b.d.	0.00051	0.000044	b.d.	b.d.	0.00069	b.d.
Mn	b.d.	0.00013	0.00024	b.d.	b.d.	b.d.	b.d.
Fe	b.d.	b.d.	0.001	b.d.	b.d.	b.d.	b.d.
Zn	0.00058	0.00010	0.00009	0.00077	0.00040	0.0021	0.0016
As	0.0027	0.0026	0.0009	0.0041	0.0037	0.0027	0.00063
Rb	0.00041	0.00021	0.00037	0.00087	0.00080	0.0015	b.d.
Sr	0.00024	0.00012	0.00007	0.00030	0.00023	0.0012	0.000026
Cs	0.00010	0.00005	0.00005	0.00021	0.00024	0.0010	0.000015
Ba	0.000049	0.000055	0.000023	b.d.	0.00002	0.000035	b.d.
Pb	0.00019	0.00009	0.00011	0.00008	b.d.	0.00010	0.000056

b) CL-analyses

element	Th.4.19 V1.2	Mu.209.4.2.5 V2.1	Th.1.4.5 V3	Th.78.3 V4	Th. 8.34 V5.1.1/2	Th. 8.35 V5.1.1/2	Th.8.23.3 V5.2.1/2
Li	b.d.	b.d.	b.d.	0.0061	b.d.	b.d.	b.d.
Na	0.79	0.55	1.23	0.92	0.53	0.67	0.36
Mg	0.045	0.060	0.238	0.097	b.d.	0.105	0.022
K	0.13	0.10	0.28	0.14	0.08	0.07	0.07
Ca	0.10	0.20	0.13	0.04	b.d.	0.04	0.04
Mn	0.0008	0.0033	0.0175	0.0015	b.d.	0.0008	0.0003
Fe	0.013	0.021	b.d.	0.083	b.d.	0.042	0.010
Cu	0.00071	0.009	0.00275	0.00100	b.d.	0.00167	0.00020
Rb	0.00053	b.d.	0.00822	0.00075	b.d.	0.00093	0.00023
Sr	0.00034	0.00034	0.00159	0.00084	b.d.	0.00120	0.00085
Cl	1.15	1.13	1.99	1.28	0.67	0.66	0.41
Br	0.0047	0.0027	0.00645	0.00073	0.00037	0.00037	0.00028
SO4	0.1012	0.072	b.d.	0.0121	b.d.	0.1572	0.072

Table 3.4: a) LA-ICPMS and b) Bulk geochemical measurements for the different fluid populations calculated to molality concentrations (mol/kg H_2O). b.d. = below detection limit.

yses done on similar fluids by Yardley et al. (1993) and Fabre et al. (2002) had lower concentrations of Mg by one to two orders of magnitude.

Rb and Sr could be detected consistently by laser ablation over different fluid inclusions from a single fluid inclusion population (Table 3.4b). The total concentrations for both elements are 0.0001 to 0.001 molal. These concentrations are similar to the data of Yardley et al. (1993) and Fabre et al. (2002).

Ba and Cs were detected only in some of the fluid inclusions from the fluid inclusion populations that were measured by laser ablation, however as trace amounts of both elements were found in most fluid inclusion populations, it can be assumed that concentrations were ≤ 0.0001 molal.

Transition metals: Fe was detectible in most crush leach samples, but only in sample Th.3.19.1 for the laser ablation analyses and at a very low concentration. Crush leach samples for V_3 and V_4 fluid inclusion populations yielded high concentrations of Fe, in the case of V_3 (sample Th.1.4.5) even higher than the Na concentration. This anomalously high value was rejected from further consideration in Table 3.4b, as it probably reflects contamination by solid phases present in the sample. Overall concentrations of Fe in the other samples are between 0.013 and 0.042 molal, which is slightly more than the concentrations measured by Yardley et al. (1993) and Fabre et al. (2002). Mn was only found in the crush leach samples at a concentration of 0.0003 to 0.0033 molal with an exception for sample Th.1.4.5 which has much higher values. This is probably also related to impurities in the sample. Mn was sporadically measured in some fluid inclusions of laser ablation sample Mu.209.4.2.5 and Th.3.19.1. Calculation of molal concentrations in these fluid inclusions yield similar concentrations as the crush leach samples. Ti, Zn, Cu and Pb have concentrations between $1\text{x}10^{-3}$ and $1\text{x}10^{-5}$ molal (Table 3.4b).

Arsenic: As was only analysed by laser ablation. Small amounts of As were consistently measured in all samples, except Th.8.23.3. This gives concentrations of As in the range of 0.0007 to 0.004 molal, which is similar to the concentrations calculated by Yardley et al. (1993).

Anions: Br concentrations in the leachate samples are relatively low, below detection limit in the case of Th.8.34 and Th.8.35 (needle quartz samples). Cl concentrations are 2 orders of magnitude larger than Br in the early V_1 and V_2 vein fluids, but more than 3 orders of magnitude in late V_3 to V_5 vein fluids. SO_4^{2-} concentrations are between 0.006 molal and 0.08 molal, which is approximately similar or slightly higher than the SO_4^{2-} concentrations

analysed by Yardley et al. (1993), Marshall et al. (1998) and Fabre et al. (2002).

Gas species: H_2S and N_2 were not detected by Raman-spectroscopy, which indicates that if these gases were present their concentrations would be very low. Yardley et al. (1993) were able to measure H_2S in amounts less than 1 wt% using mass-spectrometry on decrepitated fluid inclusions. Their study indicates a positive correlation between As and H_2S, up to concentrations near arsenopyrite oversaturation. The mineral assemblages of the V_1 to V_5 veins did not contain any sulfides, which indicates that any As present in the fluids must have come from an external source.

Summary of fluid chemistries: The data from laser-ablation and crush leach analyses demonstrate the change in amounts and types of dissolved elements in the fluids from V_1 to V_5 veins. The dissolved cations in the fluids are Na-K-Li-As-(Fe-Mg-Mn-Cu-Rb-Sr-Cs-Ba-Pb), with the last 7 elements only occasionally measured in trace amounts. Br^- and SO_4^{2-} are present in low concentrations, but the main anion is Cl^-, as is expected for most metamorphic fluids. Major and trace element geochemistry of fluid inclusion populations from veins related to Alpine metamorphism have been studied analytically by Poty et al. (1974), Luckscheiter and Morteani (1980), Yardley et al. (1993), Marshall et al. (1998) and Fabre et al. (2002) using crush leach analyses and laser induced breakdown spectroscopy (LIBS). These studies indicate that fluids from Alpine veins are mostly Na-K-Ca-Li-Cl-bearing fluids with trace amounts of Mg, Fe, Mn, Al, Sr, Ba, Cu, Zn, Pb, As, B and $SO4_{2-}$, which is similar to our findings. The fluid chemistries reported in this study are similar to the fluids related to the retrograde quartz-gold veins from the Monte Rosa nappe (Yardley et al. (1993)). Michard (1990) reports the presence of the same species in geothermal fluids from granitic areas, although in concentrations lower than $\geq 10^3$ molal.

3.5 Vein formation conditions and mechanisms

Thermometry of fluids and minerals

The ratios of dissolved cations in aqueous fluids in equilibrium with K-feldspars, particularly K/Na , have been used as indicators of the fluid temperature, particularly in the field of geothermal fluid research (e.g. Michard, 1990), but also in the in the case of Alpine fissures (Poty et al., 1974; Mullis et al., 1994; Marshall et al., 1998; Fabre et al., 2002). In the latter case these ratios were used because Alpine fissure mineralisation occured over a time span of several million years with temperatures between 300 and 450 °C. Fluids

are assumed to have equilibrated with the host rock minerals. These ratios together with stable isotope mineral pairs and their respective temperatures are shown in Figure 3.13 and Table 3.5.

K/Na ratios of fluids: Poty et al. (1974) proposed thermometric relations for total K and total Na dissolved in fluids related to low grade metamorphic vein forming fluids, using thermodynamic data gathered from experiments (e.g. Orville, 1963). The experimental data on total dissolved K and Na in fluids in equilibrium with feldspars were extended by Lagache and Weisbrod (1977). Recently, experiments by Hauzenberger et al. (2001) and Pak et al. (2003) showed that the experiments from Orville (1963) and Lagache and Weisbrod (1977) did probably buffer Na and K, but lacked the necessary buffering for Al and Si to achieve equilibrium in the mineral-fluid system and, therefore, retained different results at 600 °C and 3kb. This makes the Na/K relations deduced from experiments of Orville (1963) and Lagache and Weisbrod (1977) questionable.

Numerous thermometric equations using Na/K ratios from low temperature (25–350 °C)

	K/Na (mol)		Verma (1997)		Poty (1974)		Δ	
	LA-ICPMS	CL	T(°C)$_{LA}$	T(°C)$_{CL}$	T(°C)$_{LA}$	T(°C)$_{CL}$	(qtz-min)	T(°C)
V1.2	0.19	0.17	336	320	445	415	4.9 (bt)	439
V2.1	0.20	0.18	342	331	455	442	-	-
V2.2	0.22	-	357	-	*480*	-	-	-
V2.2/V3	0.16	*0.23*	317	*358*	395	*500*	13.4 (hm)	359
V2.3V4	0.16	0.15	317	310	395	390	5.6 (chl)	332
V4	0.17	-	320	-	415	-	6.5 (chl)	272
V5.1	-	0.16	-	313	-	*395*	6.6 (chl)	256
V5.1	-	0.10	-	266	-	305	-	-
V5.2	-	*0.19*	-	*336*	*445*	-	-	-

Table 3.5: Ratio of K/Na and the temperatures calculated by using the thermometers proposed by Verma and Santoyo (1997) and Poty et al. (1974). The last two columns show differences in the δ^{18}O values for different mineral pairs as shown in chapter 4 and the temperatures calculated using the fractionation factors between these minerals from Zheng (1991) and Zheng (1993). K/Na ratios in bold-italics are unlikely to represent equilibrium values for Na and K, while temperatures in bold-italics are too high to represent vein formation temperatures. LA= laser ablation, CL = crush leach, $\Delta = \delta^{18}$O$_{mineral}-$ δ^{18}O$_{quartz}$.

geothermal fluids originating from granites have been related to temperature (e.g. Fournier, 1979; Fouillac and Michard, 1981; Michard, 1990; Verma and Santoyo, 1997). According to calculations by Fournier (1979), these empirical equations are consistent with thermodynamic relations of K and Na exchange between K-Na feldspars and fluids. Depending on which types of feldspars (ordered or disordered) Fournier used for thermometric calculations, the lower and upper boundaries for K/Na ratios are approximately 0.05 lower or higher than the empirical thermometric calculations.

The temperature estimates for V_1 and V_2 calculated after Fournier (1979) are between 300–350 °C for the geothermal fluid thermometers, while for the relations of Poty et al. (1974) temperatures of 450 °C are obtained for the same veins. In the case of V_3 and V_4 fluids geothermal fluid thermometers produce temperatures of 305 °C and 395 °C in the case of the thermometer of Poty et al. (1974). For V_5 temperature estimates are 250 °C for geothermal fluid thermometers and 305 °C for the thermometers of Poty et al. (1974) and Lagache and Weisbrod (1977).

Stable isotope fractionations: Calculations of temperatures from $\delta^{18}O$ fractionations between different mineral pairs from stable isotope measurements yields a systematic decrease in formation temperatures (Table 3.5, of 440 °C for V_1, 350 °C for V_3 and 320 °C for V_4 and up to 260 °C for V_5.

PT-conditions of vein formation

Pressure and temperature estimates for the different veining events were made using *PVTX*-data from fluid inclusions and temperature estimates from the Na/K fluid- and stable isotope thermometry. Figure 3.14a,b) show the different vein formation conditions. V_1 vein fluids were trapped during the prograde metamorphic path. The presence of large feldspars and minor biotite indicate that temperatures of formation of V_{1a} veins were higher than 400 °C. The large grain sizes and the dynamic recrystallisation features of quartz imply temperatures of formation of 550 to 600 °C. The only time that temperatures were that high was during the formation of the Fibbia granite in the Gotthard massif during the Hercynian orogeny. The possibility that the veins are early Alpine in origin is highly unlikely due to the lack of evidence that the Gotthard massif reached these high temperatures during Alpine orogenesis. V_{1b} veins are prograde in nature and were formed during late stages of S_1 formation. Trapping conditions of the $V_{1.1}$ and $V_{1.2}$ fluid inclusion populations are estimated at 440 °C and $\sim$ 4 kbar, based on the oxygen isotopic equilib-
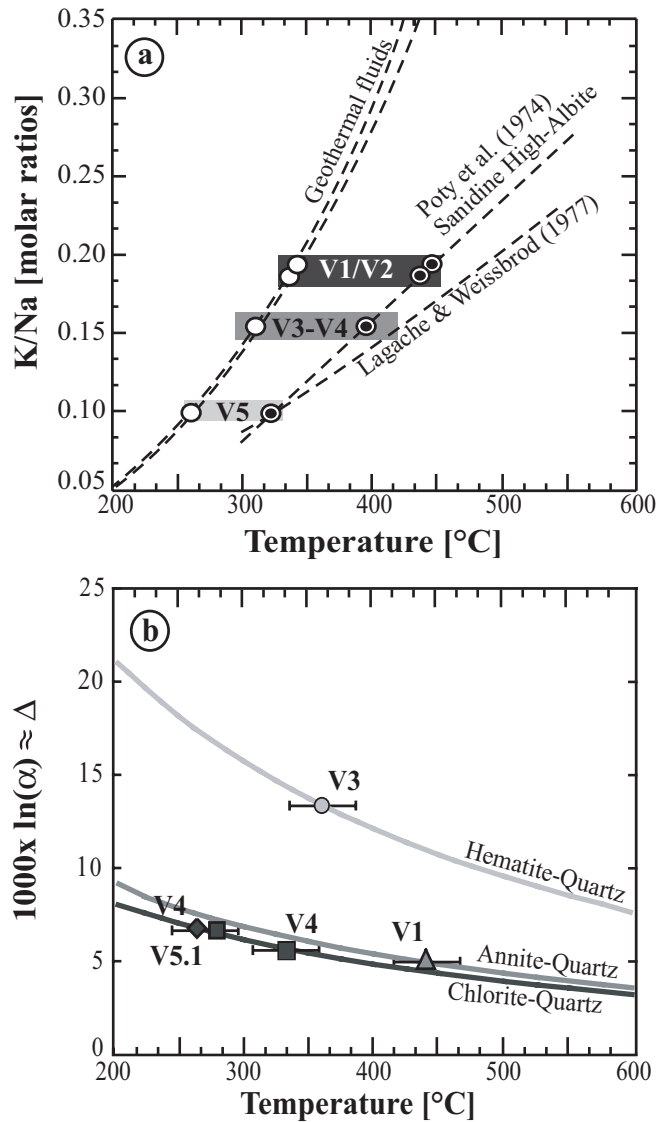
Figure 3.13: Temperature determination using a) K/Na results and temperature relations. Broken dark lines are thermometric relations from Poty et al. (1974) and Lagache and Weisbrod (1977), and empirical thermometric relations based on geothermal fluids (e.g. Fournier, 1979; Verma and Santoyo, 1997). Dots represent the K/Na ratios measured by laser ablation and crush leach analyses and their respective temperatures deduced from the thermometers above. b) Mineral-mineral oxygen isotope thermometry using different mineral pairs for different vein types. For reference the equilibrium lines from Zheng (1991, 1993) for quartz-biotite, quartz-chlorite and quartz-hematite are shown for temperatures from 200 to 600 °C.

rium between bt-qtz (Table 3.5). These trapping conditions are slightly higher than the assumed lithostatic geotherm of 30 °C/km (Clark and Jäger, 1969; Wagner et al., 1977; Mullis et al., 1994). The parallel healed fractures in which the $V_{1.2}$ fluids are hosted, indicate that the large V_1 quartz veins deformed in a brittle manner before peak metamorphic conditions. Subsequent decrepitation of fluid inclusions is attributed to further heating of the rocks after fluid inclusion trapping.

V_2 fissures opened during early stages of the retrograde metamorphic path. K/Na thermometry according to Poty et al. (1974) on early fluid inclusions from Mullis et al. (1994) indicates temperatures of formation of 415 ± 10 °C and consequently pressures of around 3 kbars. However, temperature estimates are around 350 °C using the geothermal water thermometers. A temperature of 350 °C of the fluids implies that the fluid pressure in

Figure 3.14: *PT*-diagrams of vein forma-
tion. a) Isochores of the different fluid in-
clusion populations and thermometric es-
timates and constraints. b) Equilibrium
phase diagram showing the changes in sta-
ble phase assemblages in the same P-T
range. In a) isopleths derived by Schmidt
and Bodnar (2000) of a H_2O - 10 mol%
CO_2 - 1.7 mol% NaCl equivalent fluid and
a H_2O - 4 mol% CO_2-1.7 mol% NaCl equiv-
alent fluid and the lithostatic and hydro-
static pressure conditions for a geotherm
of 30 °C/km are indicated by black dot-
ted lines. Dark to light grey lines are iso-
chores for the different fluid inclusion pop-
ulations of the veins. White points refer to
possible entrapment conditions for individ-
ual fluid inclusion populations. The thick
black and the white dotted line represent
the most probable average fluid pressure-
temperature path for the fluids from the
five vein types. Mineral abbreviations af-
ter Kretz (1983).
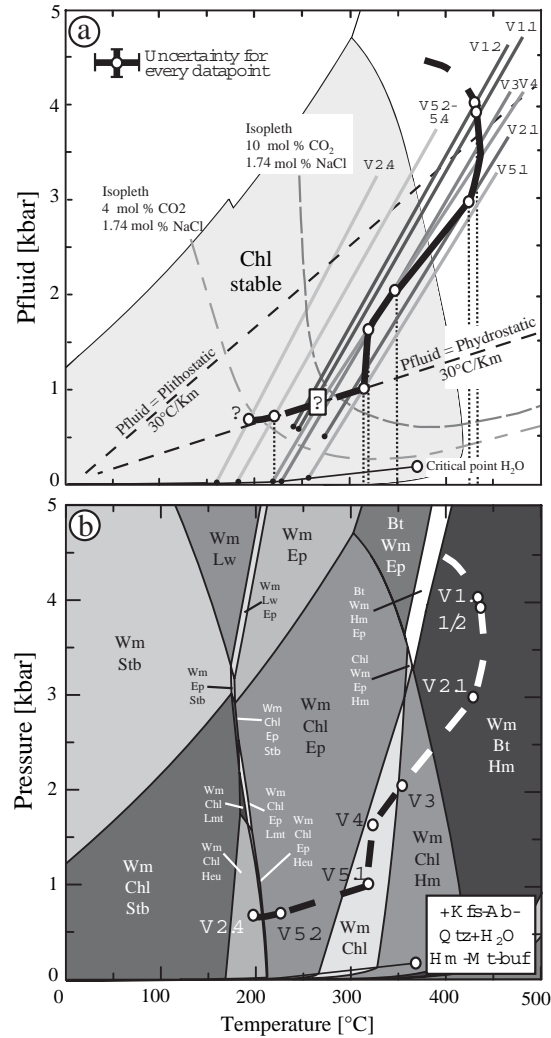
these veins was between hydrostatic and lithostatic. Ages of 18.1 Ma for biotite with a
closure temperatures of 350 °C was found by Peretti et al. (1981). These ages can be
correlated to the V_2 to V_4 vein formation events as is indicated in Figure 3.14.

During opening of V_3 and V_4 veins, *PT*-conditions of fluid trapping were at 350 to 300
°C and 2 to 1.6 kbar, while the rock pressure was still at 2.5 to 3.0 kbar. Muscovite was
dated using K/Ar at 14.1 Ma by Pürdy and Stalder (1973). This would imply an under-
pressure in the veins of approximately 1 kbar. Zeolites form after all fissure minerals in
the V_2 veins, indicating that fluids remained present at least in some of the V_2 veins to
temperatures of $\leq$ 200 °C.

The fluid chemistry and stable isotope thermometry indicate that the fluids from V_5 were
trapped between 300 and 200 °C. This implies that the fluid pressures in the veins were
near or at hydrostatic pressures of 0.5 to 1 kbar, at least during inclusion trapping. As

the measured fluid inclusion populations are all from the quartz veins that overprint the fault rocks, the deformation must have taken place at about 250 to 300 °C, probably just after V_4 formation. These temperatures are similar to the temperatures estimated from the recrystallisation characteristics of quartz in gouge$_1$ (Stipp et al., 2002). During late stages in V_2 veins, small scale badly healed secondary fluid inclusions ($V_{2.4}$) indicate that fracturing continued during late stages of the uplift of the granite body, which is also apparent by late un-mineralised fractures with similar orientation to V_5. Apatite fission track dating yields the youngest age of 7.7 Ma from Wagner et al. (1977) with a closure temperature of ~ 120 °C. This indicates that the V_5 veining event must have preceded, this stage in the exhumation path.

Fluid-mineral equilibria and mineralisation

V_{1a} consists mainly of quartz, locally in association with some large K-feldspars and biotite. The smaller inter-boudin veins (V_{1b}), overprinted by V_2 veins, consist also of quartz. The first event of V_2 vein formation is characterised by leaching of biotite and quartz from the host rock, forming a porous K, Fe, Mg and Si depleted alteration zone. The biotite removal reaction can be described as congruent dissolution of biotite:

$$1Bt + 10H^+ = K^+ + Al^{3+} + 3Qtz + 3(Fe, Mg)^{2+} + 6H_2O \qquad (3.1)$$
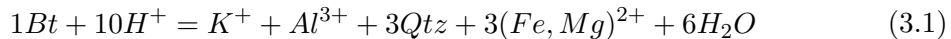
which alters the host rock and increases the porosity in the alteration zones of the V_2 veins. This requires the influx of a more acidic fluid in the early V_2 vein that was under-saturated with respect to Si, K, Fe and Mg compared to the fluid in equilibrium with the host granite. Such a fluid could originate from a different lithology or a fluid from the same lithology from a higher temperature and greater depth. In the latter case the pH of the fluid is lower and if such fluids are transported upward instantaneously are more acidic.

The depletion is followed by re-precipitation of minor biotite followed by quartz and nearly pure albite (Fig. 3.15, stage I) in the veins and pores. First albite and subsequently adularia precipitated. This implies that the vein fluid must first have been over-saturated with respect to albite and under-saturated with respect to adularia. A fluid derived from lower temperatures may become over-saturated with respect to albite, while dissolving K-feldspar (similar to Ague, 1997). During cooling of the fluid, the opposite occurs, as the Na-concentration of the fluid will increase to maintain equilibrium concentrations with the host rock and the K-concentration decreases (Ague, 2004, Fig. 3.16a). Further dissolution

Figure 3.15: One stage of alteration and three stages of mineral precipitation are identified in the alteration zones of the V_2 fissures. The newly grown minerals are indicated for the alteration zones and the fissure. Precipitation during later stages is progressively nearer to the fissures as previous pores become sealed.
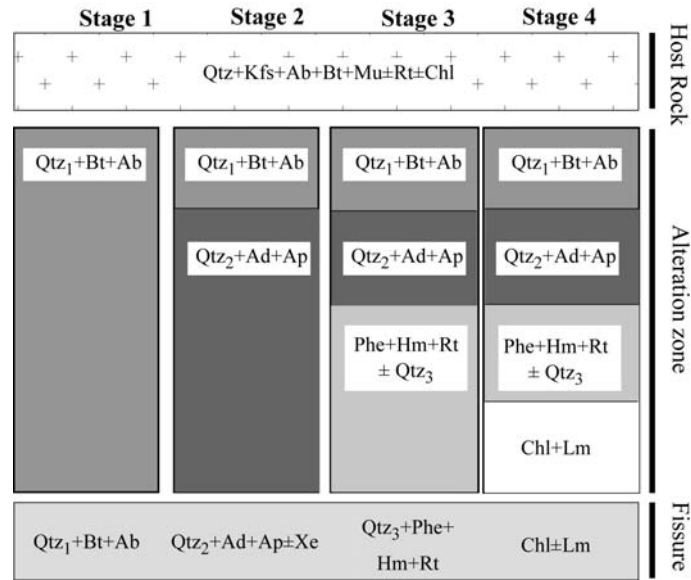
Figure 3.16: Change of Na and K concentrations with temperature in a typical 1 molal Cl-bearing aqueous solution. The stable mineral assemblage is qtz-ab-Kfs-phe-chl below 400 °C and qtz-ab-Kfs-phe-bt above 400 °C.
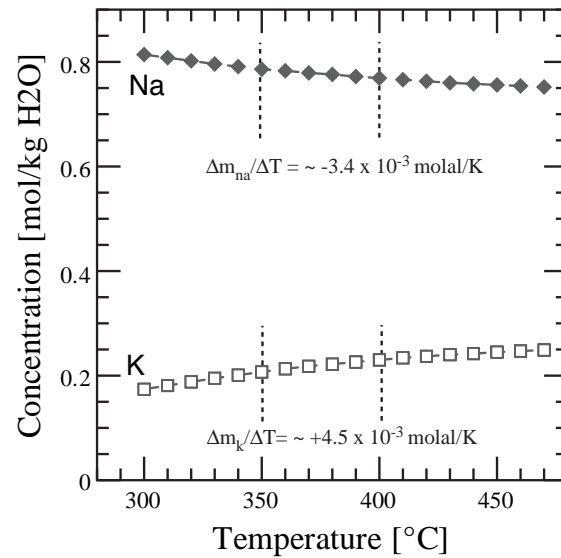
of albite from the host rock could lead to re-equilibration of the Na concentration. The addition of Al and Si to the fluid will then cause further precipitation of adularia or muscovite together with quartz as K, Si and Al will be continuously over-saturated:

$$1Ab(hostrock) + 4H^+ = 1Na^+ + Al^{3+} + 3SiO_2(aq) + 2H_2O \qquad (3.2)$$

$$K^+ + Al^{3+} + 3SiO_2aq + 2H_2O = 1Ad(vein, pore) + 4H^+ \qquad (3.3)$$
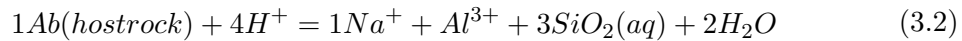
Apatite and xenotime crystallisation is related to their initial dissolution from the host rock after the initial dis-equilibrium conditions between the fluid-filled fissure and the host rock. These two events are followed by the opening of new V_3 and V_4 veins (stages III and

IV). The precipitation of phengite and subsequently hematite in V_3 veins can be described by the following end-member reactions:

$$K(Mg, Fe)_3(Al, Fe)Si_3O_{10}(OH)_2 + SiO_2 + 4H^+ =$$
$$K(Mg, Fe)AlSi_4O_{10}(OH)_2 + 2(MgFe^{2+}) + 2H_2O$$

(3.4)

$$1K(Mg, Fe)_3(Al, Fe^{3+})Si_3O_{10}(OH)_2 + 10H^+ =$$
$$K^+ + (Fe, Al)^{3+} + 3Qtz + 3(Fe, Mg)^{2+} + 6H_2O$$

(3.5)
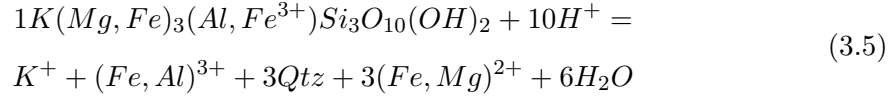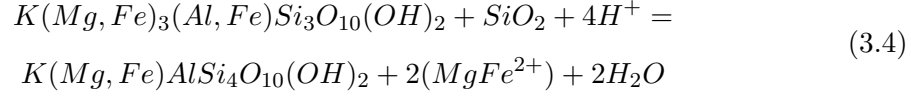
Reactions 3.4 and 3.5 show that in the cases where biotite contains Fe^{3+}, hematite is likely to precipitate, whereas in other cases phengite or chlorite will precipitate. Eventually chlorite will form as the Mg^{2+} and Fe^{2+} concentrations of the fluid will increase with increased dissolution of biotite. Calculated fluids in equilibrium with ab-kfs-qtz-bt-phg with a salinity of up to 1 molal Cl and a pH of 5 to 6 contain approximately 10^{-4} to 10^{-6} molal Mg, 10^{-6} to 10^{-8} molal Fe^{2+} and 10^{-16} to 10^{-20} molal Fe^{3+} species depending on the salinity of the fluid and the amount of secondary anions (e.g. F^-, SO_4^{2-}, CO_3^{2-}). Several parameters can explain the sequence of mineralisation and the precipitation of oxidised minerals such as hematite observed in V_3 veins: 1) the fluids were relatively oxidising and contained a higher iron concentration than the local pore fluids. 2) The fluids were derived from rocks situated at greater depths, having a higher temperature and were therefore over-saturated in Fe^{3+} with respect to the local equilibrium conditions and could therefore precipitate hematite. 3) The infiltrating fluids had different salinity with a different iron concentration than the pore fluids. 4) The pH of the infiltrating fluids was lower then Ph of the local pore fluids. 5) Breakdown of Fe^{3+}-bearing minerals along the V_3 fracture walls (e.g. biotite) can liberate significant amounts of Fe^{3+} to create hematite veins (see also reactions 3.4 and 3.5).

Possibility 1) can be disregarded because differing oxygen fugacities in fluids that infiltrate along the fracture planes will most likely be quickly buffered by the surrounding host rock. Possibility 2) requires that iron solubility increases significantly with increases in temperature or pressure. Solubility calculations show that an external fluid with a temperature of 350 °C contains up to 1.5 times (1.31×10^{-6} to 1.94×10^{-6} molal) more iron than at 300 °C in a 1 molal Cl-beariung fluid. A pressure decrease of 1 kbar (from 2.5 kbar to 1.5 kbar) upon fracturing at the same temperature increases the solubility by a factor of 2 from (1×10^{-6} to 1.94×10^{-6}) in a 1 molal Cl concentration. This will lead to an initial solubility increase of Fe-bearing minerals, which upon equilibration decreases again, thereby allow-

ing precipitation of hematite However the concentrations are so low that large amounts of fluid would be necessary to explain even the small volumes of hematite precipitated in the V_3 veins. Repeated pressure drops after fracturing is unlikely as only two stages of fracturing were observed in these veins. The size of the fractures do not warrant large scale fluid advection from a source far away. Lamprophyric dykes which cross-cut the Fibbia granite could act as a source of potentially Fe-rich fluids. 3) an external fluid with a much higher salinity might contain much higher Fe-concentrations and again upon equilibration with the host rock might decrease causing hematite precipitation. Large amounts of fluids are necessary to precipitate even the small amounts of hematite observed. Changes in pH of passing fluids (possibility 4) may also induce precipitation of hematite, but again this requires large amounts of fluids. Possibility 5) does not require (large) external fluid fluxes as biotite from the host rock is relatively Fe-rich and biotite will become unstable below $\sim$ 400 °C, and will therefore have a tendency to form more stable phases. For the creation of 1 dm^3 hematite in a fracture space of an area of 1m^2 and a width of 1 mm from a granitic rock with a modeled amount of 5 vol% biotite requires an alteration zone of 2 cm. However, a more diffuse alteration that is tapping from a larger rock-volume would diminish the observed alteration around the vein. This is the most probable explanation for the very little amounts of alteration observed around these veins.Chlorite could have formed by reactions similar to possibility 5). Biotite and white mica can form chlorite by a reaction:

$$26.8Bt + 20.9Wm + 43Qtz + 19H_2O = 1Ab + 46.7Kfs + 16.1Chl \qquad (3.6)$$
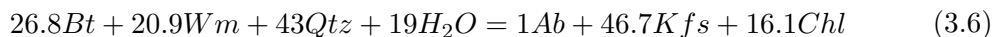
at the conditions of 380 °C and 2 kbar obtained from the calculations shown in Figure 3.14b. In the calculations of Figure 3.14b only 3 vol% of biotite is present at 400°C and 3kb and 2.6 vol% chlorite forms from this reaction. For the formation of 1 dm^3 (= 1m x 1m x 0.001m) of chlorite 38.46 dm^3 of the whole rock is involved. This corresponds to a volume of 3.8 cm wide around the vein over an area of 1 m^2. Again, when the material transfer is more diffuse from within a larger rock volume alteration would be even less pronounced. The reaction is water consuming and will therefore increase the salinity of the pore and vein fluids if the system remains closed. However as a salinity decrease was observed from $V_{3.1}$ to $V_{4.1}$ small amounts of external fluids may have precluded increasing the salinity of the fluids. However the bulk of the material was supplied from within the host-rock. It is likely that because the solubility of Fe^{3+} in a fluid is much lower compared to Fe^{2+}, Mg^{2+}, Al and Si, the fluid became saturated first with respect to hematite upon re-equilibration, causing the early precipitation of hematite and subsequent precipitation

of chlorite.

Gouge$_I$ to gouge$_{III}$ in V$_5$ contain small amounts of chlorite and white mica. These minerals formed during the cementation of small pores. Chlorite must have formed as a result of biotite breakdown similarly to reaction 3.6 from the unaltered granite and the new crystallisation of white mica can be attributed to alteration of K-feldspar. Crystallisation of needle and split-growth quartz in V$_5$ veins starts during the intermediate to late stages of fracturing. No host rock alteration is observed during this time other than small vein-lets cutting into the host granite, suggesting together with the observed increase in SiO$_2$ in the gouge zones that silica was added to the system from an external source.

Models of mass transfer in the vein systems

To determine, which models are best suited to explain the observed alteration and miner-alisation characteristics around the veins it is important to establish whether the fluid-rock system was open or closed. The geochemical and petrological characteristics of the five vein types indicate that (some) mass transport must have occurred for V$_1$ and V$_3$ to V$_5$.

V$_1$ veins: In the case of both the large V$_{1a}$ and the smaller V$_{1b}$ veins no alteration-halo has been observed or measured geochemically, or evidence of it was destroyed during metamorphism. Local diffusional transport of silica can therefore be ruled out (Yardley and Bottrell, 1992). In such an instance formation of the veins can be explained by local fluid advection within the granite body. In the case of V$_{1a}$ the size of the veins as well as their orientation indicate that they formed as pegmatites and subsequently recrystallized. At the time of V$_{1b}$ formation the Fibbia granite itself was probably quite dry (Marquer, 1990), because any fluid that could have been present in the rocks was probably expelled during the late Variscan stages of intrusion. For this reason any fluid precipitating quartz in these veins originated from dehydration of lower lying units. A model similar to Yardley and Bottrell (1992) can be proposed in which the formation of the V$_{1b}$ veins is related to embrittlement of the granite due to high fluid pressures at near peak metamorphic conditions and subsequent fluids migrating to these vein sites. Veins of over 4 m in length and sometimes 0.5 m thickness, filled with quartz, must then have tapped fluids from several hydrofracturing events (Fig. 3.17a,b).

V$_2$ veins: Around V$_2$ veins significant alteration did occur. However, this does not pre-clude the possibility of input of material from elsewhere. Rough estimates of how much
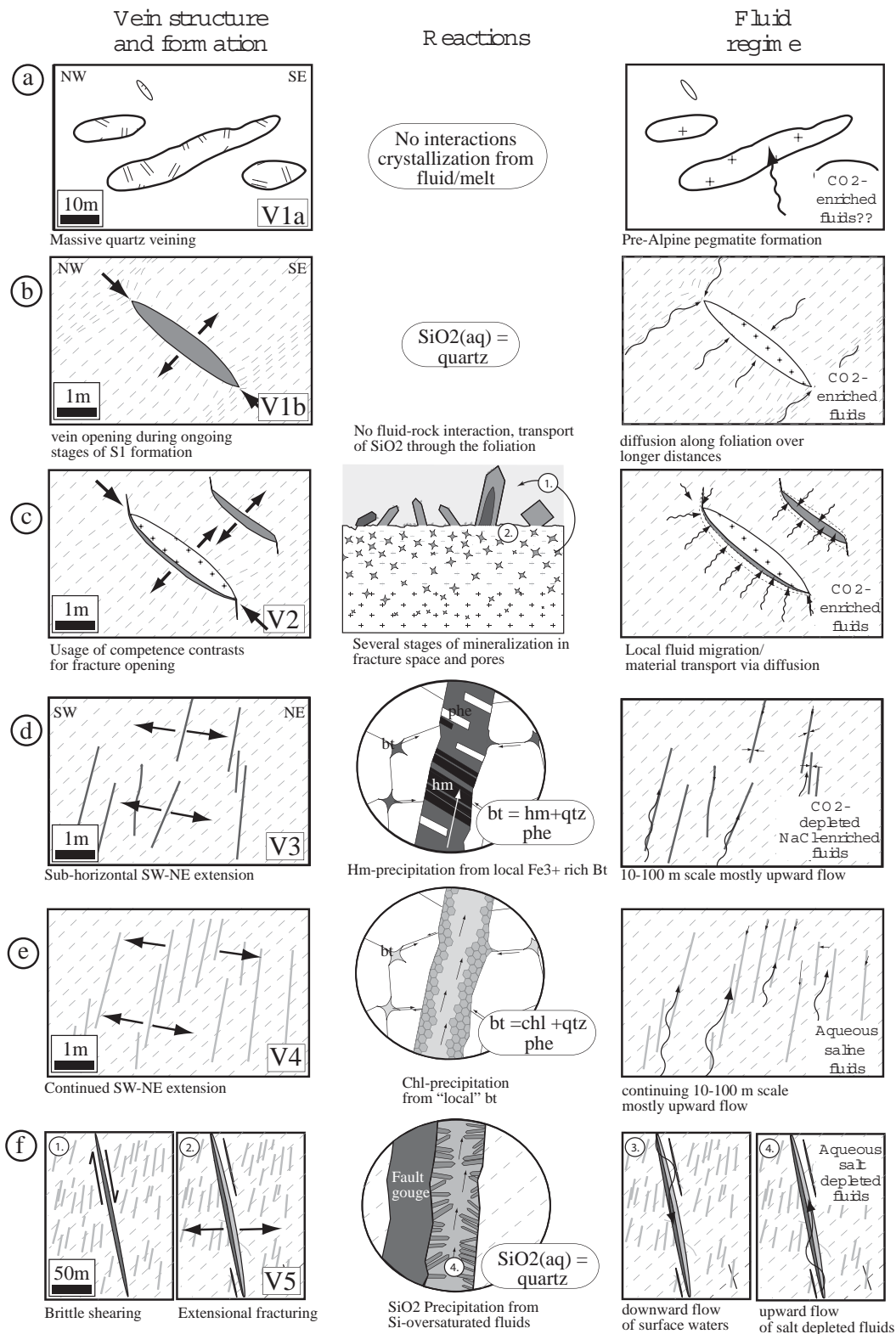
Fig. 3.17: a-f) Combined structural opening, mineralisation and fluid flow patterns around the different veins

material is needed for the observed amounts of vein mineralisation can be found by comparing the mass lost from the alteration zones with the mass gained in the vein. Using the degree of V_2 vein filling from field observation is prone to large errors. Therefore, only a semi-quantitative indication of the volume of mineralisation can be obtained. The degree of filling varies from approximately 50 to 80 vol%. The amount of vein filling observed at locality Th.1 is about 40-80 vol% and contains relatively large amounts of feldspars ($\sim$ 50 vol % adularia, 20 vol % quartz and 20 vol% albite). The volume of minimum vein fill is 0.05 m^3 x 0.4 $= \sim 0.02$ m^3 and the maximum volume of the alteration zone is 2 x 0.15 $= 0.3 \pm 0.1$ m^3 having a present pore space of 4 to 8 vol%. The volume of material extracted from the alteration zone is, therefore, approximately 0.04 x 0.3 $= 0.012$ m^3. The porosity created during the initial dissolution of minerals was slightly higher, as parts of the pores have been refilled with later mineralisation. However, as the mass that was lost initially by dissolution of quartz and biotite has now been re-precipitated from the fluids, the amount of mass lost and gained from the pores probably cancel each other out. This implies that the measured porosity difference in the alteration zones can be used for the calculation. The maximum increase of pore space volume in the alteration zone and the minimum volume of vein filling indicate that the volume lost and gained are approximately the same. The calculation above indicates that if the vein filling is nearly complete (as was the case at locality Th.1) material from elsewhere is needed to create such a vein. A possibility is that fluid flow parallel to the gneissic foliation during and after the initial vein formation may have added material to the veins (Ague, 1997), as this would not significantly alter the chemistry of the vein fluids and would be able to add material without the need of re-opening the veins (Fig. 3.17c). As there are numerous V_2 veins open at approximately the same time within the granite it is possible that in some of the veins material is added and in others material is lost without a net mass change to the whole granite. The methodology applied in this work is not able to trace these minor differences. The fact that most of the fissures were not completely mineralised indicates that not much material was added after the initial opening and dissolution stage of vein formation.

V_3 and V_4 vein types originate from mass transport from the host granite, without producing strong alteration. The size of these veins does not indicate large external fluid fluxes, although more fluid may have passed then is recorded by the fractures (Fig. 3.17d,e).

In the case of V_5 veins large amounts of fluids are necessary to explain the size and scale of the quartz mineralisation in these veins. The relatively high homogenisation temperatures

of particularly the early V_5 fluid inclusions observed in these veins imply that the fluids must have been heated, while the low salinities of the fluid gives evidence of surface derived fluids. Chapter 4 provides further evidence that these fluids were of meteoric origin and later became heated. Helgeson and Lichtner (1987) found that fluid-pressure gradients may cause both precipitation and dissolution of minerals along a fracture zone. Fluid pressure gradients may be induced by repeated fracturing, which also greatly enhances re-distribution of fluids between different previously sealed compartments along a fracture zone. Changes in the permeability, flow rate, cross-sectional areas, or direction of flow along fracture planes may also produce internal fluid pressure gradients. Particularly in downward flow quartz may precipitate when the mineralising fluid is Cl-rich or acidic and fluid pressure is temporary reduced (Helgeson and Lichtner, 1987, Fig. 3.17f). However upward flow of hotter fluids has a larger potential for precipitating large amounts of quartz as well as other minerals. In V_5 nearly only quartz precipitated, which would suggest that either quartz precipitated faster or that dissolution of quartz at the source was faster than for other minerals.

3.6 Conclusions

The physico-chemical formation conditions of Alpine veins and associated fluids were analysed using a multi-analytical approach. Five vein types formed in the Fibbia granite of which the last four formed successively from 20 Ma to 10 Ma, during retrograde metamorphic conditions.

Earliest V_{1a} veins are of pre-Alpine origin, which is indicated by high-temperature recrystallisation features of the quartz in these veins. As the rocks forming the Gotthard massif remained at about the same depth, temperatures between Variscan and Alpine orogeneses probably are similar. V_{1b} veins formed during prograde Alpine conditions and are related to schistosity formation.

Host rock alteration was most pronounced during the formation of early retrograde V_2 veins, which remained open long enough for material to be transferred between host rock and veins. At the time of V_2 formation fluid flow was limited and mineralisations can be solely explained by mass transport from the host rock to the open fractures. Later stages of vein formation are accompanied by the change in magnitude of the minimal stress directions from sub-vertical to sub horizontal SW-NE directed. During V_3 and V_4 veining V_2 veins were re-opened and new hematite and chlorite precipitated in these veins.

During later stages larger faults formed, which indicates that brittle deformation intensified. The veins which subsequently formed indicate episodical influx of silica over-saturated fluids as both the fault zones and the host rocks were infiltrated by quartz veins. Models explaining the V_5 formation by cyclic quartz over-saturation of the vein fluid, where the silica originates by diffusion of silica from the host rock are not applicable here as the host rock is unaltered and features related to pressure solution are not observed in these veins. Instead, it is concluded that the fluids and the precipitated quartz originated from external sources and that the fracture planes were used for fluid flow over longer time periods.

Equilibrium thermodynamic modeling of K-Na speciation in equilibrium with granitic bulk compositions can help to unravel possible reasons for observed mineralisations in the alpine formed retrograde veins. Actual comparison between measured fluid compositions and modelled fluid compositions in equilibrium with granite requires that existing thermodynamic datasets are integrated and extended in the number of minerals and species included.

Chapter 4

Origins and flow-paths of orogenic fluids during pro- and retrograde metamorphism in the Fibbia Area, Southern Gotthard Massif, Switzerland.[*]

Abstract

Origins and flow-paths of fluids from distinct Alpine vein sets in the Fibbia granite of the Southern Gotthard Massif in the Central Swiss Alps have been constrained by combining field relations, petrographical and fluid inclusion results with stable isotope and major element geochemistry of fluids and stable isotope compositions of host rock and vein minerals. Five veining events are associated with prograde (V_{1b}) and different retrograde stages of Alpine metamorphism (V_2-V_5). Associated with these vein formation events are at least five fracturing events. Large early V_1 veins are related to late Hercynian times, whereas smaller massive quartz veins are related to prograde Alpine conditions. Alpine recrystallisation and inclusion decrepitation obscured original characteristics of the veins. In the case of V_2 veins fracturing was associated with near lithostatic fluid pressures, while for V_3 and V_4 veins thermal contraction and the prevailing stress orientation played a key role in fracture-opening. V_5 veins are characterised by cataclastic deformation and dilation which are an expression of regional scale extension. Nine distinct fluid inclusion populations were characterised within these five vein types: CO_2-enriched saline fluids in early V_1 and V_2 veins, CO_2-free, NaCl-enriched fluids in V_3, slightly NaCl-depleted saline fluids for V_4 and salt-depleted CO_2-free fluids for V_5.

Mineral precipitation and fluid trapping in the five vein types evolved from prograde fluid pressure and temperature conditions of up to 440°C and 4 kbar for late V_1 fluids to retrograde conditions down to $\leq$ 180°C and $\leq$ 1.0 kbar for V_5.

Br and Cl ratios in fluid inclusions show that early V_1 to V_3 fluids have similar origins whereas V_4 and V_5 vein fluids have different origins. Cations indicate equilibration between feldspars and fluids. Early fluids are related to metamorphic dehydration or possibly relics of original magmatic fluids. V_4 probably originated from slightly lower-lying units and V_5 fluids from the surface. Hydrogen isotope compositions from fluid inclusions and oxygen and hydrogen isotope compositions of vein minerals show an abrupt change from equilibrated metamorphic fluids for V_1 to V_4 fluids to meteoric derived fluids, which were in disequilibrium with the host rock in late retrograde V_5 veins. The C-isotope compositions of CO_2 from fluid inclusions point to mixed origin from de-carbonatisation reactions of lower lying carbonate-bearing rocks and oxidation of organic matter. V_1-V_3 vein fluid characteristics require that the vein-host rock systems were isotopically closed. In contrast, the V_5 veins were episodically open fracture systems with near-hydrostatic fluid pressures in which surface-derived fluids were able to flow to depth of $\leq$ 10 km, become heated at depth and were episodically released, causing quartz precipitation. The middle Miocene SW-NE orogen-parallel extension and the uplift of the southern Central Alps provides suitable conditions for fluids to convect along such fracture planes.

4.1 Introduction

The origin of orogenic fluids (i.e. fluids occurring in the crust during orogenesis) and the mechanisms of fluid flow through the earth's crust have been studied for several decades by

applying different techniques (e.g. Poty et al., 1974; Hoefs and Stalder, 1977; Fyfe et al., 1978; Cathles, 1990; Koonz, 1991; Burkhard and Kerrich, 1988; Marquer and Burkhard, 1992; Thompson and Connolly, 1992; Mullis et al., 1994; Nesbitt and Muehlenbachs, 1995; Yardley, 1997; Sharp et al., 2005). However, fluid sources and fluid flow directions during exhumation stages in collisional belts and especially in the Central Alps have not been well characterised. As the Alpine mountain belt has a very complex architecture and geologic history, fluid sources and fluid flow can vary significantly between different parts of this orogen. This study is confined to rocks representative of middle to upper crustal conditions, where fluid flow occurs along faults, fractures, joints or lithological boundaries. In order to understand the modes and scales of mass transport in the Alpine geodynamic setting it is necessary to characterise the type of fluids present in veins and their geochemical compositions.

Rocks from the crystalline nappes in the Central Alps have generally not been isotopically equilibrated during Alpine orogenesis, mainly due to lack of pervasive fluid flow during metamorphism (Hoernes and Friedrichsen, 1980). However, previous oxygen and hydrogen stable isotope investigations on minerals and fluids showed that fluids from early formed veins in the Central Alps were generally isotopically equilibrated with the host rocks (e.g. Mullis et al., 1994; Lucchini, 2002; Sharp et al., 2005) and showed typical metamorphic values. Carbon from fluid inclusions in hydrothermal quartz and carbonates from Alpine fissures generally has isotopic compositions reflecting devolatisation of carbonates or oxidation of organic matter (Hoefs and Stalder, 1977; Mazurek, 1999). In addition, recent studies established that fluids in veins formed during Alpine orogenis may retain meteoric H- and O-isotope compositions even though these fluids must have penetrated to depths ≥ 8 km in the northern Penninic nappes and the southern Gotthard massif (Mullis et al., 2001; Sharp et al., 2005; Mullis et al., in prep.). This requires a change in fluid regime which is related to the exhumation history, changes in stress conditions, fluid pressure and the permeability of the crystalline rocks of the Central Alps.

The purpose of this paper is to point out the origin and flow paths of fluids during the pro- and retrograde metamorphic events and to use constraints on PT-conditions and timing of vein formation and mineralisation to make conceptual models on evolving Alpine fluid regimes. The following topics are addressed: 1) Tectonic setting and scale of fluid movement are determined by a detailed field study of veins and fractures in the Southern Gotthard Massif. 2) Changes in physical and chemical conditions are characterised by detailed petrographic investigations of veins and wall rocks. 3) Fluid origins, temperatures of vein formation and equilibrium conditions between veins and host rocks, are evaluated

using H, C, and O isotope compositions of included fluids in quartz and of vein- and wall rock minerals (biotite, quartz, chlorite, phengite, feldspar, fault gouge). 4) Additional information on the origin of components within the fluids were obtained from laser ablation and crush leach analyses on cation- and anion-ratios in fluids. 5) These constraints on fluid origin and flow during retrograde metamorphic evolution of the Gotthard massif are related to the regional tectono-metamorphic settings and related to the thermal evolution of the Central Alps.

4.2 Geology and metamorphic history

The Gotthard massif is the southern-most part of the External Alpine Massifs (Helvetic nappes, Aar and Gotthard massif) and has been described by Schmid et al. (2004) as sub-Penninic (see also Milnes, 1974), belonging paleo-geographically to the distal part of the European margin. It consists of a crystalline basement that was affected by poly-phase pre-Alpine metamorphic events together with a meta-sedimentary cover. It is bordered to the South by the Penninic nappes and is separated from the Aar-massif by the Tavetch intermediate Massif and the Urseren-Garvera zone (Fig. 4.1a,b). For more detailed lithological descriptions see chapter 3.

Grujic and Mancktelow (1996) and Maxelon and Mancktelow (2005) showed that the Lepontine area experienced five phases of ductile deformation (D_1 to D_5) between 40 Ma and $\leq$ 20 Ma. The Gotthard massif was involved in the D_1 deformation event at around 35 Ma, during which the Gotthard was tectonically partly separated from the European plate. This was at approximately the same time as the temperature peak was reached. During Alpine orogenesis the southern Gotthard area was metamorphosed at upper greenschist, lower amphibolite facies conditions (T = 500°C and P $\sim$ 4 kbar, (Frey et al., 1980)). The peak Alpine metamorphic event in the area is dated at around 37 Ma (Deutsch and Steiger, 1985) using K/Ar on amphiboles from meta-sediments. Schmid et al. (1996) place the timing of the formation of "Chièra" synform and the "Northern Steep Belt" at around 23 Ma, affecting the southern parts of the Gotthard massif and the northern parts of the Penninic (Lebendun, Lucomagno/Leventina, Simano, Maggia and Antigorio) nappes. The timing of exhumation of the southern Gotthard massif was constrained by K/Ar and Rb/Sr analyses on mica and amphibole, and fission-track data on zircons and apatite from Pürdy and Stalder (1973); Wagner et al. (1977); Peretti et al. (1981); Michalski and Soom (1990). An exhumation rate of $\sim$ 0.1-1 mm/yr for the Fibbia area is proposed by Michalski and Soom (1990) for the past 35 Ma. In contrast Hurford (1986); Mullis (1996); Sharp et al. (2005) show that there is a clear shift in cooling rates between 23 to 16 Ma and 16 to 8
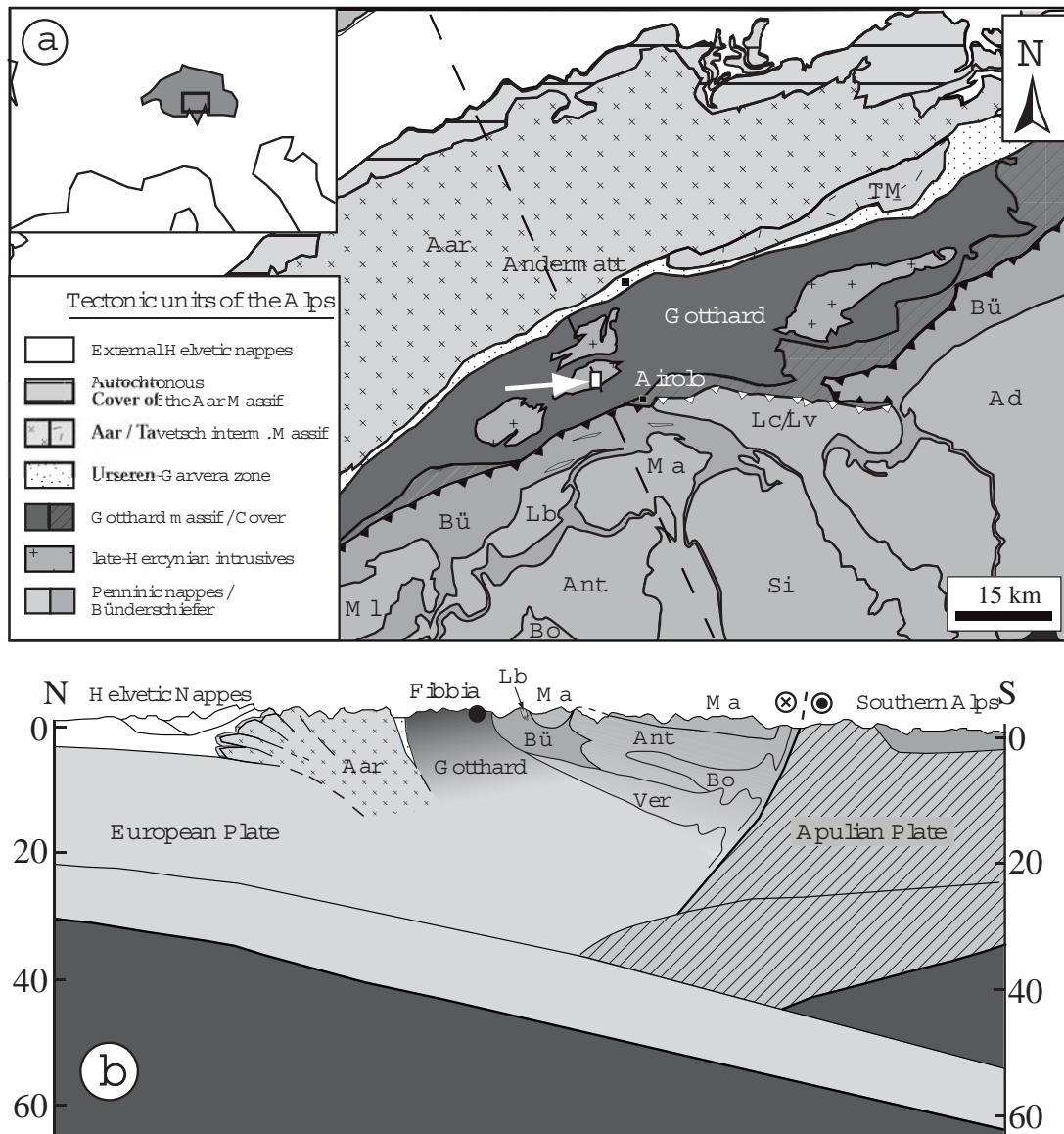
Fig. 4.1: a) Tectonic map of a part of the External and Central Alps after Spicher (1980): the white box and arrow indicate the area of study ("Fibbia" Granite). b) Interpreted NW-SE cross-section through Fibbia area in the Central Alps (modified after Schmid et al. (1996) and Pfiffner et al. (1997)). Bü = Bündnerschiefer, Ver = Verampio nappe, Ant = Antigorio nappe, Bo = Bosco unit, Ma = Maggia nappe, Si = Simano nappe, Ad = Adula nappe, Lb = Lebendun nappe, Lc/Lv = Lucomagno/Leventina nappe and Ml = Monte Leone Nappe

Ma in the southern Gotthard massif and the northern Penninic units, implying changes in exhumation rates. Analyses of molar K/Na ratios of the earliest fluid population from Alpine fissures yielded a ratio of 0.156 (Mullis et al., 1994). This ratio was used for fluid thermometry by applying the relations of Poty et al. (1974), yielding a minimum fissure formation temperature of approximately 420 °C. This temperature estimate was linked to the approximate timing of fissure opening at approximately 20 Ma (Mullis, 1996; Sharp et al., 2005) and the main quartz growth stages in the Alpine fissures took place between 19 to 14 Ma.

According to the fluid zonation map of Mullis (1995) (see also Fig. A.1) the Central Alps are divided into four zones (from North to South): the higher hydrocarbon zone, the methane zone, the water zone and the CO_2 zone. The early fissure fluids in the Aar- and Northern Gotthard massif are generally characterised by ≥ 90 mol% H_2O (H_2O zone). Early retrograde fissure fluids from the southern part of the Gotthard massif and Penninic nappes contain ≥ 10 mol% CO_2 and belong to the CO_2 zone. The Fibbia area is located slightly North of the boundary between the water and the CO_2 zone. Three different saline aqueous fluid populations were distinguished in Alpine fissures from the Fibbia granite by Mullis (1995).

4.3 Location, distribution and orientation of mineralised fractures and veins

Fractures and veins are considered to be macroscopic pathways of fluid flow. Scale, orientation, geometry and interconnectivity are important parameters to determine the macroscopic porosity and permeability of the rock during the vein forming event. Figure 4.2 shows the locations and orientations of the five vein types. The plotted orientations represent the average of several measured veins from one locality. The distribution of the mapped veins demonstrates that V_1 to V_4 veins often occur at the same place. V_{1a} veins represent a small number of veins larger than 2 meters (Samples: Th.2, Th.4, Th.53, Th.63) which are commonly sub-parallel to the S_1 foliation (Fig. 4.2a) and many smaller veins (V_{1b}), which are perpendicular to the S_1 foliation (Fig. 4.2b). These are often associated with V_2 veins (Fig. 4.2c). The separation between V_3 and V_4 veins is based on field observation of fracture fillings of either black hematite (V_3) or green chlorite (V_4). Chlorite-filled fractures were observed more often as is displayed in Figure 4.2e, but could not all be resolved spatially on the map. V_5 veins are constrained to the NW-SE striking lineament in Figure 4.2f.
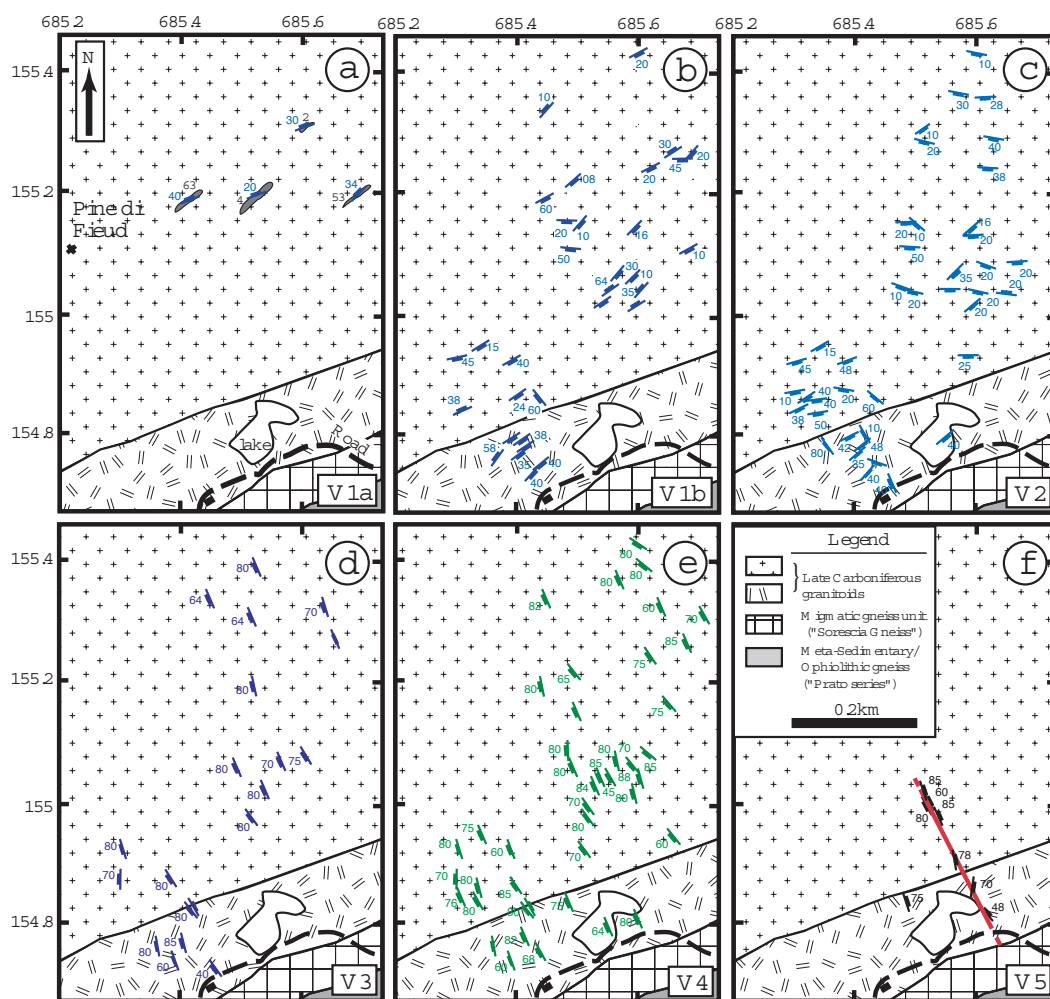
Fig. 4.2: a to f) localities and orientation of the five vein types (V_1 is subdivided into V_{1a} for early pre-Alpine veins and V_{1b} for prograde Alpine veins.

4.4 Analytical techniques

Geochemistry of fluid inclusions

Microthermometry, laser-ablation ICPMS and crush leach methods, by which the fluid inclusion populations were analysed are the same as in chapter 3. In this study only the average physical and chemical properties of the fluid inclusions and calculated concentrations of Na, K, Ca, Li, Br and Cl from the analysed fluid inclusion populations are reported. The ratios of molal concentrations for the different fluid inclusion populations are the same as the molar concentrations that can be calculated directly from the analyses. For more detailed information on the setup and methods of analyses see chapter 3 and

reference therein.

Stable isotope analyses of fluid inclusions and minerals

To acquire $\delta^{18}O$ (‰ vs VSMOW) values from quartz and δD (‰ vs VSMOW) values of H_2O for fluid inclusions, different quartz generations and fluid inclusion populations were carefully separated from each other. Mineral pairs of quartz-chlorite, quartz-hematite, quartz-phengite were separated for stable isotope thermometry.

Quartz (1 to 2 mg) was finely crushed and washed with dilute (10%) HCl to remove included calcite. Oxygen form quartz and other silicates and oxides was extracted using a CO_2 laser-line and fluorine reagent (method as described in Kasemann et al., 2001). Isotopic composition of extracted oxygen was measured using a ThermoFinnigan MAT 251 and later a MAT 253 mass spectrometer. Results are normalised against an in-house quartz standard (Ls-1; 30-50 mesh, $\delta^{18}O = 18.1$‰, calibrated against NBS-28 of $\delta^{18}O = 9.64$‰). The standard reproduced to within $\pm$ 0.1‰.

For the δD measurements of silicates the samples were weighed into silver cups, tightly folded and closed, and analysed using a ThermoFinnigan high Temperature Conversion Elemental Analyser (TC-EA). This method involves reduction in a He carrier gas stream with graphite at 1450°C, separation of the gases produced on a gas chromatographic column held at 85°C prior to transfer into the mass spectrometer (ThermoFinnigan Delta plus XL) for isotopic analyses of H_2 (method adapted after Sharp et al., 2001). Measurements were normalised using in-house biotite and kaolinite standards (δD of -63 and -125‰, respectively), both calibrated against NBS-30 biotite (δD of -65‰), and which reproduced to within $\pm$ 2‰.

Separations of different fluid species, mainly CO_2 and H_2O in fluid inclusions, were done using a simplified extraction line of Vennemann and O'Neil (1993) without conversion of H_2O to H_2 using the Zn reagent. Fluids contained in fluid inclusions of quartz were extracted through heating and decrepitation in a vacuum extraction line. Maximum temperatures of decrepitation were in the range of 550°C. This was judged on the basis of changes in pressure detected by the vacuum gauge located between the sample and a U-trap held at liquid nitrogen temperatures. In contrast to the experiences obtained in a number of other laboratories (e.g. Gleeson et al., 2000; Simon, 2001; Faure, 2003), our experience has been that for the present suite of samples, the bulk of the fluid is present as fluid inclusions within the quartz and that these fluids are best extracted using the method of thermal decrepitation rather than crushing of the sample at lower temperatures (Kesler

et al., 1997; Vazquez et al., 1998). Results from Mazurek (1999), both for vacuum decrepitation and crushing of splits of the same samples have also confirmed that the two methods of extraction provide very similar results for the given types of samples analysed here. In addition, his measurements of the chemical and isotopic composition of the fluid inclusions in quartz were very similar to those of the pore fluids within the rocks hosting the veins, suggesting that the fluids in inclusions of quartz veins are representative of the fluids in the rocks. This may well be different for quartz samples formed at both higher temperatures in igneous-hydrothermal systems (Simon, 2001) and/or for quartz precipitated from active geothermal systems (Faure, 2003), where a more substantial proportion of water may be structurally bound within the quartz and hence have a different isotopic composition compared to that in the fluid inclusions. In addition, the presence of other contaminants in quartz (e.g., minerals, organic matter, etc.) will also complicate extraction procedures, in particular the thermal decrepitation method and hence pure quartz samples are needed.

Released H_2O and CO_2 were trapped under vacuum in a liquid nitrogen-cooled U-tube and then separated cryogenically using an ethanol-liquid nitrogen slush trap at about $-90°C$, where CO_2 is released as a vapour once more. CO_2 and H_2O were then cryogenically transferred into small Pyrex® glass tubes for the transfer to the mass spectrometers. As part of this transfer, the amount of CO_2 was measured using a calibrated capacitance manometer (calibrated with CO_2 derived from precisely weighed pure graphite samples). Amounts varied between <0.5 μmol up to several μmol for CO_2. The isotopic composition of CO_2 was analysed by dual inlet mass spectrometry on a Finnigan MAT 253 (251), or for samples less than 3 micro-moles in size using a GasBench II and carrier gas system linked to a ThermoFinnigan Delta plus XL mass spectrometer with all gas being passed through a gas chromatograph to isolate the CO_2 for analyses (see above). Standards reproduced to within 0.3 ‰

The H_2O was transferred cryogenically into a small 1/4 inch (outer diameter) stainless steel U-tube of a specially constructed vacuum line linked to the TC-EA via a 1/16th inch outer diameter stainless steel line. After thawing of the water at $100°C$, it was flushed with He into the He-stream of the TC-EA, allowing it to react with graphite at $1350°C$ and passing the product H_2 (and CO) over a gas chromatograph into the mass spectrometer as for the measurements of D/H from the solid samples. The δD values for H_2O from the fluid inclusions, were calibrated against those of three laboratory standards with δD values of +3, −58, and −160‰. The standards, introduced into the same vacuum line via injection with a vacuum-tight micro-syringe, reproduced to within ± 5‰.

4.5   Results

Structural and petrographical characteristics of veins and vein mineralisation
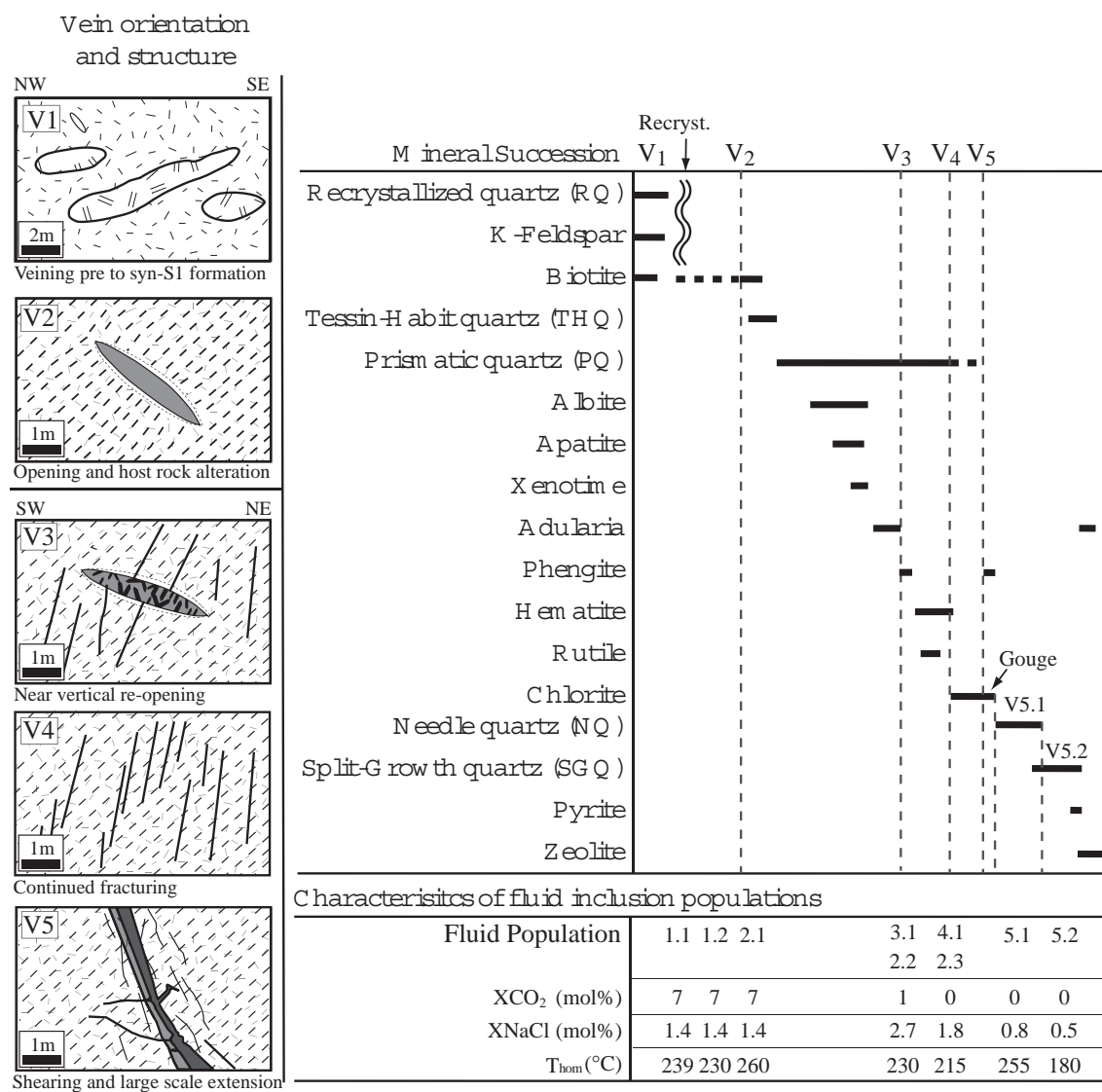
Fig. 4.3: Combined data obtained from chapter 3 showing the structures and orientations of the five different veining events, the succession of mineralisation in the veins and the physical and chemical characteristics of the different fluid inclusion populations

Vein mineralisation and fluid inclusions were studied in chapter 3. Figure 4.3 summarises the most important results on the mineralisation and the characteristics of fluid inclusion populations. Veins are classified based on the relative age as V_x; a terminology irrespective of the geometrical characteristic and mode of formation of the vein. In the case of V_5 veins a numbered classification was used to describe the different stages of cataclastic

deformation, vein-formation and fluid inclusion trapping. V_5 gouge$_I$ to gouge$_{III}$ denote the different stages of fault gouge formation, 5.1 points to the first fluid population in needle-quartz veins and 5.2 denotes the first fluid inclusion population in split-growth quartz veins.

Early V_1 veins are large quartz veins without any host-rock alteration and contain minor "pegmatitic" K-feldspar, biotite and some muscovite. Fluid inclusions in these veins contain CO_2 and were trapped during prograde conditions as can be inferred by typical stretching and decrepitation patterns within previously recrystallized fluid inclusion free quartz. Early V_2 veins are characterised by a succession of minerals starting with biotite-quartz and albite. Early low salinity fluids associated with this mineral paragenesis are also CO_2-enriched (7 mol%), containing 1.4 mol% NaCl.

During V_3 veining, phengite and especially hematite formed and fluids became depleted in CO_2 but slightly enriched in salt (2.7 mol%). V_4 veins are correlated with chlorite formation and CO_2-free fluids with lower salinity. These veins were followed by localised intense brittle failure with fault gouge formation and succeeded by V_5 veins. These veins are characterised by large-scale quartz precipitation and a lack of host rock alteration. Fluids related to the V_5 veining event are CO_2-free and depleted in salt (0.7 mol%).

The bulk fluid inclusion homogenisation temperature evolves from 240 to 260°C for V_1 to V_2 veins and decrease for earliest fluid inclusion populations in V_3 (about 230°C) and V_4 veins (about 215°C). Early $V_{5.1}$ fluids have again higher homogenisation temperatures, up to 260°C, while later $V_{5.2}$ fluids have lower homogenisation temperatures down to 180°C for the youngest $V_{5.2.2}$ fluid inclusion populations from split-growth quartz.

Geochemical characteristics of vein fluids

Knowledge of the electrolyte chemistry of the fluids places further constraints on the origin and evolution of the vein fluids. Electrolyte concentrations of the different fluid inclusion populations from the Fibbia area are shown in Table 4.1 and in Figure 4.4 and Figure 4.5.

The relations between the Cl and Br concentrations in fluids are indicative of their origin. V_1 to V_4 fluids have Cl concentrations between 4.3 and 4.6 log units. These are near to the Cl concentration of sea-water and the Cl concentrations measured for the vein fluids from Brusson, Pointe Hellbronner and Mont Chemin (Fig. 4.4a). The Br concentrations (2.1 to 2.5 log units) for V_1 to V_3 vein fluids are slightly higher than the halite precipitation line and the fluid inclusion populations from Brusson. The Br concentration of V_4 vein fluids

a)		Th.4.15.3	Mu.209.4.2.5	Th.3.19.1	Mu.209.4.1.2	Mu. 209.4.1.3	Th.78.3	Th.8.23.3
	Element	V1.1	V2.1	V2.1	V2.2	V2.3	V4.1	V5.2
	Li	0.0087	0.0326	0.0169	0.0280	0.0324	0.0439	b.d.
	Na	0.70	0.65	0.65	0.84	1.15	0.87	0.26
	K	0.13	0.128	0.143	0.134	0.187	0.145	b.d.
	Ca	b.d.	0.0289	0.0096	b.d.	b.d.	0.070	b.d.

b)		Th.4.19	Mu.209.4.2.5	Th.1.4.5	Th.78.3	Th. 8.34	Th. 8.35	Th.8.22.2	Th.8.23.3
	Element	V1.1*	V2.1*	V3.1*	V4.1*	V5.1	V5.1	V5.2	V5.2*
	Li	b.d.	b.d.	b.d.	0.0034	b.d.	b.d.	b.d.	b.d.
	Na	0.50	0.33	0.71	0.52	0.30	0.39	0.09	0.20
	K	0.084	0.060	0.159	0.080	0.047	0.039	0.048	0.037
	Ca	0.062	0.120	0.076	0.020	b.d.	0.025	0.013	0.021
	Cl	0.67	0.59	1.08	0.67	0.345	0.340	0.208	0.208
	Br	0.0027	0.0014	0.0035	0.00038	b.d.	b.d.	0.000078	0.00014

Table 4.1: Compilation of Li-Na-K-Ca-Cl-Br data obtained from a) laser-ablation ICPMS b) and crush leach data from chapter 3. All elements are tabulated in molal concentrations. Symbol ∗ are samples shown in Figure 4.4b. b.d. = below detection limit.

.

is 1.5 log units, which is slightly lower than those of sea-water and Brusson. $V_{5.2}$ fluids have much lower Cl (3.8 to 3.9 log units) and Br concentrations (0.75 to 1.1 log units) than the earlier V_1 to V_4 fluids.

The Cl/Br ratios (Fig. 4.4b) of the V_1 to V_3 fluids are between 250 and 550. These are lower than standard sea-water Cl/Br ratios (650). V_4 and $V_{5.2}$ fluids have higher Cl/Br ratios (1500-1800). Na/Br ratios of V_1 and V_3 fluids. The early vein fluids (V_1 to V_3) have similar Cl/Br and Na/Br ratios as crush-leach data obtained by Marshall et al. (1998) and Fabre (2000) for the Mont Chemin and Pointe Hellbronner fluids in the Mont-Blanc Massif. Fluids from Brusson measured by Yardley et al. (1993) plot near the sea-water point: Cl/Br ratios are slightly lower and Na/Br ratios are higher than Na/Br ratios for sea-water. The Cl/Br ratios for V_1 to V_3 fluids are in the range of Cl/Br ratios of vein fluids, formed during peak to retrograde metamorphic settings (Munz et al., 1995; Yardley, 1997).

Dissolved Na, K, Li and Ca readily participate in exchange reactions with mineral phases at metamorphic conditions. These cations can, therefore, be used to determine the degree of interaction and equilibration between fluid and rocks. Figures 4.5a,b display Na/K against Na/Ca and Na/K against Na/Li for the V_1 to V_5 fluids.

In Figure 4.5a the Na/Ca ratios have a large spread from 2 to 65, even among a single fluid inclusion population. This is due to a relatively high background for Ca in the laser ablation analyses. In the case of the crush leach analyses there is less spreading in Na/Ca values, which were more easily measurable. The Na/K ratio is often used as a fluid thermometer, provided that the fluid was at equilibrium with two feldspars and other Na and K-bearing host rock minerals. The V_1 and V_4 fluids have nearly the same ratios as the Pointe Hellbronner sample (Fabre, 2000) and one of the Mont Chemin samples (Marshall et al., 1998). V_2 fluids have a quite large scatter in Na/Ca values, from 2 to 20 for one particular sample, but have approximately the same Na/K values. The V_5 fluids show more scatter (from 1 to 10) in Na/K ratios and have higher values than V_1 to V_4 samples. The Na/Ca and Na/K ratios cover particularly the field of geothermal fluids,
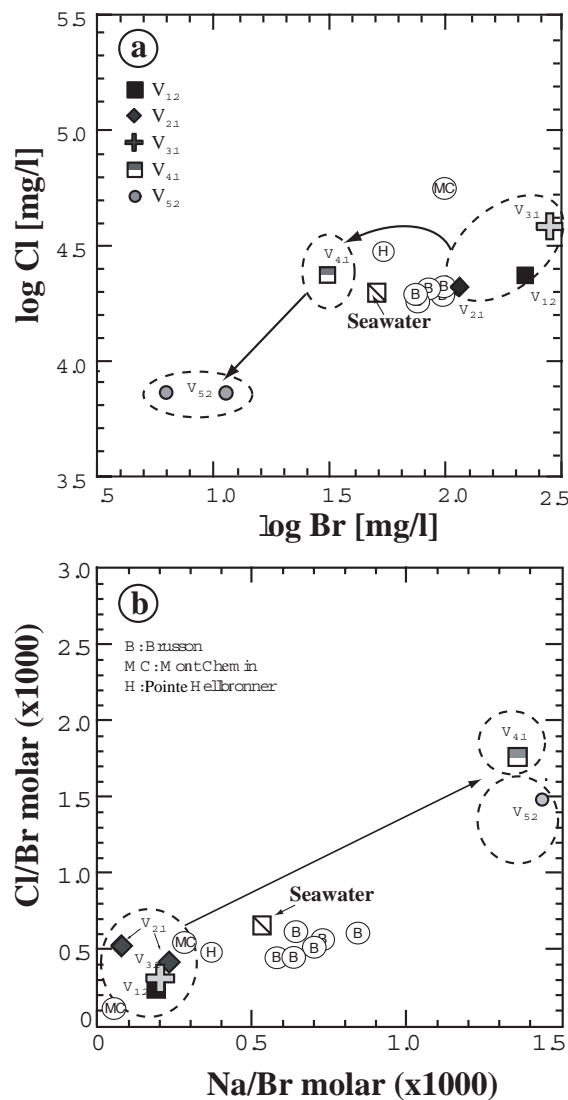
Figure 4.4: a) Cl-Br diagram after Carpenter (1978) and b) Na-Cl-Br diagram after Walter et al. (1990). Fluid data of V_1 to V_5 are shown together with data measured by Yardley et al. (1993) for quartz-gold veins from the Monte Rosa nappe (B), Marshall et al. (1998) for quartz-muscovite and quartz-chlorite veins from Mont Chemin in the Mont-Blanc area (MC) and Fabre et al. (2002) for an Alpine fissure from Pointe Hellbronner (H) of the Mont-Blanc Massif.
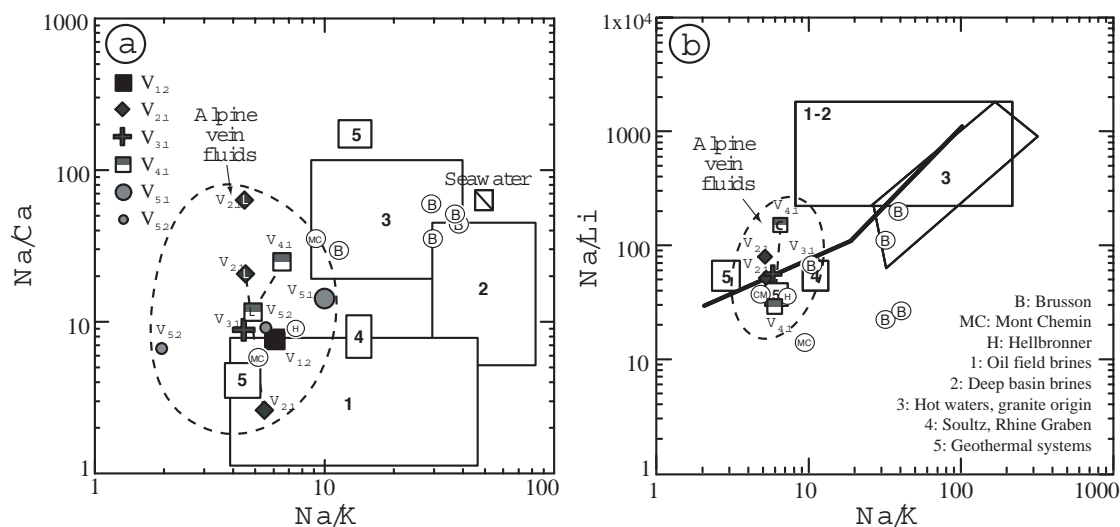
Fig. 4.5: a) Na/Ca-Na/K and b) Na/Li-Na/K diagrams with fluid data of the five vein types from laser ablation and crush-leach analyses (Table 4.1). Fluids from different geologic settings are indicated with boxes 1 to 5. (1) Oil field brines after Carpenter et al. (1974); Kharaka et al. (1987), (2) Deep basin brines after Fischer and Kreitler (1987), (3) Hot water granites after Michard (1990) (4) deep waters from Soultz, Rhine Graben after Pauwels et al. (1993) and (5) Geothermal waters after Barnes (1979) and Henley et al. (1984). B, MC and H are from the same sources as in Figure 4.4. In a) results for LA-ICPMS are indicated by "L" inside the data-point and in b) data from crush-leach analyses are indicated by "C". Data from the Alpine fluid population are connected by a striped line.

near to values of geothermal system and hot waters of granitic origin.

Na/Li ratios of V_1 to V_5 fluids range between 30 to 110 (Fig. 4.5b) with the main ratios between 50 and 60. The heavy line marks the conditions where Na/K and Na/Li thermometers give the same temperatures. V_1 to V_5 fluids plot near fluids from geothermal systems and from Soultz (France) and from Mont Chemin and Pointe Hellbronner. Fluids from Brusson have similar Na/Li ratios but higher Na/K ratios.

Stable isotope compositions of H-O for minerals and H-C-O of fluids

Stable isotopic compositions of oxygen, hydrogen and carbon for minerals and fluids are compiled in Table 4.2 and shown in Figure 4.6 to Figure 4.9. Approximate formation temperatures as determined from stable isotope thermometry, fluid chemistry and the

approximate O-H isotopic values of water are shown in Table 4.2.

Vein type	Sample nr.	Mineral V=vein H=Host rock	Fluid inclusion population	Approx. Tf (°C)	δ18O mineral (‰ vs. VSMOW)	calculated δ18O H2O (‰ vs. VSMOW)	δD fluid inclusions (‰ vs. VSMOW)	δD minerals (‰ vs. VSMOW)	δD H2O calculated (‰ vs. VSMOW)	δ13C fluid (‰ vs. PDB)
V1	Th.4	Qtz (H)	-	-	9.4	-	-	-	-	-
	Th.5	Bt(V)	-	450	5.3	7.3	-	-106	-61	-
	Th.6	RQ(V)	1.2	450	-	-	-	-	-	-10.3
	Th.23.2	RQ(V)	1.2	450	10.1	7.0	-84	-	-	-6.9
	Th.53	RQ(V)	1.2	450	10.1	7.0	-92	-	-	-9.7
	Th.63.2	RQ(V)	1.2	450	10.0	7.1	-86	-	-	-9.6
	Th.63.2	RQ(V)	1.2	450	10.2	7.0	-	-	-	-10.3
V2	Mu 209.A.4	Fsp(H)	-	-	9.1	-	-	-	-	-
	Th.1.9	Bt(Lam)	-	-	4.9	6.9	-	-77	-32	-
	Mu. 209.4 (1-6)	THQ	-	420	9.8-10.4*	6.1-6.7	-	-	-	-
	Th.1.5.1	THQ(V)	2.1	420	10.5	6.8	-66	-	-	-10.3
	Th.1.5.2	THQ(V)	2.1	420	10.6	6.9	-78	-	-	-9.9
	Mu.209.8	THQ(V)	2.1	420	10.5	6.9	-65	-	-	-6.7
	Mu.209.9	THQ(V)	2.1	420	10.5	6.8	-88	-	-	-10.3
	Th.37	Ms(V)	-	350	-	-	-	-54	-16	-
	Th.1.4.5	Hm(V)	eq V3	350	-2.2	7.7	-	-	-	-
	Th.1.10	Chl(V)	eq V4	300	4.9	5.3	-	-89	-49	-
	Th.1.11	Chl(V)	eq V4	300	4.1	4.5	-	-76	-37	-
V3	209.1.0	Qtz(H)	-	-	9.1	-	-	-	-	-
	209.1.3	Phe(V)	-	350	6.0	5.0	-	-58	-20	-
	Th.1	Phe(V)	-	350	7.1	6.0	-	-	-	-
	Th.1	Hm(V)	3.1	350	-2.8	7.1	-	-	-	-
	Rh.1	Hm(V)	3.1	350	-3.6	6.3	-	-	-	-
V4	Th.78	Qtz(H)	-	-	10.9	-	-	-	-	-
	Th.78	Chl(V)	4.1	300	3.8	4.2	-	-78	-39	-
	Th.7	Chl(V)	4.1	300	4.1	3.9	-	-96	-57	-
V5	Th.8.0	Qtz(H)	-	-	9.9	-	-	-	-	-
	Th.8.30	Chl(gouge III)	-	300	-0.8	-1.0	-	-	-	-
	Th.8.12 (1-6)	Wr(gouge I-III)	-	300	8.2 to 5.9§	-3.1 to -7.0	-	-119 to -145	-77 to -100	-
	Th.8.12 (7-9)	NQ(V)	5.1	250	6.1 to 5.8§	-2.9 to -3.2	-	-	-	-
	Th.8.1a	NQ (V)	5.1	250	5.4	-3.6	-98	-	-	-
	Th.8.1b	NQ/SGQ(V)	5.2	250	6.1	-5.5	-90	-	-	-22.8
	Th.8.40	NQ (V)	5.1	250	4.5	-4.4	-88	-	-	-20.5
	Th.8.12 (10-11)	SGQ	5.2	200	5.2 to 4.9§	-6.5 to -6.8	-	-	-	-
	Th.8.36	SGQ/NQ (V)	5.1/2	200	6.5	-2.5	-121	-	-	-
	Th.8.35	SGQ/NQ (V)	5.1/2	200	5.8	-3.2	-129	-	-	-
	Th.8.17a	SGQ(V)	5.2	200	5.5	-6.2	-115	-	-	-
	Th.8.17b	SGQ(V)	5.2	200	6.1	-5.5	-134	-	-	-
	Th.8.22	SGQ(V)	5.2	200	5.2	-6.5	-120	-	-	-14.5

Table 4.2: O and H isotope compositions of minerals and H and C isotope compositions of included fluids. RQ = recrystallized quartz, THQ = Tessin habit quartz, NQ = needle quartz, SGQ = split growth quartz, Chl = chlorite, Ms= muscovite, Phe = phengite, Bt = biotite and Hm = hematite, Wr = whole rock, Lam=Lamprophyre. Symbols ∗ and § point to the data shown in Figure 4.6 and Figure 4.7 respectively.

Oxygen isotopes: $\delta^{18}O$ values of the host-rock quartz sampled near the five vein types are between +9.1 and +10.9‰, feldspars have values of +9.1‰. Early V_1 recrystallized quartz

Figure 4.6: δ^{18}O (‰ vs VSMOW) of host rock quartz and vein quartz. Note that for V$_3$ and V$_4$ the δ^{18}O of vein quartz is calculated to be in equilibrium with measured values for phengite and chlorite at T = 350 and 300 °C, respectively. $\Delta = \delta^{18}$O$_{Hr} - \delta^{18}$O$_{Veinquartz}$
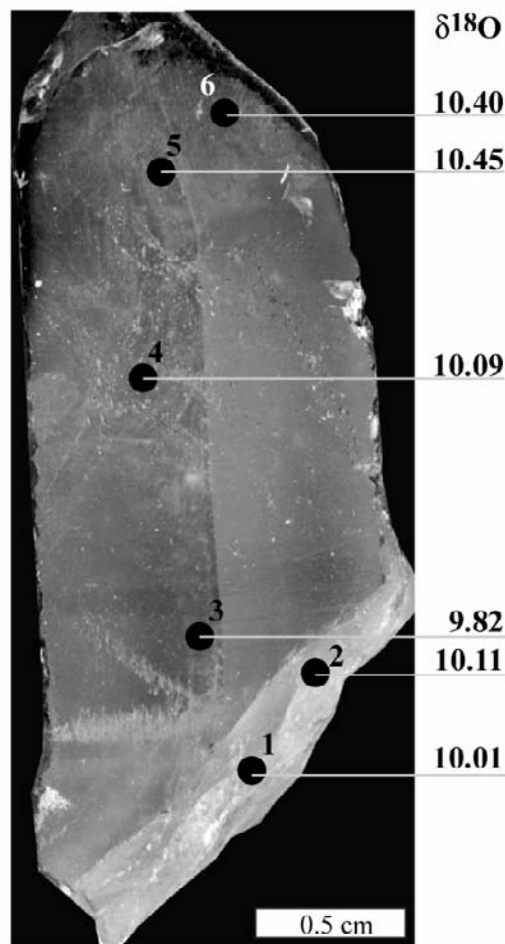
and early V$_2$ Tessin habit quartz have constant values of δ^{18}O values of +10.1‰ (Table 4.2 and Fig. 4.6) whereas the δ^{18}O values of Tessin habit quartz increases to +10.4‰. Biotite from V$_1$ veins has a value of +5.3‰. δ^{18}O values of hematite in V$_3$ are −2.2 to −3.6‰ and of chlorite in V$_4$ are +3.8 to +4.1 ‰. Both hematite and chlorite of V$_3$ and V$_4$ have similar isotopic compositions as the chlorite and hematite precipitated contemporaneously with Tessin habit quartz in V$_2$ veins. Phengite, which preceded hematite formation has δ^{18}O values of +6.0 to +7.1 ‰.

In the V$_5$ vein system δ^{18}O values of the 3 fault gouges (gouge$_I$ to gouge$_{III}$) and vein quartz (needle and split-growth) were measured (Fig. 4.7). δ^{18}O values in fault gouge changes from +8.2‰ in gouge$_I$ to +5.9‰ in gouge$_{III}$. δ^{18}O values from the gouge zones are mixtures of the δ^{18}O values from components of the original granite (quartz, K-feldspar, albite, ± muscovite and ± chlorite) with chlorite and muscovite formed by later healing and new needle and split-growth quartz during veining. It is impossible to distinguish between these minerals macroscopically as the gouge is too fine-grained to measure individual
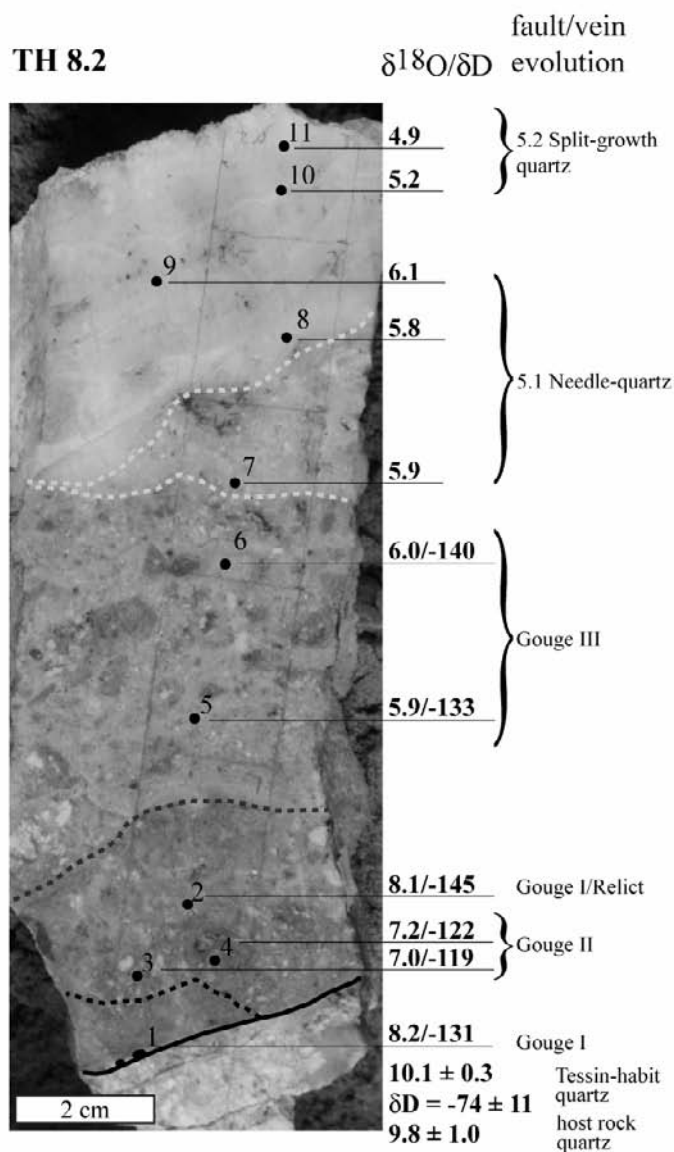
Figure 4.7: Changes in oxygen and hydrogen isotope compositions of V_5 fault gouge and the late V_5 vein quartz (sample Th.8.2).

grains and modal amounts are not constant over the gouge zones. Care was taken to sample only the fine-grained parts of the gouge, to avoid measuring relict clasts. The $\delta^{18}O$ values of gouge$_{III}$ are similar to the values measured for the early vein formation stages (+5.8 to +6.1‰). The values, are lower (+4.9 to +5.2‰) during later split growth quartz formation.

The $\delta^{18}O$ values of the host rock quartz and vein quartz suggest that the fluids introduced later have equilibrated with the host during V_1 to V_4 formation (Fig. 4.8). Late V_2 vein quartz as well as $\delta^{18}O$ values of quartz calculated to be in equilibrium with chlorite and hematite were compared to the measured values for host rock quartz for the V_3 and V_4

Figure 4.8: $\delta^{18}O$ (‰ vs VS-MOW) of host rock quartz and vein quartz. Note that for V_3 and V_4 the $\delta^{18}O$ of vein quartz is calculated to be in equilibrium with measured values for phengite and chlorite at T = 350 and 300 °C, respectively. $\Delta = \delta^{18}O_{Host-rock} - \delta^{18}O_{Vein}$
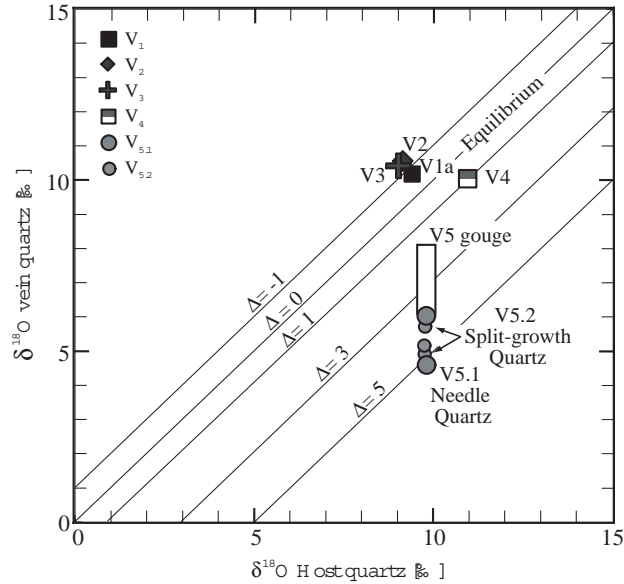
veins. Only in the case of the V_5 veins can significant differences be observed between host rock and vein quartz (+4 to +5‰).

Hydrogen isotopes: Hydrogen isotope compositions were measured for both fluid inclusions from quartz and hydrous vein minerals (biotite, phengite and chlorite, mixtures of gouge material) (Table 4.2). The values for hydrous minerals represent an average of two analyses, the fluid inclusion values are single analyses. Biotite from V_1 has a low δD of -106‰. The $V_{1.2}$ fluid inclusion population has δD values between -84 and -92‰. δD of early CO_2-bearing fluid inclusions from Tessin habit quartz (fluid inclusion population $V_{2.1}$) are slightly higher (-65 to -88‰) and is similar to biotite with -77‰. Chlorite sampled from V_2 vein has values of -76 to -89‰. In the case of V_3 only phengite was measured and had a δD of -58‰. Chlorite sampled from the V_4 veins has δD values similar to those precipitated in V_2 veins. V_5 fault gouge has a spread in values of -119 to -145‰ for the gouge mineral mixtures and values of -88 to -134‰ for the fluid inclusions in needle and split-growth quartz. Gouge$_I$ mixture has δD values of -131 to -145‰ (points 1 and 2 in Fig. 4.7), whereas δD of gouge$_{II}$ has higher values of -119 to -122‰ (points 3 and 4 in Fig. 4.7). Gouge$_{III}$ has again values of δD of -133 to -140‰, which is similar to gouge$_I$. Fluid inclusions from needle quartz have δD values between -88 and -129‰. Needle quartz often contains tiny fluid inclusions from later populations, associated with split growth quartz. These are probably reflected in the lower δD values observed in some of the samples (-121 and -129‰). Split growth quartz has values between -115 to-134.

Carbon isotopes: Carbon isotopes of CO_2-bearing fluid inclusions were only measured

for early V_1 and V_2 and late vein quartz samples from V_5 veins. The early V_1 and V_2 values are between -6.9 and $-10.3‰$, which implies that the carbon isotope composition of the fluids did not change significantly from entrapment of V_1 fluids to V_2 fluids. The $\delta^{13}C$ values of -22 to $-14‰$ obtained for V_5 vein fluids are significantly lower than those obtained from V_1 and V_2 veins. The lack of carbon-bearing gases in the fluids (Fig. 4.3) signifies that the $\delta^{13}C$ values obtained for V_5 vein fluids are probably contaminations of organic matter and are not representative of the original vein fluids and are, therefore, not discussed any further.

Stable isotope geochemistry of vein fluids

The stable isotopic composition of the vein fluids were approximated by calculating the oxygen and hydrogen stable isotopic compositions to be in equilibrium with the minerals at the corresponding formation temperatures. The following oxygen isotope fractionation factors were applied: for quartz-water calibrated in the range of 200 to 500°C from Matsuhisa et al. (1979). For annite-water, phengite-water and chlorite-water from Zheng (1993) and for hematite-water the oxygen isotope fractionation factor from Zheng (1991) was used (all determined in the range of 0 to 1200°C). The hydrogen isotope composition of water from fluid inclusions is taken to represent the value of the original composition of the fluid, whereas for hydrous minerals the appropriate fractionation factors have been applied to calculate the isotopic composition of the fluid in equilibrium with the hydrous mineral. Fluids in equilibrium with muscovite and biotite were calculated using fractionation factors of Suzuoki and Epstein (1976). According to Graham et al. (1987) equilibrium fractionation between chlorite and water is up to $40‰$ at temperatures between 200 to 500°C. These maximum values were used for V_4 and V_5 chlorite analyses. δD values of inclusion fluids are assumed to have remained constant after fluid inclusion entrapment. The measured and calculated isotopic values are displayed in Table 4.2 and Figure 4.9.

The $\delta^{18}O$ value of V_1 fluids is around $+7‰$ as calculated to be in equilibrium with biotite and recrystallized quartz and δD of this fluid is between -60 and $-95‰$, which is indicated by vein biotite and fluid inclusions. These are approximately the same values as for V_2, which has slightly lower $\delta^{18}O$ values because of the lower formation temperature of quartz. The $\delta^{18}O$ values of fluids calculated in equilibrium with chlorite are slightly lower than the $\delta^{18}O$ values of fluids calculated from quartz probably because of the lower formation temperature of chlorite in the V_2 veins. Early V_2 vein fluid has a δD value of -66 to $-88‰$, whereas chlorite has higher values.

V_3 fluid has calculated $\delta^{18}O$ values between $+5$ and $+7.1$ ‰ and one phengite measurement provides a δD value for water of -20‰. V_4 fluids have similar $\delta^{18}O$ values as the late chlorite from V_2 veins at 4‰ ± 0.2 and δD values of -39 to -57.

Fluids from V_5 are separated in gouge, needle quartz and split-growth quartz fluids. The gouge fluids are derived from bulk samples, which makes it difficult to determine the exact H and O isotopic composition of of the fluid. However, the δD values for the gouge fluids demonstrate that these values are probably mixtures of fluids from older muscovites and chlorites and younger V_5 fluids which have values of -88 to -134‰. This is also implied by the differences in the three gouge generations as is indicated in Figure 4.7. The lower $\delta^{18}O$ values of quartz ($+4.9$ to $+6.1$‰, Figure 4.7, points 8 to 11) imply that these fluids also had a lower $\delta^{18}O$ value than V_2 to V_4 fluids.

4.6 Discussion

Stress-orientation and tectonic setting during the different vein formation events

The vein formation mechanisms for V_{1a} and V_{1b} vein opening are largely unknown. However the size and texture of V_{1a} veins imply that the "veins" were formed as quartz-pegmatites during late Hercynian conditions. In such a case silica enriched fluids could easily create such large veins. Whether differential stress played a role in opening these veins or whether they are caused by hydrofracturing cannot be determined on the basis of present field relationships. V_{1b} veins have smaller volumes and therefore need less fluid to precipitate. As V_{1a} and V_{1b} veins are commonly related to the S_1 foliation and the S_1 foliation was refolded during the formation of the Chièra synform to the South of the Gotthard massif and steepened during early Miocene times their orientations were probably sub-horizontal and near vertical, respectively during their formation.

The vein orientations and shapes imply that the stress orientation remained constant from V_2 to V_5 during retrograde metamorphic conditions. The formation of V_2 veins can be attributed to a stress regime with a vertical least principal stress (σ_3) and a near horizontal SE-NW directed largest principal stress (σ_1). However, they commonly overprint V_{1b} veins and open the lower interface between host rock and massive quartz veins, which act as weak planes. Grujic and Mancktelow (1996) and Maxelon and Mancktelow (2005) indicate a late phase of vertical shortening (their D_5 as this was the prevailing stress regime in the Central Alps at the time.
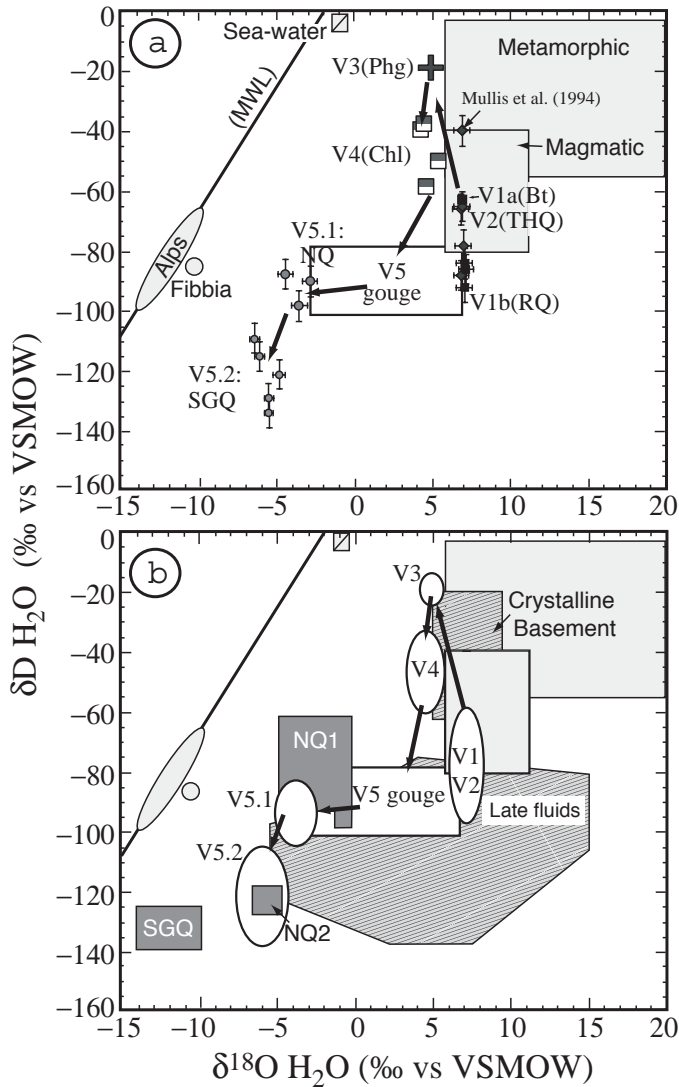
Figure 4.9: a) Stable isotope constraints on fluid origins of V_1 to V_5 fluids. Symbols for stable isotope measurements on fluids from the different vein generations are the same is in Figure 4.4. The metamorphic, magmatic fields and the "meteoric water line" (MWL) denote the H and O isotopic compositions of water from Hoefs (1997). Recent meteoric fluids from the Central Alps are indicated as well as own measurements of lake water from the Fibbia ($\delta D = -85.4‰$ and $\delta^{18}O = -10.3‰$). One measurement from the Fibbia area was taken from Mullis et al. (1994) b) Relation between hydrogen and oxygen isotopic composition of fluids from this study and fluids from Mullis et al. (2001); Sharp et al. (2005); Mullis et al. (in prep.). Fluids from Mullis et al. (2001, in prep.) are indicated by dark grey areas and fluids from Sharp et al. (2005) by grey-striped areas.

Near vertical V_3 to V_4 vein formation is attributed to a change in magnitude of principal stress axes, which is related to the progressive exhumation of the Fibbia granite and the Miocene NE-SW extension, coeval with the normal faulting along the Simplon fault (Mancktelow, 1990; Grosjean et al., 2004) and the progressive exhumation of the Lepontine area. According to Sibson (2000) such changes in tectonic stress magnitudes can lead to redistribution of fluids and changes in fluid pressures. V_5 veins are considered to have formed in a similar stress regime as V_3 and V_4. These veins record more intense shearing and SW-NE extension and in some cases re-use the V_3 and V_4 fracture planes.

Vein fluid temperature and pressure evolution

Pressure and temperature estimates for the different veining events were made in chapter 3 using $PVTX$ data from fluid inclusions and temperature estimates from stable isotope and K/Na fluid thermometry on mineral pairs and fluid chemistry from the different vein types. Large V_{1a} veins formed during pre-Alpine conditions, after granite intrusion, which is also confirmed by the presence of large felspar clasts. Smaller V_{1b} veins formed during prograde metamorphic conditions at around 450 °C. After V_{1b} vein formation fracturing led to the incorporation of SE-NW oriented new parallel trails of fluid inclusions. Subsequent decrepitation of some of these fluid inclusions is attributed to further heating after V_{1b} vein formation and fluid trapping. V_2 fissures opened during temperature maximum to early stages of the retrograde metamorphic path. Na-K thermometry on early fluid inclusions from Mullis et al. (1994) and in chapter 3 provided temperatures of formation of 420°C and consequently pressures of around 3.5 kbars.

Fluid temperatures and pressures of V_3 and V_4 vein formation are constrained at 350 and 320°C, 2.0 and 1.6 kbar respectively, on the basis of measured isotopic fractionations of V_3 and V_4 vein minerals (chapter 3). This indicates relatively large differences in fluid pressure in the vein and the lithostatic pressures on the host rock. Formation temperatures of V_5 veins were at $\leq 300°C$ during early stages of needle quartz formation and $\leq 220°C$ during for split-growth quartz formation and fluid pressures were between 1 to 0.6 kbar, at approximately hydrostatic levels.

Origin of vein fluids

Inferences from anion and electrolyte geochemistry: According to Cesare et al. (2001) high Cl contents (≥ 20 wt% NaCl eq.) in a fluid can be related to fluid-unmixing, external sources such as evaporite-rich sedimentary formations, or to retrograde uptake of water, for example the alteration of biotite to chlorite. Biotite and chlorite are known to exchange Cl or F for OH in their crystal structures to different amounts. Bromine is not known to be taken up by either mineral, although trace amounts such as are present in fluids are not ruled out. Biotite to hematite or chlorite reactions may, therefore, cause selective addition or loss of Cl in the fluids and changes in the Cl/Br ratio. This is probably reflected in the increased salinity observed from V_2 to V_3 and V_4 fluids. However, mixing with fluids of slightly different salinity and Cl/Br ratios is also possible.

During V_5 vein formation the salinity of the fluid decreases and Cl/Br and Na/Br ratios

change compared to V_1 to V_3 fluids, but are similar to V_4 fluids. A salinity decrease of 5 to 6 wt% NaCl for V_2 to V_4 fluids to ≤ 2 wt% NaCl for V_5 fluids is indicative of mixing of local fluids with fluids from an external salt-depleted source. These external V_5 fluids probably gained small amounts of Cl from leaching Cl-bearing hydrous minerals or salts. The molar Na/Ca, Na/ Li and Na/K ratios of the V_5 fluids imply similar element ratios as high temperature geothermal fluids, which have been in contact with granites. This is expected for V_2 vein forming fluids in a relatively closed system granitic metamorphic environment. The presence of Li, K, Na and other elements in V_4 and V_5 vein fluids show that these fluids had time to take up some cations from infiltrated host rocks.

Inferences from stable isotope chemistry: Figure 4.9a,b) show that the stable isotope composition of oxygen and hydrogen of the vein fluids changes from fluids with compositions typical for metamorphic or magmatic fluid sources for V_1 to V_4 to those typical for mixed metamorphic-meteoric sources for V_5 fault gouge and needle quartz and finally meteoric sources for the split-growth quartz. The hydrogen stable isotope composition of V_1 and V_2 vein fluids is relatively low (between -65 and $-92‰$) compared to normal metamorphic fluids (-5 to $-55‰$) or magmatic fluids (-40 to $-80‰$) and may be related to slight contaminations from later fluids. The higher δD values of fluids calculated from phengites from V_3 (at $-20‰$) and chlorites from V_2 and V_4 veins (with an average of $-44.7‰$) are probably related to fluids with a slightly different hydrogen isotopic composition entering the system although still typical for a metamorphic fluid. The δ^{13}C values of V_1 and V_2 CO_2 have values that are indicative of an input of both devolatisation fluids from carbonates and oxidation of organic matter. Both processes occurred during the Alpine metamorphic events.

Reasons for very negative δD values: Gleeson et al. (1999) proposed several reasons for measuring δD values that do not represent the original δD values of the fluids. These can be divided into: 1) processes causing fluid inclusion populations with strongly inhomogeneous δD values during fluid inclusion trapping, 2) by post-entrapment processes and 3) by using different analytical methods.

Processes affecting the δD value of the fluid during the time of entrapment are related to changes in the physical and chemical properties of the fluid by external processes. These can in turn be related to processes like fluid mixing, boiling, fluid un-mixing and probably to a lesser extend fluid-rock interactions and addition or loss of fluid. The fluid inclusions within a single fluid inclusion population measured in the V_1 to V_5 veins are relatively homogeneous in both physical and chemical properties (volume and homogenisation temperature, salinity and electrolyte chemistry) and the petrography of the fluids suggest that

boiling or fluid unmixing did not occur at the time of entrapment. The fluid rock interactions that did occur represent longer time scales than the entrapment of single inclusion populations and could not cause inhomogeneities of δD values in the fluid inclusions.

Post-entrapment changes of the fluid inclusions can occur due to diffusion of hydrogen through the quartz at high temperatures ($>200\,^\circ$C) and can explain extreme low values of δD (Mavrogenes and Bodnar, 1994). Recrystallisation, decrepitation and re-equilibration of fluids and diffusive interaction with minerals containing H_2O in the crystal structure or as impurities are the main processes that can affect the δD values of the fluid inclusions. However, the low values of δD are found in late quartz veins, which were formed in a temperature range of around 200 to 250 $^\circ$C (chapter 3), whereas the earlier formed quartz retained higher δD values and so it is unlikely that in this case the original δD values are significantly changed by diffusion.

The effect of different extraction techniques on δD values of fluids from different natural quartz was studied by Simon (2001). His analyses show that δD values from fluid inclusions from quartz samples measured using extraction by thermal decrepitation and mechanical crushing is dependent on the grain size of the sample material. The cause of this grain size dependence on δD values is tapping of different sources of hydrogen from the quartz during extraction. The samples that were thermally decrepitated in this research had grain-sizes up of about 1–5 mm, which is considered large enough, so that fluid-inclusion fluid was extracted and values consequently must be near to the original fluid value. In some extractions, however, small grain-sizes may have caused some mixing. Especially for V_5 split-growth quartz also water from small flakes of micas could have been included in the analyses. As thermal decrepitation was the only method used in this study, the observed differences in δD values probably represent real changes, although the measured values may be systematically off-set from the "real" values.

The effect of pressure on hydrogen isotopic fractionation between water and gas or minerals was considered by Driesner (1997). Hydrogen isotopic fractionation between water and minerals is very strong at temperatures and pressures where water shows critical behaviour. This effect can be up to 20‰. However, at the higher pressures that prevail in the earth's crust this factor is reduced to only several permil, which for hydrogen analyses is within the range of the standard error of the technique. Elevated salt concentrations in water may also influence hydrogen isotope fractionation between H_2O and minerals (Chacko et al., 2001), particularly for $CaCl_2$ solutions at salt concentrations larger than 4 molal (Horita et al., 1993). Regression equations of Horita et al. (1993) indicate that the salt effect becomes less important at temperatures of around 300°C, but can be substantial at

lower temperatures. However, the salinity of at least the V_5 fluids is relatively low (>1 molal), which decreases the hydrogen fractionation effect induced by additional salt for these fluids and implies that the very low hydrogen isotopic compositions observed for split-growth quartz are primary

Ultimate fluid sources: The V_1 to V_2 fluids are probably derived from original formation waters together with an input of metamorphic dehydration reactions. This can be inferred from the Cl/Br signatures (near modern sea water) and the presence of CO_2 and its stable isotopic composition. These fluids were at equilibrium with the host rock as is indicated by the equilibrium between the host rock and vein minerals. Particularly in the case of V_1 the equilibration probably occurred later during heating towards the metamorphic peak temperature. V_2 veins equilibrated during the vein formation as V_2 fluids interacted readily with the host rock. V_3 and partly also V_4 vein fluids originated from the pores of the host granite and evolved V_2 vein fluids. However in the case of V_4 external derived fluids also played a role as is indicated by the change in its Cl/Br ratios. In the case of V_5 fluids, the low δD values values support a large change in the isotopic composition of the vein fluids. The low δD and $\delta^{18}O$ values of the minerals suggest infiltration of meteoric water derived from a high altitude catchment area (e.g. Mullis et al., 2001; Mulch et al., 2004; Sharp et al., 2005, Appendix A). Recent average rain waters from the Fibbia area have a δD of $-80‰$ and values above $-130‰$ would imply a meteoric origin of the fluids from a mountain range with an average height that was at least 2000 meters higher than the current altitudes in the Alps, which was also proposed by (Sharp et al., 2005).

Fluid flow models for the five vein types.

In collisional mountain belts the fluid flow regime in rocks is dependent on the position with respect to the surface, whether the rock is in the internal or external part of the orogen and what the architecture of the orogen and in particular the architecture of the major fault zones is. Koonz (1991) proposes a model for fluid flow regimes in orogens, suitable for the Southern Alps (New-Zealand), the European Central Alps and the Himalaya. He considers fluid flow to be separated in an internal wedge (e.g. Penninic Nappes), a transition zone (e.g. Aar and Gotthard Massifs) and an external wedge (e.g. External Helvetic Nappes). In the external wedge, fluids tend to move upward by compaction driven flow, whereas in the transition zone topography driven meteoric fluid flows downward and buoyancy driven fluid flows upward are both present. Fluids are considered to be capable of flowing down to 10 km depth. In the internal wedge zone fluids are transported upwards by a high geothermal gradient and tectonic transport. Of central importance is the geometry of the

major fault zones that can act as major fluid pathways for downward flow. This simple model fits the observation that hot meteoric fluids are found in Central Alps. However, there are no major fault zones nearby which could act as fluid pathways, and it is unlikely that meteoric fluids could flow penetratively downwards through the crystalline basement. It is therefore neccesary to find additional models to explain the presence of fluids with a meteoric isotopic composition in Alpine formed veins.

Fluid regimes in V_{1a} veins: The fluid flow regime is constrained by the observations of large volumes of quartz precipitation, no-detectable host rock alteration as documented in chapter 3, equilibrated oxygen isotopic compositions, low-saline fluids, temperatures of around 450°C and pressures of 3 to 4 kbar and no observable pathways that could have been used for fluid flow. These data only contribute indirectly to the understanding of the fluid flow processes causing the V_1 veins. In the case of V_{1a} late fluid rich melts, segregated from the granite can readily produce such large amounts of quartz. Two fluid flow regimes are thought to be likely for producing V_{1b} veins: either progressive devolatisation with several events of hydrofracturing (Yardley, 1997) with silica-oversaturated fluids that originated from slightly higher temperatures and/or pressures than the veins or the mobile hydrofracturing model (Bons, 2001) in which fluids originated from much higher temperatures or pressures and are, therefore, very silica-supersaturated. The model of Yardley (1997) requires more fluids to flow through the veins, while in the model of Bons (2001) the presence of narrow flow paths that let deep crustal fluids escape are necessary. In either case fluids should not have the possibility of interacting with the host-rock as there is no indication of silica depletion or enrichment in the host rock. However, because the fluids recorded as $V_{1.1}$ and $V_{1.2}$ represent fluids that were trapped after vein formation, but probably still during prograde conditions, these data do not contribute to understanding of vein formation itself but to stages after vein formation.

Fluid regimes in V_2 veins: In the case of V_2 veins fluid flow was constrained by infiltration of fluids from neighbouring rocks during vein opening and later enlargement of the veins during opening of the V_3 and V_4 veins. In the period between opening and the enlargement of veins, fluids were able to interact with the porous host rock near the vein wall as is indicated by the silica-depleted alteration zone surrounding these veins. The anion and cation chemistry of the fluids as well as the stable isotope compositions of vein fluids and minerals imply that vein fluids equilibrated with the host granites and that the veins were chemically closed. Minerals were able to precipitate continuously without being disturbed by brittle deformation, during this period of closed system interaction. Fluid pressures must have remained at the levels necessary to keep the fracture open i.e. near

to lithostatic pressures. Several mechanisms causing the vein mineralisations have been proposed (Mullis, 1996; Ague, 2004; Sharp et al., 2005). These include quartz precipitation due to temperature and fluid pressure decrease, continuous vein-host rock interactions due to gradients in fluid pressure or chemical potential between veins and host rocks. Sharp et al. (2005) argued that temperature decrease was probably not a dominant factor for causing the precipitation of quartz as large amounts of fluid would be required to precipitate such amounts of quartz. Instead they proposed a "breathing" model in which small pressure fluctuations caused small extensions and contractions of the veins and thereby providing changes in chemical potential to grow quartz inside the vein. Such diffusive transport models can create 1-meter thick quartz veins in ~ 1 Ma (Wangen and Munz, 2004). The V_2 veins in the Fibbia area are commonly only partly mineralised with free growing crystals. The total V_2 vein volume in the Fibbia area is mostly up to 0.1–0.5 m^3, and therefore would require much less fluid passage (by a factor of 10 to 100) than the largest veins described by Sharp et al. (2005) in a temperature decrease model. However, these vein systems were at isotopic equilibrium with the host rock so large fluid passage is unlikely. In addition, chapter 3 shows that the porous alteration zone acted as the main source for the mineralisation of V_2 veins. The host rock minerals were fractured during vein opening and were partially still strained from the S_1 foliation formation. Possibly the bending of the host-rock around the veins might have caused fracturing of minerals in the altered zones near the veins. Relict minerals in the alteration zones, therefore, have a higher strain and surface energy then the newly grown strain free minerals in the V_2 veins. These effects provide additional energy to let diffusive transport of material from the alteration zone to the veins take place.

Fluid regimes in V_3 and V_4 veins: V_3 and V_4 mineralised fractures cut the V_2 veins and form a fracture set with similar orientations. Single fractures can be several meters in length. The mesh produced by the V_3 and V_4 veins probably constituted a fracture system as these type of fractures are observed elsewhere in the Central Alps as well (Grosjean et al., 2004). However, from field observation it is unclear whether these fractures were interconnecting over distances larger than the outcrop scale and therefore could form large-scale flow systems. The oxygen isotope composition of vein minerals and the cation chemistry of the fluids imply that the fluids in the Fibbia area were in contact with metamorphic rocks. Hydrogen isotope composition of V_3 and V_4 vein fluids indicate higher values for these fluids than for V_1 and V_2 fluids. However the dataset on these veins is small and the hydrogen fractionation factors between muscovite or chlorite and water are poorly known. Therefore, the observed change in hydrogen isotopic composition may not be real. The anion chemistry of V_4 suggests that external fluids with a different

Cl/Br ratio may have played a role in the formation of V_4 chlorite veins and that V_4 fractures were locally partially interconnected, and thus temporarily partly permeable.

Fluid regimes in V_5 veins: Nesbitt and Muehlenbachs (1989) suggested, on the basis of permeability data, that surface-derived waters could be common in the brittle crust up to 16 km depth, provided that there is an interconnected fracture network. However, they also show that circulation of surface- derived fluids is limited in a compressional setting. The Alps were in a phase of SE-NW compression and NE-SW orogen parallel extension at the time of V_5 formation. Two dimensional models, such as proposed by Nesbitt and Muehlenbachs (1989) and Koonz (1991), did not contain such three dimensional features. The V_5 veins are an expression of this late stage extension environment in the Central Alps and are very suitable for fluid flow because of their scale and near vertical orientation. The relatively high homogenisation temperatures (between 180 and 260°C) of fluid inclusions and the high silica content of the fluids (as indicated by the scale of quartz precipitation) imply that hot fluids were derived from greater depth. On the other hand, the low hydrogen and oxygen isotope compositions estimated for these fluids suggest that they are surface-derived. These results and observations point to a fluid flow system in contact with the paleo-surface at scales much larger than the outcrop scale. However, large-scale faults, which could have acted as flow path, are absent from the area. The mineralised extensional fractures observed in the northern Penninic nappes (Appendix A) have similar orientation and dip as the V_5 veins, but can be considerably larger. In contrast to Sharp et al. (2005) these veins were mineralised with mainly quartz after the V_2 quartz mineralisations and A even observed typical V_5 quartz crystals overgrowing V_2 vein quartz. As the oxygen isotopic composition of quartz from V_5 and the host rock differ significantly, the V_5 veins must have formed during disequilibrium conditions, which also points to externally derived fluids. As these different fracture sets have relatively uniform fluid characteristics and stable isotopic compositions, they were probably interconnected and open during the same period. V_5 veins are, according to appendix A, mineralised fractures that were at least partly open for longer periods of time down to 10 km depth within the crust. The large-scale extensional conjugate en-echelon fracture meshes can remain open in relatively competent rocks undergoing extension down to 4 km depth (Sibson, 1996). This may be deeper for less competent rocks. Appendix A suggests that an interplay of topography, gravity, density differences between cold surface fluids and deep hot fluids and possibly sub-hydrostatic fluid pressures in dry re-hydrated crystalline rocks are parameters that could have induced downwards directed fluid flow in long term open fractures. Additionally seismic pumping (Sibson, 1981) or a modified seismic pumping mechanism proposed by McCaig (1988) may induce further fluid redistribution upward as well as downward along

a fault zone.

4.7   Conclusions

Five vein generations have been distinguished based on their structural, petrographical and geochemical characteristics and the different geochemical compositions of their vein fluids. This is essential to constrain the origin of the vein fluids and to help interpret the tectonic framework of the orogen. The combination of cation and anion and the C, H stable isotope composition of fluids together with the O, H stable isotope compositions of minerals point to the following:

1) The earliest veins (V_1) were strongly re-equilibrated by deformation and recrystallisation during pro- and early retrograde metamorphic conditions. Fluids were at equilibrium with their host rocks. The granitic host rock buffered the cations and the oxygen and hydrogen stable isotope compositions in the earliest vein fluids (V_1 and V_2).

2) Early nucleation of vein crystals is probably related to disequilibrium conditions during vein opening. During later stages V_2 vein fluid interacted strongly with the host rock, suggesting a longer period of fluid presence. Dissolution of minerals with higher surface and strain energy from the alteration zone led to continued crystallisation of new minerals in the veins.

3) V_3 and V_4 veins are related to deformation in the brittle regime and partially interconnected open joint systems. The Br/Cl and Na/Br ratios of these fluids as well as δD values of the fluid suggest a possible input from external fluids during V_4 formation, whereas the cation fluid chemistry and oxygen stable isotopic composition of vein chlorite and hematite indicate that these fluids were equilibrated with granitic rocks, as is also indicated by the chlorite mineralisation. However, the overall data suggest that the V_4 fluids were different from those during V_1 to V_3 vein formation.

4) In the case of V_5 veins fluids were externally derived, meteoric fluids. The V_5 veins in the Fibbia area are related to a system of meso-scale sub-vertical extensional brittle shear zones, which extends spatially over large parts of the Northern Penninic nappes and the southern Gotthard Massif. Early needle quartz mineralising fluids were of mixed metamorphic-meteoric origin and can be attributed to the earliest stages of vein opening after cataclastic deformation and extension along the V_5 faults. Later split- growth quartz mineralisation is attributed to the influx of high altitude, heated meteoric fluids, that penetrated the same fault systems and which returned to the surface over-saturated in silica.

5) Particularly during retrograde conditions did the stress regime of SE-NW compression and first sub-vertical extension (V_2) and later SW-NE extension (V_3 to V_5) contribute to vein forming events.

Chapter 5

Origin and pathways of mineralising fluids associated to vein formation, Amsteg, Northern Aar massif, Switzerland[§]

Abstract

Sigmoidal en-echelon qtz-ab-ad-chl-cc-PbS-ZnS-FeS-veins from the northern part of the Aar massif, which were formed by brittle fracturing of meta-sedimentary rocks and mineralisation from aqueous saline fluids were studied using structural methods, fluid inclusion micro-thermometry, geochemical and stable isotopic techniques. These veins formed during or slightly after peak Alpine (low-grade) metamorphic conditions at T = 350 °C and at approximately 3.5 kbar (11 km depth) and remained fluid filled until T = 250 °C and 2.5 kbar (8 km) depth. The veins are related to late Alpine exhumation stages of the Aar massif between 18 and 13 Ma. Early veins are small, but become extended and interconnected upon further straining of the rock. A stress regime with sub-vertical extension and SE-NW compression together with high fluid pressures is a probable cause for the opening and enlargement of the fractures.

mineralisation of the veins indicates that mineralising fluids must have contained small amounts of sulfur, whereas the main mineralisation is dominated by quartz and different alumino-silicates. Three fluid inclusion populations indicate slight salinity decreases upon cooling, without large changes of the Na/K ratios as obtained from crush-leach analyses. In addition the Cl/Br and Na/Br ratios are highly variable, which implies variable fluid compositions present in the veins. Fluid circulation within the meta-sediments in which the veins formed is therefore likely. The amount of material leached from the host rock is small and the veins are nearly completely mineralised, which substantiates this. Stable isotope values of fluids and minerals indicate that these fluids were metamorphic fluids equilibrated with the crystalline basement, without large changes in H_2O compositions among subsequent fluid inclusion populations. Short intervals of albite precipitation during K-feldspar precipitation can be explained by influx of fluids from lower temperatures, as the K concentration of fluids tends to decrease with temperature at even constant chlorinity, whereas the Na concentration is increased.

keywords

Vein formation, Aar massif, fluid inclusions, fluid-rock interactions, fluid sources.

5.1   Introduction

Veins and mineralised fractures are ubiquitous in regional metamorphic terrains and give important information on style of deformation, fluid movement, fluid-rock interaction and fluid sources. In the Alps different types of mineralised fractures and veins have formed during different events in the Alpine metamorphic cycle. Given that veins can form in very different geologic environments - with varying physical and chemical conditions, imposed during vein opening and mineralisation - it is logical that the end-products can be categorised using different structural and geochemical parameters.

In the external Central Alps veins formed during peak or early retrograde conditions have been thoroughly excavated over the past centuries and studied for their mineralogy. (e.g. Koenigsberger, 1917; Niggli et al., 1940; Parker, 1973). In the last decades studies on geochemical relations with the host rock, fluid chemistry from either petrological measurements or fluid inclusions contributed to the understanding of the vein mineralisation and formation conditions (e.g. Stalder, 1964; Poty, 1969; Stalder and Touray, 1970; Poty et al., 1974; Mullis, 1976; Hoefs and Stalder, 1977; Mercolli, 1979; Luckscheiter and Morteani, 1980; Ramsay, 1980; Mercolli et al., 1984; Ramsey and Huber, 1987; Diamond, 1990; Marquer and Burkhard, 1992; Yardley et al., 1993; Mullis et al., 1994; Henry et al., 1996; Mullis, 1996; Marshall et al., 1998; Fabre, 2000; Fabre et al., 2002; Lucchini, 2002; Sharp et al., 2005; Tarantola, 2005).

In this study freshly excavated veins from the new NEAT ("Neue Eisenbahn Alpen Transversale") -Cable tunnel through the Aar and Gotthard massif, Switzerland were studied for their structural, mineralogical and fluid evolution. Geochemical relations between the veins and the host rock and the geochemistry of the fluids were investigated in detail. Veins were studied in a 2-D section along the tunnel walls and contained unweathered mineralisation. Previous studies in this particular area (Mullis et al., 1994, locality Mu.19) showed that late episodic CO_2 enriched fluids penetrated in these types of fractures and caused formation of skeletal quartz. The CO_2 involved was interpreted to originate from graphite bearing volcanoclastic sediments situated some 100 meters below. Such instances of tapping fluids from different sources than the local host-rock occur more often in the Alps, but did not occur everywhere.

Additionally veins in the area are known to contain REE-minerals (Köhler, 1997). The relatively heterogeneous rocks of the Aar massif contain many relics of pre-Alpine magmatic and metamorphic phases and locally PbS-ZnS mineralisations, which can be partly re-mobilised. This study is concerned with the mineralogical evolution of the veins, geo-

chemical changes from host rock to veins, re-mobilisation of major rock forming elements during Alpine vein formation and whether externally derived fluids were also involved in the veins formed in the NEAT-Cable tunnel. Combining all structural and geochemical results yields an overall assessment of vein evolution, fluid characteristics, sources and flow paths in the the Amsteg area.

5.2   Geological setting

The Aar massif is part of the external crystalline massifs of the Central Alps (Fig. 5.1a). Amsteg is situated at the northern boundary between the crystalline units and Helvetic-cover of the Aar massif. The crystalline Aar massif consists of pre-Varsican gneiss units, pre-Variscan granitoid units, migmatic granites and gneiss units, lower Carboniferous intrusives, Carboniferous volcanics and upper Carboniferous intrusives (Abrecht, 1994). In the Amsteg area the main lithologies are chlorite-sericite schists (belonging to the pre-Variscan gneiss units), volcanoclastic sediments, belonging to the Carboniferous volcanics and volcanoclastic sediments, granitic-tonalitic gneisses which belong to the migmatic granites and gneisses, and Jurassic sediments which belong to the cover units of the Aar massif (Fig. 5.1b).

The volcanoclastic sediments were, according to Schenker (1986) and Schenker and Abrecht (1987), overprinted by three metamorphic events: 1) syn- to post volcanic low temperature hydrothermal metasomatic changes, 2) contact metamorphism during the formation of Variscan intrusions, with temperatures up to 500 °C and 3) regional Alpine metamorphism up to 300-350 °C and 2 kbar, which is based on the stilpnomelane-out reaction (Frey et al., 1980; Frey and Ferreiro-Mählmann, 1999). The Alpine induced metamorphic grade of the Aar massif increases from 300 °C in the north to 450 °C in the South (Frey et al., 1980).

The NEAT-Cable and Base tunnel are situated mainly in the chlorite-sericite schists (Fig. 5.1b). The Aar massif was uplifted during late Tertiary, but was not eroded before 10 Ma (Trümpy, 1980). Schmid et al. (1996) showed that the timing of the main foliation formation in the Internal Aar massif was at around 30 to 28 Ma, after which further deformation occurred during the "Ruchi" phase. Zircon and apatite fission tracks indicate that cooling through the 300 °C isotherm in the Amsteg area occurred at 15.8 Ma and through the 120 °C isotherm at 6.5 Ma (Schaer et al., 1975; Wagner et al., 1977; Michalski and Soom, 1990).

The fluids from early Alpine fissures in the crystalline and cover units of the Aar massif

are mainly mixtures of H_2O and NaCl with small amounts of CO_2, CH_4 or other volatiles (Mullis et al., 1994). This zone is bordered to the North by the methane zone (Frey et al., 1980; Mullis et al., 1994; Tarantola, 2005). To the South fluids are mainly saline aqueous fluids. In veins at locality Mu.19 (Mullis et al., 1994) five different fluid populations were distinguished. The first population is mainly water rich, the second contains 72 mol% CO_2, the third population has a heterogeneous composition and the last two populations are depleted in CO_2. Their fluid temperature and pressure estimates, based on the intersection with the 30 °C/km geotherm show an evolution from 350°C and 3.7 kb to 250°C and 1.2 kb for the second population. Unfortunately, the geometry of the vein systems at locality Mu. 19 of Mullis et al. (1994) could not be studied any further.

5.3   Analytical techniques and sample preparation

Localities of sampled vein systems are numbered based on their distance from the NEAT-Base tunnel and sample numbers (e.g. 1160 meter, Th.101).

The whole rock bulk geochemistry of the chlorite-sericite schists 1 m away from veins, and at 5 cm intervals towards the vein-wallrock interface was measured using wavelength dispersive X-ray spectrometry on fused glass beads which contained a mixture of 300 mg powdered sample material and 4700 mg lithium tetraborate. The analyses were carried out on a Siemens SRS3000 wavelength dispersive sequential X-ray spectrometer with a Rh end-window tube (4 kV) at the University of Basel. The analyses were calibrated with well defined in-house standards. Porosity and density measurements of approximately 7 g of material per sample were performed with a Hg-porosimeter at the University of Fribourg.

A Chaixmeca heating-freezing stage was used to perform the microthermometric measurements. It was designed to work in the temperature range of –160 °C to 600 °C (Poty et al., 1976). The heating-freezing stage was mounted on a Leitz cross-polarised light microscope calibrated as described by Mullis et al. (1994). Heating was done manually, but always at the slowest rate possible. Well characterised double-polished (0.2-0.5 mm thick) sections of quartz samples from the veins were used for the measurements. In all cases only ice melting (T_m ice) and bulk inclusion homogenisation (T_h) were observed.

Salinity of the fluid inclusions was calculated using the experimentally determined T_m-weight% NaCl equation of Potter and Clynne (1978). The total fluid inclusion density was determined with the program BULK, from the FLUIDS software package of Bakker (2003). Isochores of the fluid inclusions were calculated using the equations of Zhang and Frantz (1987) for the H_2O-NaCl fluid system. Additionally the same fluid inclusion
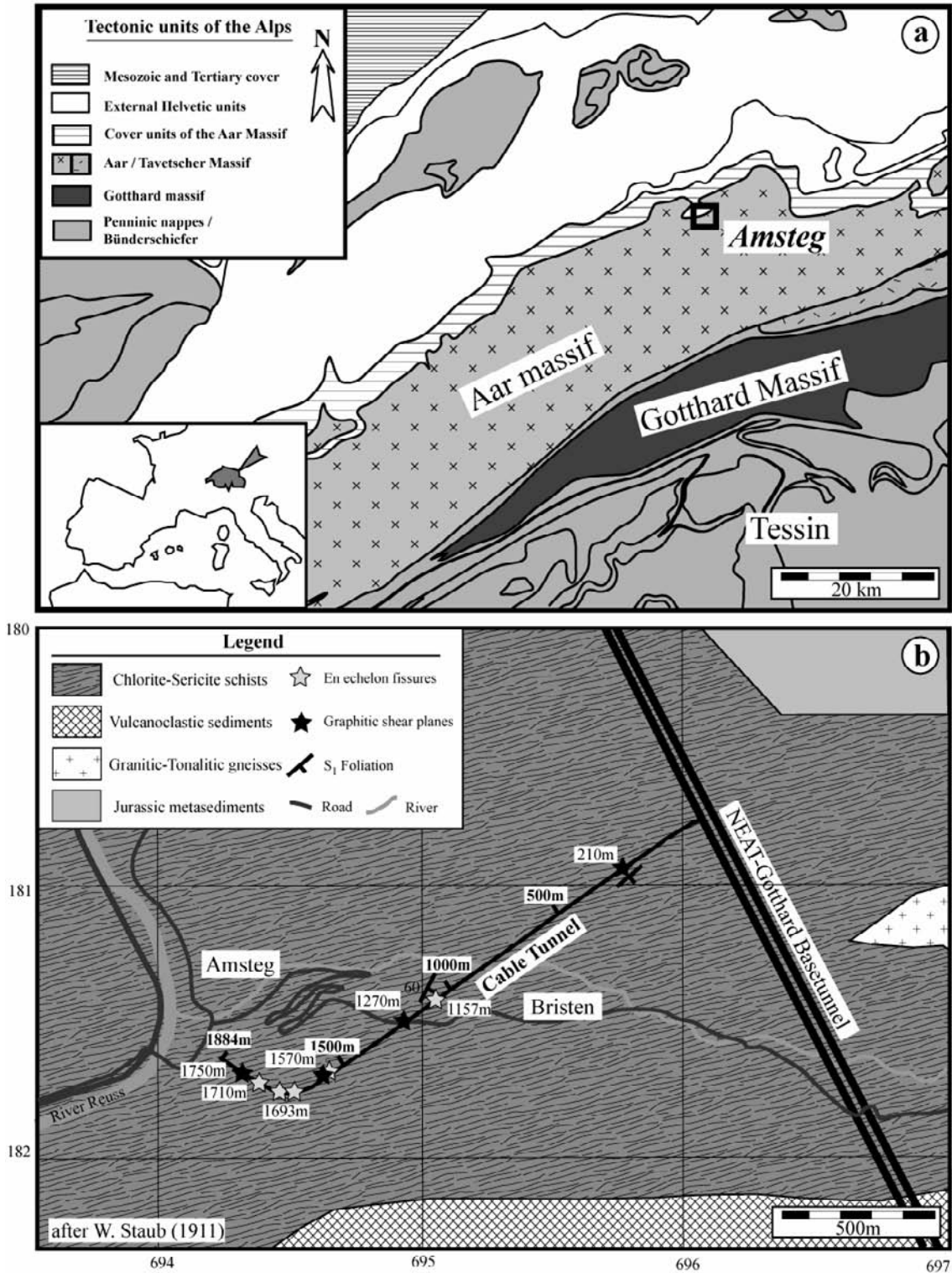
Fig. 5.1: a) Tectonic map of the Central Alps (modified after Schmid et al., 2004). b) Detailed geological map of the area around the NEAT-Cable tunnel near Amsteg (after Mercolli et al., 1994).

populations were checked for minor quantities of volatiles using Raman spectroscopy on the vapor bubble at room temperature. Raman analyses were performed with a Dilor Labram spectrometer connected to a Olympus BX40 microscope using a Innova 90C Ar-laser with wavelength of 488 nm at the ETH, Zürich.

Approximately 1 g of quartz was prepared for crush leach analyses using samples of three different quartz types from the three vein systems. Crush leach analyses were performed by D. Banks in Leeds, using techniques described by Bottrell et al. (1988) and Banks and Yardley (1992). For further details of the analyses procedure and anlytical uncertainties as described in chapter 3.

Vein and host-rock quartz and vein-chlorite and -calcite were manually separated for oxygen stable isotope thermometry on mineral pairs. In the case of quartz and chlorite oxygen was extracted by letting F_2 react with the sample material during laser ablation. For more information on the analytical procedure see chapter 4. In addition fluid inclusion extractions of H_2O and CO_2 were done using techniques described in chapter 4.

The oxygen and carbon isotopic compositions of calcite were measured using samples of 100 to 200 μg. Calcite was dissolved using phosphoric acid at 70 °C, which liberated CO_2. CO_2 and H_2O in the resulting gas mixture were separated by gas-chromatography before being analysed in a ThermoFinnigan Delta plus XL mass-spectrometer (Spötl and Vennemann, 2003). Oxygen and carbon were analysed at the same time. Carrara marble was used as a standard for the analyses. The carbon isotopic composition of inclusion fluids was determined by breaking a pyrex tube in the sample holders used for the carbonate analyses and analysed in the same way as the carbonates. All stable isotope analyses were performed at the University of Lausanne.

5.4   Results

Vein structure

The vein systems are characterised by relatively complex geometries, related to progressive stages of fracture opening. The veins in this area were formed during a single phase in which several fracturing events played a role. The early formed veins are oriented NE-SW and dip to the NW, nearly perpendicular to the S_1 orientation, whereas the later formed veins are often orientated in a more horizontal manner. Fig. 5.2a shows all the different stages present in a vein system at 1670 meter into the Cable tunnel on the South side. During progressive stages of vein opening the veins may become slightly rotated compared

to the earlier veins. The central parts of the veins are mostly extended, forming cavities in which single elongated blocky quartz crystals (Bons, 2000) (further-on termed fibre-quartz) stretch from vein-wall to vein-wall. Small early veins are commonly distributed in an en-echelon geometry with a length of up to 0.5 m and a width of up to 2 cm and are mostly completely filled with fibre-quartz or in some cases adularia. As the veins continue to extend, the previously formed fibrous minerals were broken in two halves in the centre of the veins and prismatic quartz rims overgrow the separated parts of the fibre-crystals. Veins can be up to 5 m in length and 30 cm wide, but these often comprise several smaller fractures which were linked upon further opening. Near the fracture tips the veins have less open spaces and form a relatively dense aggregate of fibrous crystals.

Host rock petrography

The green chlorite-sericite schists contain additionally to chlorite and muscovite, partly serizitised K-feldspar, quartz and graphite as well (Fig. 5.4a). Patches of up to 1 cm large feldspar clasts are often included in a fine-grained mica-rich matrix. The S_1 schistosity is marked by anastomozing mica-rich layers around feldspar clasts. The S_1 schistosity is occasionally cut on thin-section scale by more graphitic mica-rich layers, which may comprise a weak second foliation, having a slightly different orientation to the S_1 foliation.

Vein petrography

The veins can be characterised as quartz-feldspar-chlorite-sulfide-carbonate veins (Fig. 5.3). Mineralisation is divided into three intervals. Interval 1) fracture opening and fibrous quartz growth, 2) increased fracture opening, fracturing of fibre-quartz and euhedral quartz infill and 3) fracturing of euhedral crystals with late stage mineralisations. The early vein systems are mainly filled with fibre-quartz (Fig. 5.4b,c) and fibre-adularia. The positions of fractured K-feldspar clasts show that there was no horizontal displacement along the fracture (Fig. 5.4b). In the case where cavities were able to remain open for prolonged periods elongated fibre-quartz extend from the lower to the upper vein walls. The fibre-quartz clearly exhibits crack-seal-type bands of inclusions and their c-axes are often slightly rotated during continuous growth. After their formation they were overgrown by small phyllosilicates and finally by prismatic quartz parallel to the c-axes of the fibre-quartz (Fig. 5.4c). These are in turn overgrown by prismatic quartz crystals, which can contain numerous layers of chlorite, which originally were deposited upon upward growing rhombohedral and prism planes (Fig. 5.4d). Chlorite in the veins is often associated with
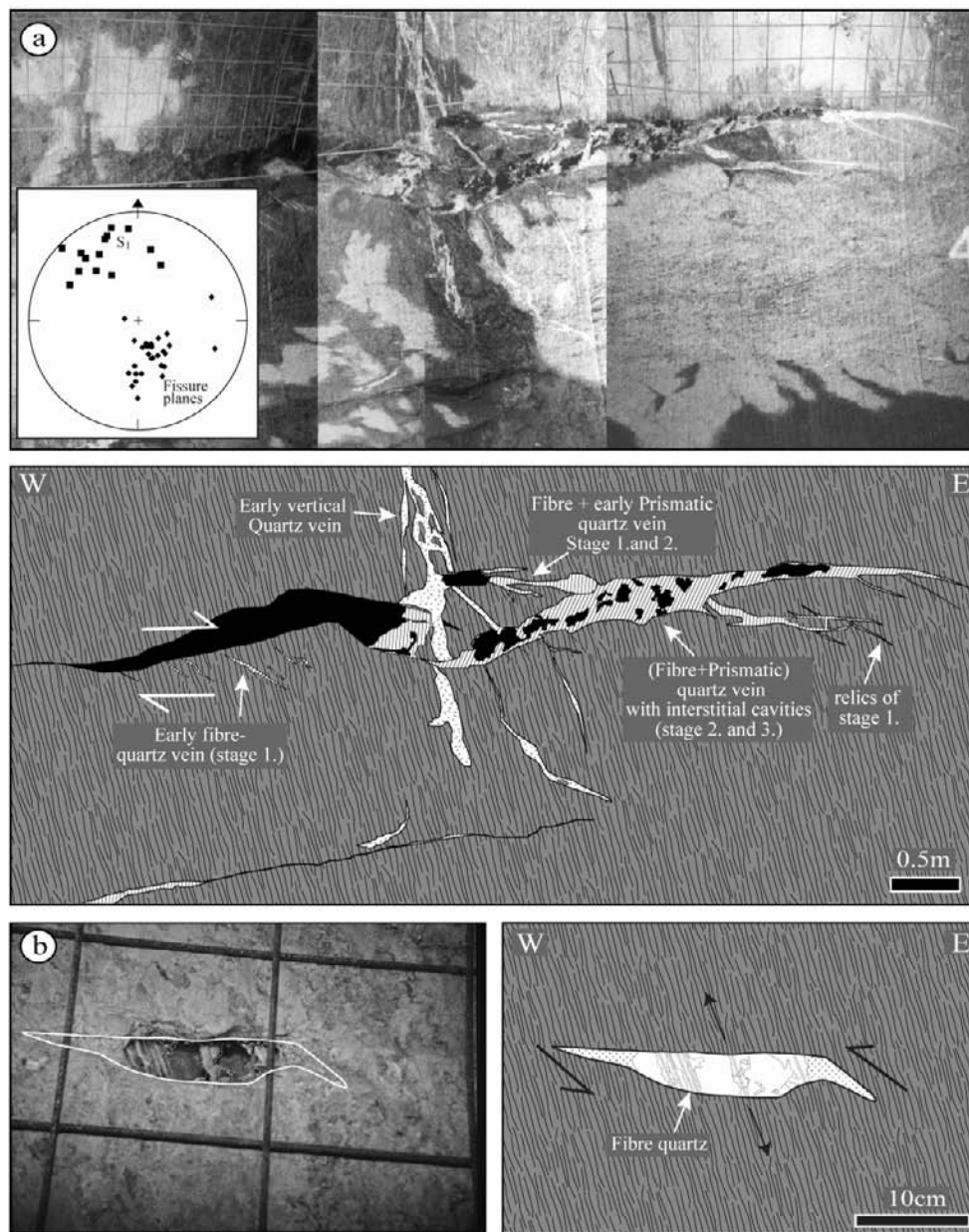
Fig. 5.2: a) Photograph's and sketches of different stages of Alpine fissure formation at locality 1670 meter (not further sampled). b) Photograph and sketch of small Alpine fissure with wall-to-wall fibre-quartz and adularia in a cavity at locality 1572 m.

adularia and at some stages with late albite (Fig. 5.4e) and during late precipitation events REE-carbonates and anatase (TiO_2) may have formed together with pyrite (Fig. 5.4f).

Petrography and geochemistry of the V_2 alteration zones

Bulk geochemical, density and porosity measurements of the alteration zones from three vein systems at 1160 m, 1570 m and 1710 m were performed to determine the amount of mass loss and gain near the vein interface (Fig. 5.5 and Table 5.1). Fig. 5.5 shows that within the alteration zone of Th.101 the SiO_2 content varies substantially from 70 to 63 wt%. However, the SiO_2 content of Th.106 remains nearly the same from 61 wt% to 58 wt%. The SiO_2 increase in the alteration zone of Th.103 is probably caused by microscopic interstitial veins in the alteration zones, such as shown in Fig. 5.4b. This is substantiated by the porosity increase of the alteration zone near Th.103. The Al_2O_3 concentrations also vary from 15.5 to 20 wt% in Th.101, whereas for Th.106 the values only fluctuate. The chemical composition of the host rock near the Th.103 vein is nearly constant for the three measured samples. The Na_2O, K_2O, MgO, CaO, Fe_2O_3 and TiO_2 compositions of the three studied veins are all relatively constant (Fig. 5.5e-h). This indicates that these components were not noticeably exchanged during the mineralisation in the veins. A relatively large density decrease can be noticed (Fig. 5.5i). These can be associated with differences in minor oxide or sulfide minerals in the veins.

Figure 5.3: Succession of deformation events and fissure and vein mineralisation.
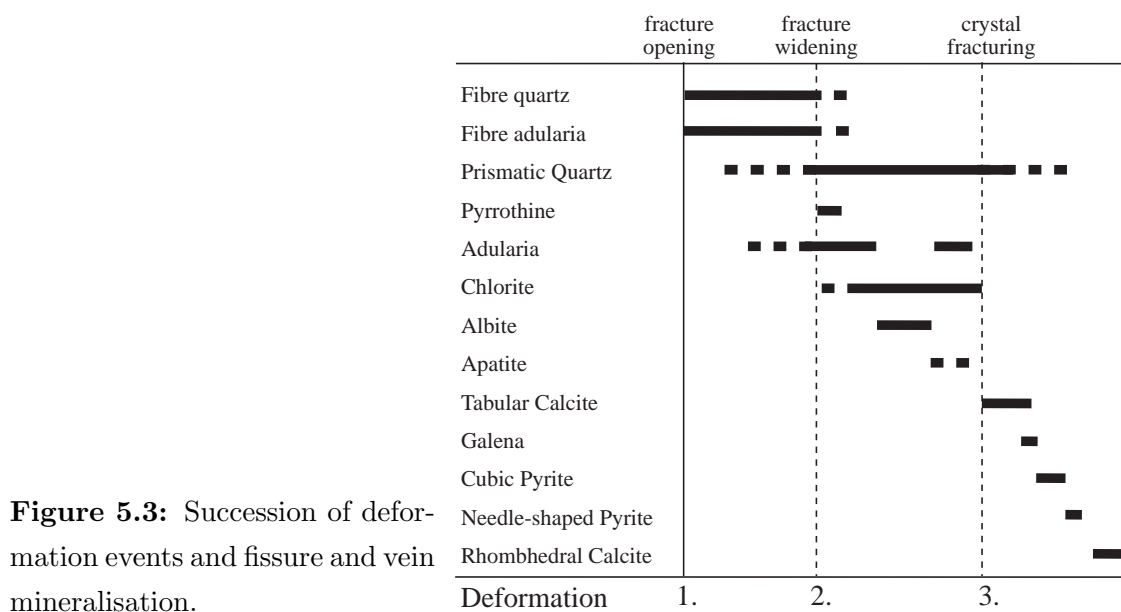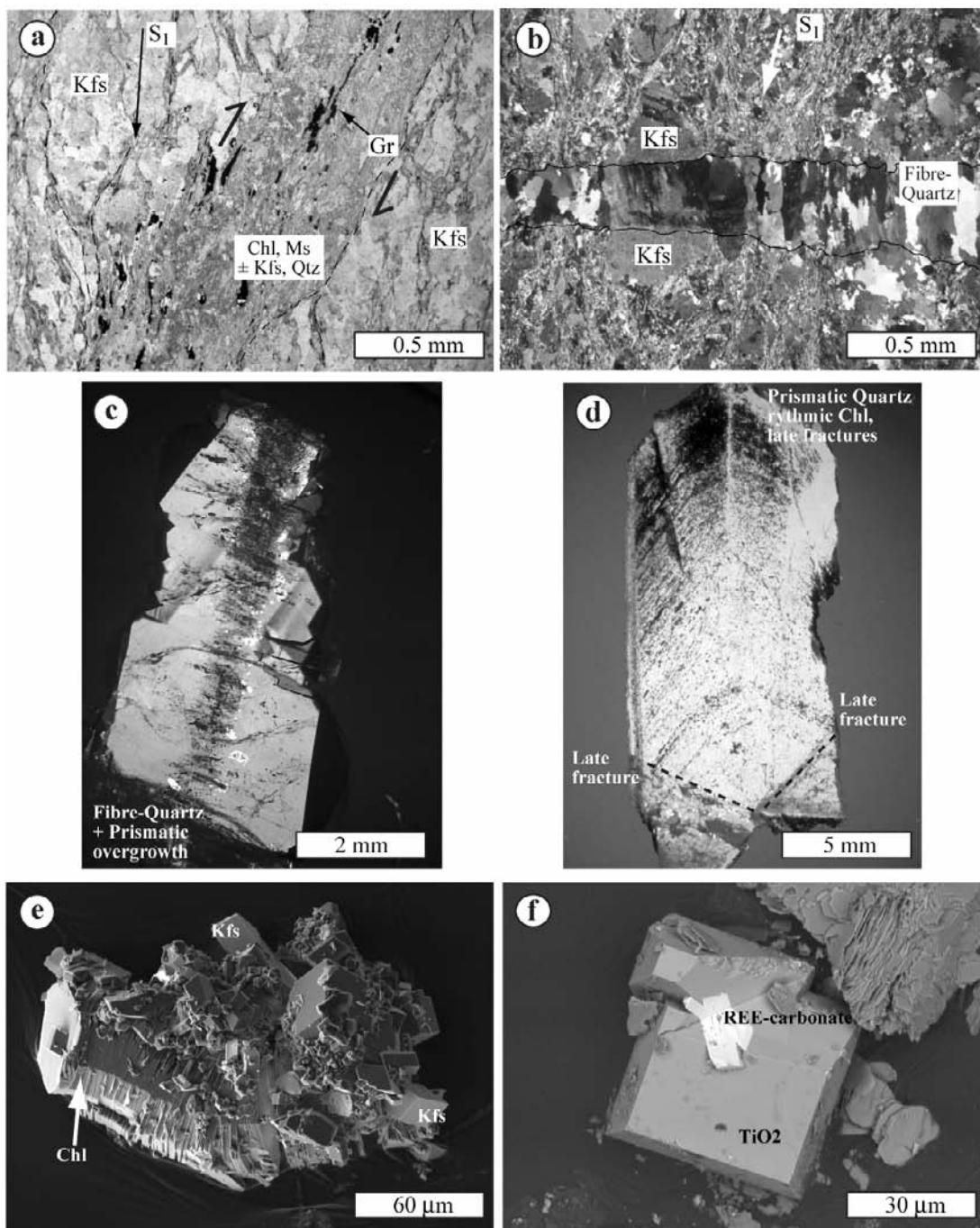
Fig. 5.4: Micrographs of host rock and vein microstructures: a) Kfs-chl-mu-qtz-gr schist with meandering S_1 foliation, cut in a slightly oblique orientation by mica and graphite rich layer (plain polarised light). b) Early fibre-quartz vein cutting the main foliation horizonatlly (crossed polarised light). c) Thick-section of fibre-quartz (middle) overgrown by prismatic quartz. (crossed polarised light). d) Thick-section of prismatic quartz with many cycles of chlorite precipitation on the rhomboedral and prismatic planes (crossed polarised light). e) BSE-SEM image of typical wormy chlorite with small adularia grown on top. f) BSE-SEM image of late anatase (TiO_2) crystal with REE-bearing carbonate.

Fig. 5.5: Geochemistry (a-h), density (i), and porosity (j) of altered wall-rocks around the veins from localities Th.101, Th.103 and Th.106.

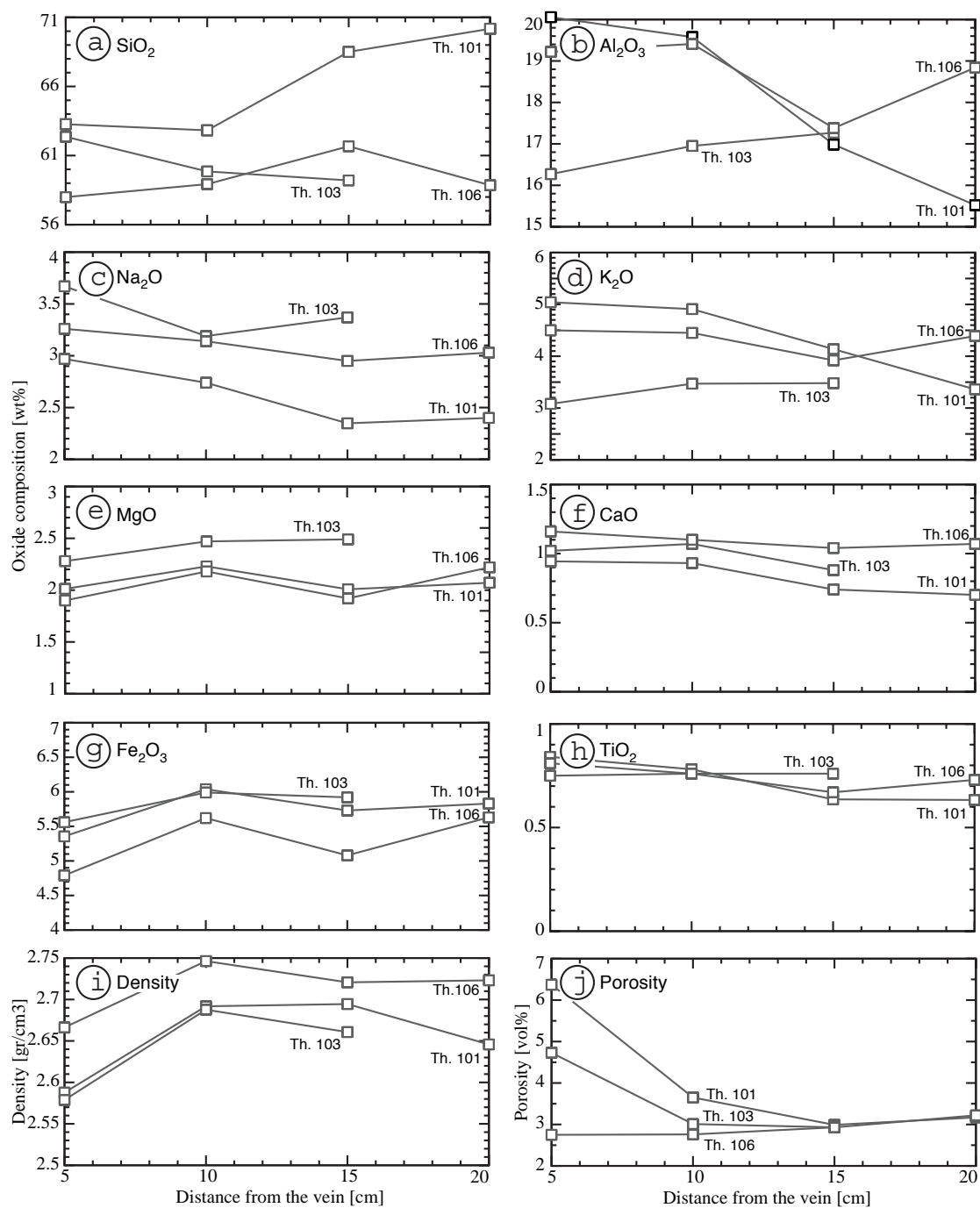| Vein system	Sample Nr.	Distance from vein [cm]	Porosity [vol%]	Density [gr/cm3]	SiO2 wt[%]	TiO$_2$ wt[%]	Al$_2$O$_3$ wt[%]	Fe$_2$O$_3$t wt[%]	MnO wt[%]	MgO wt[%]	Na$_2$O wt[%]	K$_2$O wt[%]	CaO wt[%]	Total wt[%]
1160 m	101	20	3.17	2.65	70.21	0.63	15.52	5.83	0.08	2.07	2.40	3.36	0.70	101.02
		15	2.99	2.69	68.40	0.64	16.98	5.73	0.08	2.01	2.35	4.14	0.74	101.32
		10	3.65	2.69	63.73	0.78	19.58	6.04	0.08	2.23	2.74	4.91	0.93	101.30
		5	6.37	2.59	63.67	0.84	20.06	5.36	0.07	2.01	2.97	5.04	0.94	101.23
1570 m	103	15	2.93	2.66	59.20	0.76	17.27	5.92	0.13	2.49	3.37	3.48	0.88	96.97
		10	3.01	2.69	59.85	0.76	16.95	5.99	0.14	2.47	3.19	3.47	1.07	97.55
		5	4.73	2.58	62.36	0.75	16.27	5.56	0.13	2.28	3.67	3.08	1.02	98.27
1710 m	106	20	3.22	2.72	58.85	0.73	18.84	5.63	0.07	2.22	3.03	4.39	1.07	98.13
		15	2.93	2.72	61.67	0.67	17.38	5.08	0.07	1.92	2.95	3.92	1.04	97.56
		10	2.76	2.75	58.93	0.76	19.41	5.62	0.08	2.18	3.14	4.45	1.10	99.03
		5	2.75	2.67	57.99	0.81	19.22	4.79	0.07	1.90	3.26	4.50	1.16	96.99

Table 5.1: Porosity, density and geochemistry of alteration zones around the veins from threelocalities.

Fluid inclusion topology and physical and chemical characteristics

Three different fluid inclusion populations from the three stages of vein formation were distinguished based on changes in melting and homogenisation temperatures (Fig. 5.6 and Table 5.2). Inclusions from early fibre-quartz are relatively large (up to 60 μm in size) and well healed (Fig. 5.6b). Fluid inclusions in fibre-quartz are perpendicular to the c-axis. Fluid inclusions in prismatic quartz are well-formed with an approximately negative quartz-shape and are between 2 and ≥ 20 μm in size (Fig. 5.6c). Late inclusions in prismatic crystals have irregular shapes, are often elongated parallel to the fracture plane in which they are situated and can be up to 60 μm (Fig. 5.6d). On these fracture planes fine prismatic quartz can newly precipitate and cause a late stage prismatic quartz growth (Fig. 5.4d). All inclusion populations are two-phase with vapour bubbles of between 5 and 15 vol% in size. The three fluid inclusion populations measured in all the veins did not always yield the same fluid inclusion properties, although their properties are very near near to one-another (e.g. melting temperatures between -2.6 and -4.8 °C and homogenisation temperatures between 154 and 180 °C, Fig. 5.6a). No volatile phases were detected by direct observation, by clathrate dissociation or by Raman-spectroscopy.

Crush leach analyses

Crush leach analyses were conducted on the analysed fluid inclusion populations (Fig. 5.7 and Table 5.3). In most cases only Li, Na and K were present in the inclusions. Except in

Th.103.3, Th.103.2.17 and Th.106.1 substantial amounts of Mg, Fe, Ca, Mn and to a lesser extend Cu, Rb and Sr were measured. However the high Fe/Na ratio indicate that the high Fe concentrations are probably caused by small particles of chlorite in the samples. Cl/Br ratios are rather typical of these types of fluids.

H-C-O compositions of fluid inclusions fluids and minerals.

Stable isotopic data (Table 5.4) of oxygen from minerals and hydrogen from fluid inclusions and hydrous minerals like chlorite allow to determine the isotopic compositions of the paleo-fluids. $\delta^{18}O$ values of vein quartz are between +8.9 and +9.9 ‰, while values of host rocks are between +7.5 and +8.2 ‰. Vein chlorite has values of +3.0 and +3.4 ‰
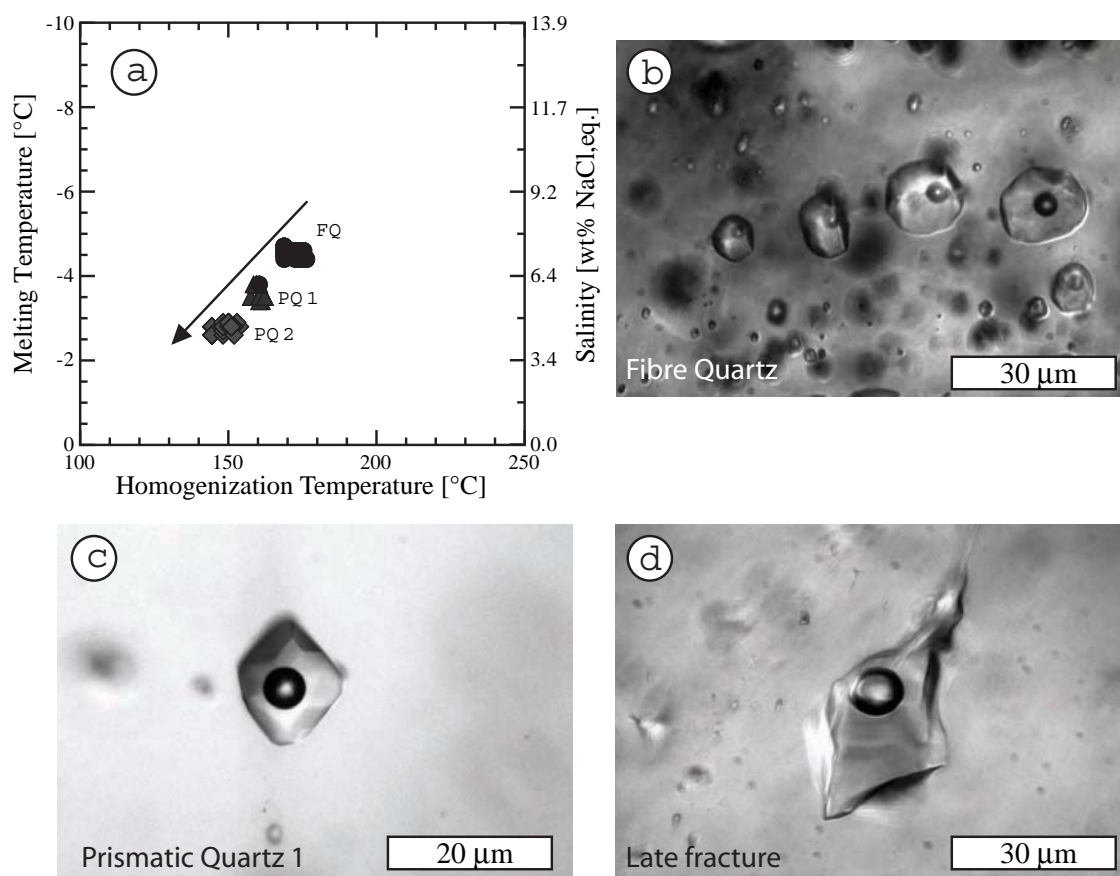

Fig. 5.6: a) Homogenisation and melting temperatures of the fluid inclusion populations of the three vein systems. Also shown are the converted salinities in weight% of the fluids. FQ = fibre-quartz, PQ = prismatic quartz. b-d) Characteristic fluid inclusions of the three investigated populations.

Locality	FP	HM	IT	nI	VoT	V%	Tm (ice)			Th (bulk)			wt% NaCl	Mol%		Density	Other features
							Average	Min	Max	Average	Min	Max		H_2O	NaCl	gr/cm³	
1160 Th.101	1	FQ	*	15	H2O	10	-4.5	-4.7	-4.4	169.0	168	171	7.1	97.7	2.3	0.88	crack seal
	3	PQ	PS	35	H2O	7	-3.5	-3.8	-3.4	161	160	162	5.69	98.2	1.8	0.94	internal fracture
	3	PQ	S	11	H2O	5	-3.8	-3.8	-3.8	159.0	158	160	6.1	98.0	2.0	0.94	on late fracture
1570 Th.103	1	FQ	*	15	H2O	10	-4.5	-4.6	-4.4	173.6	168	176	7.1	97.7	2.3	0.88	crack seal
	2	PQ	PS	35	H2O	6	-2.8	-2.9	-2.8	151.0	150	151	4.4	98.6	1.4	0.96	near Chl incl
	3	PQ	S	11	H2O	6	-2.8	-2.9	-2.6	149	147	153	4.7	98.6	1.4	0.96	on late fracture
1710 Th.106	1	FQ	*	17	H2O	15	-4.6	-4.8	-4.6	169.0	168	170	7.2	97.6	2.4	0.88	crack seal
	2	PQ	PS	15	H2O	15	-3.5	-3.5	-3.4	175	174	180	5.9	98.1	1.9	0.87	none
	3	PQ	S	15	H2O	15	-4.0	-4.0	-3.9	154	154	160	6.4	98.0	2.0	0.87	none

Table 5.2: Overview of the measured fluid populations from the three vein systems. FP: fluid population, HM: host mineral, IT: inclusion type (P = primary, PS = pseudo-secondary, * = can be interpreted to be both primary and pseudo-secondary), nI: number of inclusions, VoT: volatile type, V%: volume percent, T_m: melting temperature, T_h: homogenisation temperature, wt% NaCl: weight percent NaCl equivalent, Mol%: molar percent.
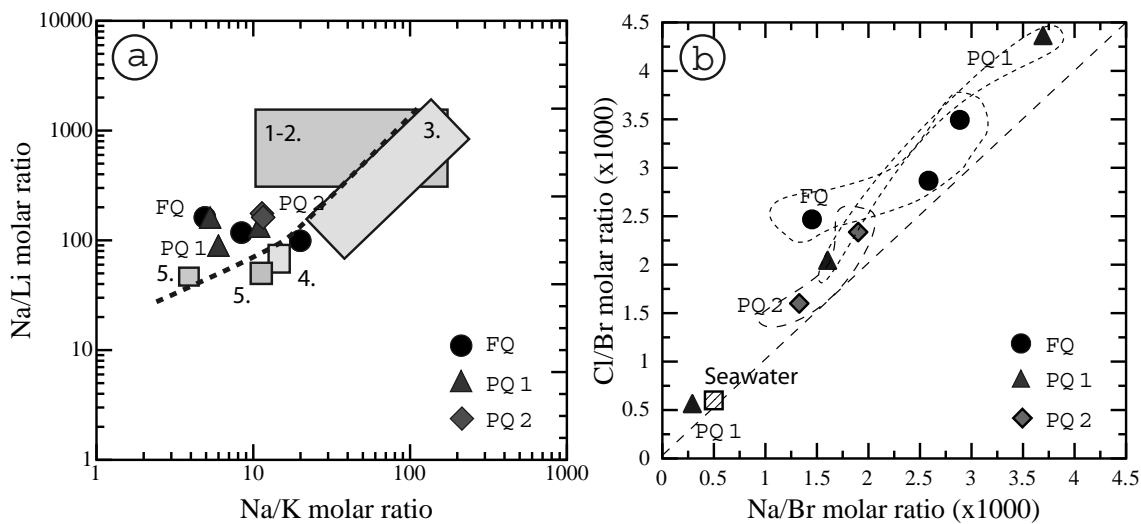
Fig. 5.7: Molar ratios of a) Na-K and Na-Li of the three fluid populations from the investigated localities and b) Na-Br and Cl-Br. In a) numbers 1-5 represent reference fluids: 1) Oil field brines after Carpenter et al. (1974); Kharaka et al. (1987), (2) Deep basin brines after Fischer and Kreitler (1987), (3) Hot water granites after Michard (1990) (4) deep waters from Soultz, Rhine Graben after Pauwels et al. (1993) and (5) Geothermal waters after Barnes (1979) and Henley et al. (1984). In b) the reference seawater Na/Br and Cl/Br values are indicated by the striped-square.

and calcite has $\delta^{18}O$ between +9.2 and +7.1 ‰. δD values of the extracted fluid inclusion fluids from the three quartz types scatter between −40 and −73 ‰, without an observable trend. δD values from fluid extracted from chlorite range between −71 and −55 ‰, similar to the inclusion fluids. If these values are converted to a maximum fractionation between water and chlorite of 40 ‰ the δD values of chlorite are approximately 10 ‰ higher than the inclusion fluids. (Fig. 5.8a). Carbon isotopes were measured for tabular calcite and rhomboedral calcite and for traces of CO_2 derived from fluid inclusions and for graphite from shear planes parallel to the host rock. Values for carbonate from Th.103 are relatively constant between −8.6 and −9.8 ‰, whereas the values measured from the inclusion fluids are lower between −13.2 and −19.5 ‰. Values for graphite are between −24.7 and −30.8 ‰. Recalculation of the measured oxygen values for quartz to water at the approximate temperatures of formation for the different fluid inclusion populations yields $\delta^{18}O$ of water between +3.3 and +4.3 for fluid population 1 from fibre-quartz, between 2.0 and 3.0 ‰ for fluid population 2 and between 2.3 and 2.9 ‰ for fluid population 3. As there is nearly no

Nr.	1	2	3	4	5	6	7	8
Mineral Type	FQ	FQ	FQ	PQ1	PQ1	PQ1	PQ2	PQ2
Sample number	Th.101.2	Th.103.3	Th.106.2	Th.101.2b	Th.103.2.17	Th.106.1	Th.103.17b	Th.106.1b
Fluid type	H2O-NaCl	H2O-NaCl	H2O-NaCl	H2O-NaCl	H2O-NaCl	H2O-NaCl	H2O-NaCl	H2O-NaCl
Fluid pop	1	1	1	2	2	2	3	3
Amount (gr)	0.35	1.53	0.4	0.4	1.1	1.32	0.2	0.35
Wt% NaCl	7	7	7	6	4.8	6	4.8	5.6
Li	7.4	1.2	0.9	0.2	0.7	0.1	0.45	0.5
Mg	-	14	-	-	18	13.875	-	-
Na	2567	616.25	358	88	224	51.25	247	257
K	252	185.5	70	14	57.5	14.5	38	39
Ca	-	165	-	-	5	31	-	-
Mn	-	9.76	-	-	9.76	0.76	-	-
Fe	-	210	-	-	334	19	-	-
Cu	-	1	-	-	0.8	0.5	-	-
Rb	-	1	-	-	0.3	<0.1	-	-
Sr	-	6	-	-	0.9	0.9	-	-
Cl	4709	1587	602	170	401	151	460	469
Br	3.08	1.47	0.48	0.19	0.21	0.61	0.45	0.67
SO4	-	38	60	7	60	-	-	9

Table 5.3: Crush-leach analyses indicating the cation and anion compositions of the fluid inclusion populations (abbreviations as in Table 5.2). Fluid pop = fluid population.

fractionation of $\delta^{18}O$ between water and chlorite at these temperatures the measured $\delta^{18}O$ composition approximately represents the isotopic composition of the paleofluid. They are also comparable to the $\delta^{18}O$ composition calculated from quartz and tabular calcite. $\delta^{18}O$ calculation of rhomboedral calcite is 3 ‰ lower at the lower temperature estimated.

5.5 Discussion

Stress orientation during vein opening and dilation

The orientation of the regional stress regime during and after the tectonic separation of the Aar massif was characterised by a SE-NW σ_1 (Schmid et al., 1996) and a vertical or horizontal SW-NE σ_3. This is also reflected in the orientation of small fibre-quartz veins which are mainly NE-SW oriented and dipping to the NW and the similar oriented but SE dipping S_1. Early veins that were further extended and later veins may be re-oriented with respect to the earlier vein orientation, but this does not reflect a change in stress orientation as the veins themselves were only formed within a relatively short time-span. The re-orientation of the veins is related to changes in the response of the rock to the prevailing stress regime or consequently to local inhomogeneities. The complex vein-set geometry as is observed in the tunnel is more a result of viewing the veins parallel to their strike than actual changes in sense of deformation. As noted by Smith (1995) and Smith (1996) the three dimensional pattern of en-echelon veins is relatively complex and accurate.

Thermometry of fluids and minerals

K/Na ratios of fluids: K/Na ratios of K-feldspar and albite bearing rocks have been used to infer the temperature of the fluids (e.g. Poty et al., 1974; Lagache and Weisbrod, 1977; Fournier, 1979; Fouillac and Michard, 1981; Michard, 1990; Verma and Santoyo, 1997), based on thermodynamic data and analyses of geothermal fluids of known temperature. In this study the relation of Verma and Santoyo (1997) was used to establish the temperature as this provides nearly similar temperatures as previous calibration of Michard (1990). The temperatures obtained from this thermometer coincides with temperatures obtained from stable isotope data and the Na/Li ratios in the fluids (see paragraphs below). The K/Na thermometer of Poty et al. (1974) (Fig. 5.9a) has 50 °C higher temperatures than the Verma and Santoyo (1997) thermometer at temperatures $< 250°C$. At temperatures $> 300 °C$ for the Verma and Santoyo (1997) thermometer this difference becomes approx-

Veinsystem Distance Nr into tunnel	Sample nr	Mineral V=vein, H=Host rock	$\delta^{18}O$ mineral (‰ vs. VSMOW)	1σ	δD (‰ vs. VSMOW)	1σ	$\delta^{13}C$ (‰ vs. PDB)	1σ	Approx Tf (°C)	$\delta^{18}O$ H2O (‰ vs. VSMOW)	δD H2O (‰ vs. VSMOW)
Th.100 210m	100.1	Graphite(H)	-		-		-24.7		-	-	-
Th.101 1160m	101.0	Qtz(H)	8.25		-				-	-	-
	101.1	FQ(V)	9.93		-55	5	-17.5		350	4.33	-55
	101.2	Chl(V)	3.44		-67	3			300	3.44	-27
	101.3	PQ.1(V)	9.83		-73	5			300	3.03	-73
Th.102 1270m	102.1.1	Graphite(H)	-		-		-30.8		-	-	-
Th.103 1570m	103.0	Qtz(H)	7.52		-				-	-	-
	103	Chl(V)	-		-53	3			300	-	-13
	103.40	FQ(V)	9.94		-71	5			350	4.34	-71
	103.1.3.1	PQ.1(V)	8.86		-69	5			300	2.06	-69
	103.1.3.2	PQ.2(V)	9.78		-46	5	-16.9		300	2.979	-46
	103.1.5.1	TCc(V)	8.7		-		-9.8		300	4.61	-
	103.2.27	TCc(V)	9.2		-		-8.6		300	5.11	-
	103.1.1.2	RCc(V)	7.6		-		-9.8		250	1.88	-
	103.1.2b	RCc(V)	7.1		-		-9.2		250	1.34	-
	103.2.19	Graphite(V-H)	-		-		-27.1		-	-	-
Th.106 1710m	106.0	FSP/Qtz(H)	7.6		-				-	-	-
	106.1	FQ(V)	8.96		-57	5	-13.2		350	3.36	-57
	106.2	Chl(V)	3.01		-70	3			300	3.01	-30
	106.3	PQ.1(V)	9.49		-40	5	-19.7		300	2.69	-40
	106.3.2	PQ.2(V)	9.10		-53	5	-11.6		300	2.30	-53

Table 5.4: H-C-O stable isotope compositions of chl-qtz-cc-gr and C-H compositions of vein-fluid populations. FQ: fibre-quartz, PQ1: early prismatic quartz, PQ2: late prismatic quartz, TCc: Tabular calcite, RCc: Rhomboedral calcite, Chl: Chlorite, FSP: K-feldspar, Qtz= Quartz.
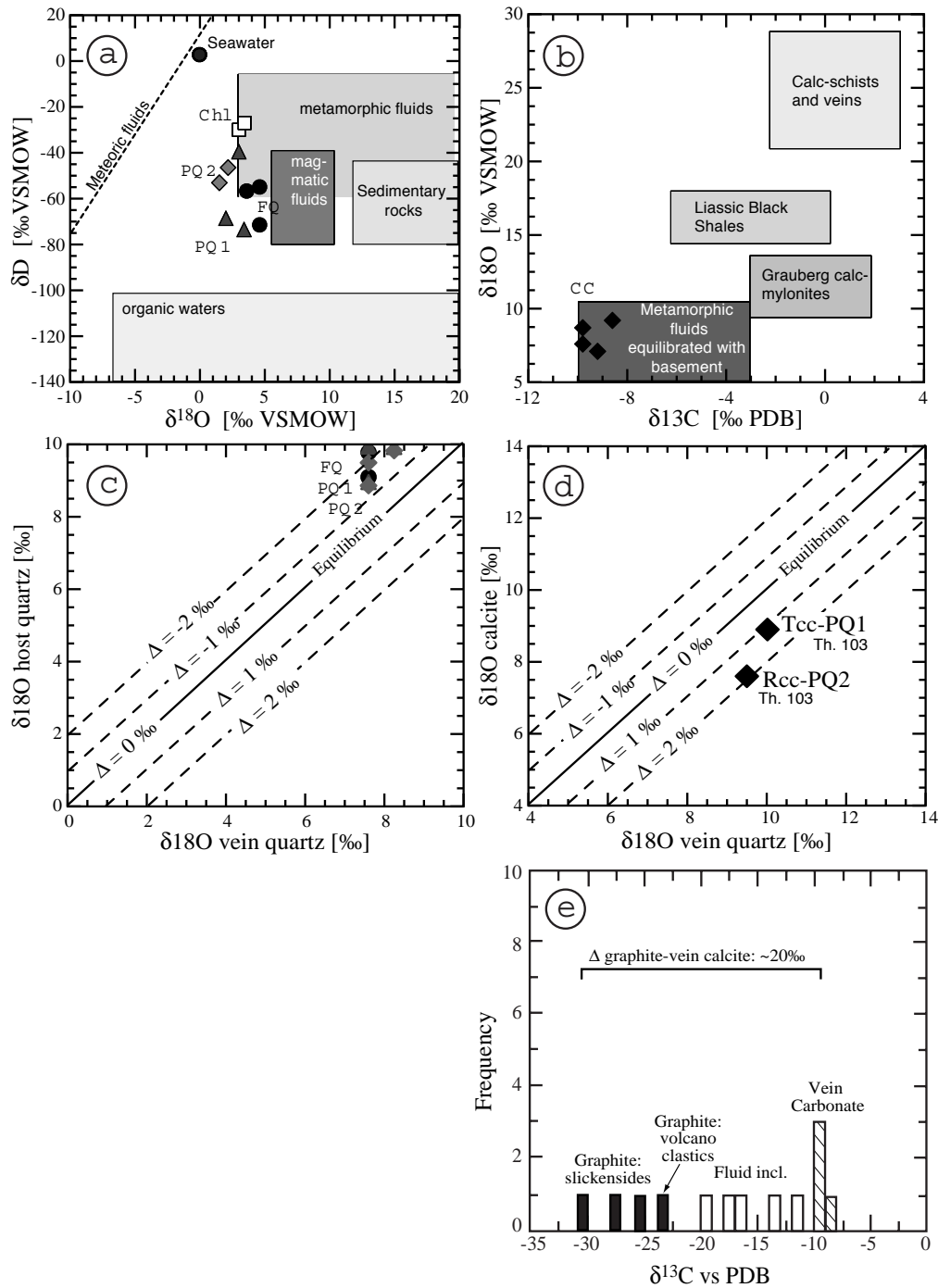
Fig. 5.8: H-C-O systematics of fluids and minerals. a) Recalculated oxygen and hydrogen isotopic values for vein fluids based on H isotope measurements from fluid inclusions, oxygen isotope measurements of quartz and H,O isotope measurements of chlorite. Organic water field is from Sheppard (1986). b) C-O isotope measurements of vein carbonates. Different fields are from Henry et al. (1996). c) Comparison of oxygen isotopic composition of vein and host rock quartz. ($\Delta = \delta^{18}O_{vein} - \delta^{18}O_{Host-rock}$) d) Comparison of the oxygen isotopic composition of vein calcite and vein quartz. e) C-isotope comparison of carbon bearing minerals from veins, graphite slickensides, underlying volcanoclastics and fluid inclusions.

imately 90 °C, which is relatively large. The Verma and Santoyo (1997) thermometer was calibrated between 100 and 350 °C, while the thermometer of Poty et al. (1974) and of others were calibrated between 300 and 600 °C. It is likely that the real temperatures are somewhere in between both thermometers. Figure 5.9a also indicates a tendency of increasing Na/K ratios from early to late fluid inclusion populations and therefore decreasing temperatures.
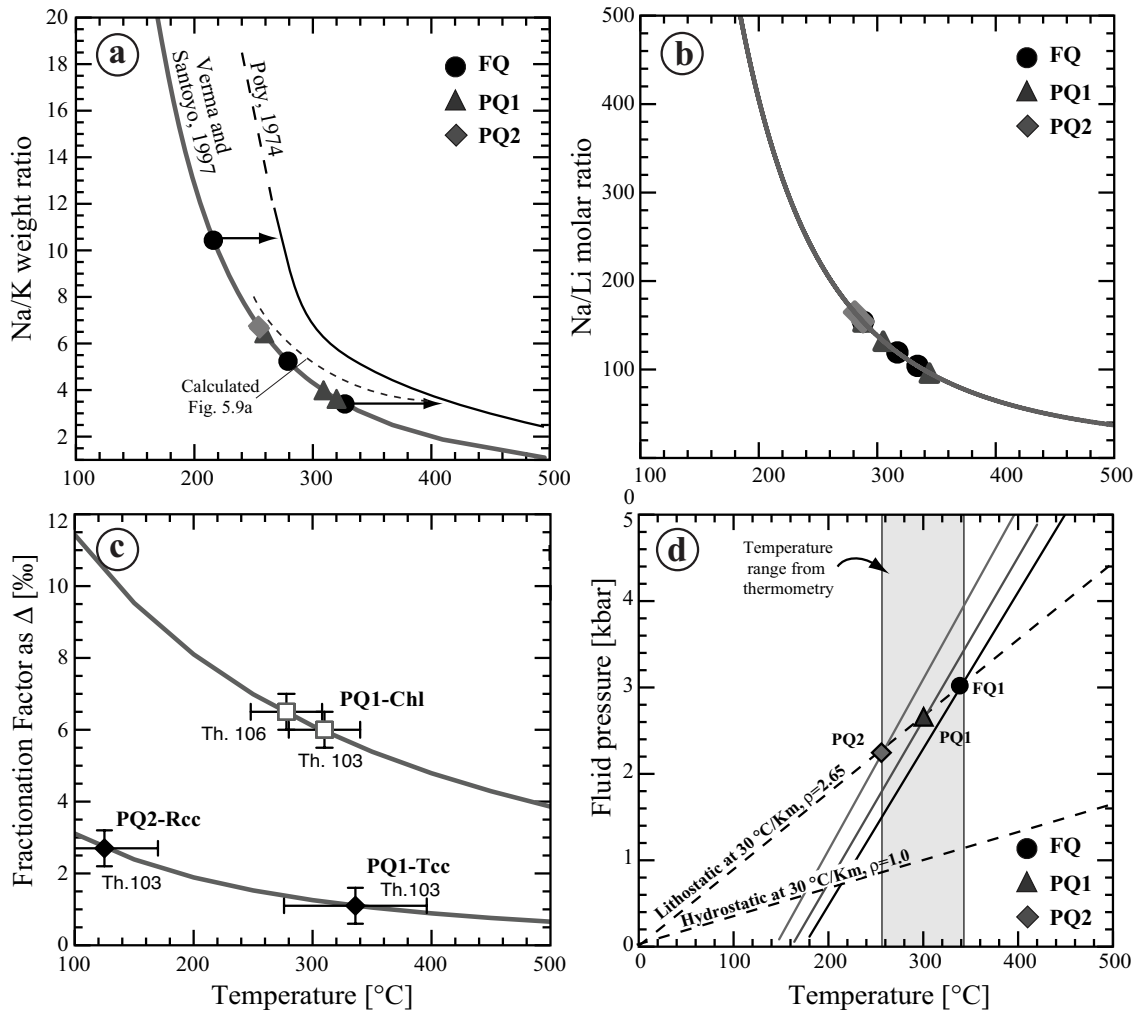

Fig. 5.9: Thermometric calculations by using a) the Na/K ratios from the crush-leach analyses, b) Na/Li ratios of the crush-leach analyses, c) fractionation factors of qtz-cc and qtz-chl. Thermometric relations of a) and b) are from Verma and Santoyo (1997) while for c) The qtz-cc is from Zheng (1993) and the qtz-chl relation is calculated from qtz-H_2O and Chl-H_2O fractionation. d) shows the temperatures inferred from a-c) in a *PT*-diagram together with the calculated isochores for the three different fluid populations (FP1-3) and the lithostatic and hydrostatic geothermal gradient of 30°C/km.

Na/Li ratios of fluids: Molar Na/Li values show a variation between 90 and 160, with

the earliest fluid populations, 1 and 2, having lower values and fluid population 3 slightly higher values (Fig. 5.9b). These ratios result in temperatures between 340 and 270 °C. The relatively consistent Na/Li ratios also indicate that the estimated temperatures are probably close to the real trapping temperatures.

Stable isotope mineral pairs: Temperature determinations were also done using chlorite-quartz and calcite-quartz mineral pairs (Fig. 5.9c). As chlorite precipitated mainly during prismatic quartz growth the values for these quartzes were used for temperature determination. Values for quartz, tabular calcite and rhomboedral calcite were calculated from samples of locality Th.103. (Table 5.4). The fractionations for tabular calcite were calculated using prismatic quartz I and for rhomboedral calcite with prismatic quartz II as these grew on top of tabular calcite. Both quartz-chlorite values are between 280 and 300 °C. PQI-Tcc is at 340 °C and PQII-Rcc is at 120°C. However, as the quartz-calcite fractionation is relatively small the temperature calculations are expected to be larger than for quartz-chlorite.

PT-conditions of vein formation: The temperatures calculated for the vein formation can be directly related to the fluid isochores, giving pressure estimates of approximately 3.1 kbar at a temperature of 340 °C for early fibre-quartz (fluid population 1) formation (Fig. 5.9d). Prismatic quartz formed at slightly lower pressures of 2.6 kbar at a temperature of around 300 °C and late prismatic quartz formed at a pressure of 2.3 kbar at a temperature of 260 °C. These pressures would represent approximately 10.6, 10 and 8 km depth at a geotherm of 30 °C/km. If it is correct to assume this geotherm the fluids were at approximately lithostatic pressure during fluid trapping and mineralisation. The formation temperature was established independent from fluid inclusion isochores. Fluid-pressures determined from this study may not be the same as the pressure in the host rock, because under dis-equilibrium conditions fluid pressure can easily fluctuate. However, it is not likely that large fluid over-pressures existed as the host rock was repeatedly fractured forming fibre-quartz and chlorite deposition on the prismatic quartz. Similarly, under-pressures would have caused collapse of the veins, which was not observed. The geothermal gradient may have been up to 5 °C lower than the assumed 30 °C/km, which in that case would imply sub-lithostatic fluid pressures in the veins.

Origin of mineralisations and mineralising fluids

The calculated paleofluids as indicated in Fig. 5.8a show that they are positioned at the lower end or slightly below the metamorphic water field with respect to δD and δ^{18}O of

water. Apart from the slightly decreasing δ^{18}O values, there is no systematic trend from early to later fluids. This trend is caused by converting δ^{18}O of quartz to δ^{18}O values of water at the specific temperatures of formation. δ^{18}O and δ^{13}C values of calcite (Fig. 5.8b) show that the calcite was derived from fluids equilibrated with basement rocks as is to be expected for a the meta-sedimentary host rock, which is part of the crystalline basement of the Aar massif. As is indicated by the δ^{18}O values of host-rock and vein quartz (Fig. 5.8c) the oxygen system was close to an equilibrium, albeit the host rock values may have been a bit lowered due to possible impurities in the samples. Comparison of the δ^{18}O values of the measured vein calcite and vein quartz samples (Fig. 5.8d) indicates a difference between +1 and +2 ‰, showing that the samples were equilibrated. These values were used for thermometry.

Na, K and Li compositions are typical of high temperature metamorphic fluids (see also Fabre et al., 2002, and in chapter 4). The relatively high variability in Br/Cl ratios and Na/Br ratios might imply that the fluids were mixed with several metamorphic fluids that each have different Cl, Br and Na compositions. This is explained by heterogeneous Cl and Br concentrations in surrounding pore fluids, which are possibly relicts of different extends of hydration, dehydration and mixing during pre-Alpine and Alpine metamorphism.

The observed 2.4 wt% NaCl-depletion requires the addition of 0.5 kg pure H_2O to every 1 kg H_2O available in the vein. External fluids probably also contain some salt, so the value of 0.5 kg H_2O is only a minimum value. Mullis et al. (1994) have shown that this salt depletion is common in the Central Alps with only incidentally large episodic increases in salinity due to retrograde boiling or fluid mixing with fluids derived from evaporitic sequences. This implies that the dilution observed in the studied veins is regional and generally occurring. There are four possibilities to explain the salinity decrease: 1) Surface derived salt-depleted fluids slowly permeated the Aar massif upon cooling and exhumation, but their H and O isotopic compositions and their Na, K and Li cation compositions were equilibrated with the rocks through which they have moved. 2) Salt-depleted formation fluids flowed downwards from structurally higher positions, but were not directly derived from the surface. 3) Salt-depleted fluids are derived from below, which would equally explain their stable isotopic and geochemical compositions. 4) During ongoing mineralisation the salinity of the fluid decreased, due to incorporation of anions as well as cations in minerals.

As the host rocks in which the vein systems occur are generally impermeable it is unlikely that meteoric fluids could penetrate to depths of approximately 8 km, without the presence of additional permeable structures. In the case of Mullis et al. (2001) and in chapter 4, large

vertically dipping fracture systems were observed which are more likely to transport fluids downwards, when they form an interconnected fracture system. However, these fractures are highly localised both on a meso- and a macro scale and will therefore not be able to dilute vein fluids pervasively. In fact, in chapter 4 retrograde depletion of saline fluids was also documented in the typical Alpine fissures, which did not record the meteoric influence and only when they were cut by late vertical fractures did late quartz precipitate from meteoric fluids (Mullis et al., 2001). Sharp et al. (2005) did record meteoric compositions for late chlorite precipitated in Alpine fissures, but this was only in a few instances of their total sample collection, which for the rest mainly showed metamorphic values. This therefore indicates that possibility 1) is unlikely but possible. Similarly possibility 2) and 3) are also possible, but more likely as they do not require large scale flow patterns. Possibility 4) is unlikely because mineralisation within the vein is mainly H_2O consuming when relatively large amounts of chlorite precipitate and would therefore tend to increase the salinity of the mineralising fluids.

Fluid-mineral equilibria and vein formation
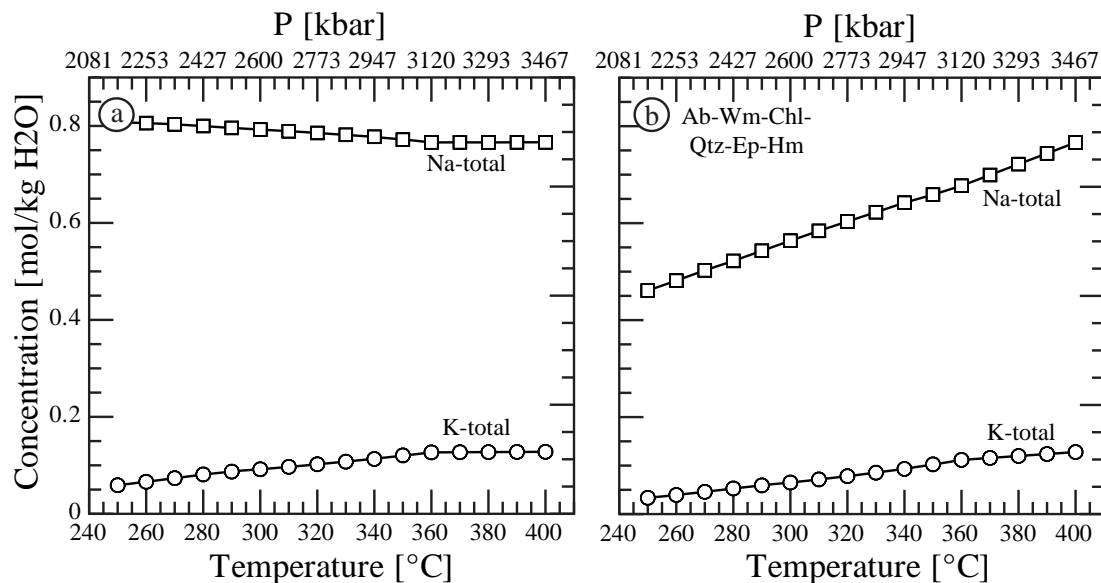
Fig. 5.10: Evolution of Na and K concentration in the metasedimentary host rock over a geothermal gradient of 30 °C/km where a) total Cl concentration remains constant at 0.9 molal and b) total Cl concentration changes continuously from 0.5 to 0.9 molal and b) . Note the same trends are produced only temperature changes when pressure remains constant. The total Cl concentration is buffered by the amount of HCl dissolved in the solution.

Fluid-mineral equilibria were calculated by applying an extension to the Theriak/Domino software of de Capitani and Brown (1987), which is capable of calculating the speciation of a fluid related to the equilibrium mineral assemblage of a bulk rock system. The influence between bulk-rock chemistry, stable mineral assemblages and the speciation of pore-fluids can be predicted for different P, T and different Cl concentrations in the fluids (see also chapter 3).

The mineralisation in the veins was influenced by four factors: 1) decreasing temperature upon cooling at near lithostatic fluid pressures, 2) increased opening of the fractures leading to larger amounts of fluid available to the vein, 3) little host-rock alteration, which suggest addition of material in the vein was either solely from the fluid in the vein or more likely with additional material from infiltrating fluids, 4) decreasing salinity from early to late fluids from 7 to 4.6 wt% eq. implies dilution of the fluid with small amounts of external low-saline fluids, as indicated in the previous section.

Early vein mineralisation is related to repeated fracturing and quartz precipitation. It is likely that diffusion of material due to chemical potential gradients induced by pressure and/or small differences in chemistry between pore-fluids and the fluids in the open fractures led to continued precipitation during early opening phases (see also Fisher and Brantley, 1992; Wangen and Munz, 2004). During continued fracturing more fractures formed and older fractures were inter-linked, making it possible for fluids to flow at a scale ~ 10 m.

Figure 5.10a,b shows modelled Na and K concentrations in both constant and changing Cl concentrations along a geothermal gradient of 30 °C/km. The bulk chemistry of sample Th.103.1 (Table 5.1 was converted to molar amounts and used as input for the routine, yielding a constant assemblage of ab-wm-chl-qtz-ep-hm-sph. In the case of constant Cl concentrations, the Na concentration in the fluid tends to decrease with increasing temperatures (Fig. 5.10a). In the case of decreasing Cl contents in the fluids (dilution), K and Na concentrations of the fluids both decrease as they are directly linked to the amount of Cl. However the Na concentration is more affected by the Cl decrease than the K concentration, but it would imply that albite and K-feldspar would be precipitated together (Fig. 5.10b). As the Si concentration decreases with temperature and pressure quartz will precipitate additionally. In the studied veins, albite formed only during one event and not continuously like K-feldspar. It is therefore likely that there was a short interval of up-temperature flow (as implied by Fig. 5.10a) in the host rocks around the veins causing albite precipitation.

5.6 Conclusions

En-echelon veins were studied using structural methods and geochemical and stable isotopic techniques and shows that:

1. Early veins were small, but became extended and interconnected upon further fracturing of the rock. A stress regime with sub-vertical extension and SE-NW compression together with high fluid pressures is a probable cause for the opening and enlargement of the fractures.

2. These veins formed during or slightly after peak Alpine (low-grade) metamorphic conditions at T = 350 °C and at approximately 3.5 kbar (11 km depth) and remained fluid filled until T = 250 °C and 2.5 kbar (8 km) depth. The veins are related to late Alpine exhumation stages of the Aar massif between 18 to 13 Ma.

3. The main mineralisation was dominated by quartz and different alumino-silicates, but also traces of sulphides were found. The fluid inclusion characteristics of the three fluid inclusion populations imply slight salinity decreases upon cooling, without large changes of the Na/K or Na/Li ratios as obtained from crush-leach analyses. In addition the Cl/Br and Na/Br ratios are highly variable, which suggests variable fluid compositions present in the veins. The amount of material leached from the host rock is small and the veins are nearly completely mineralised. Short intervals of albite precipitation during K-feldspar precipitation can be explained by influx of fluids from lower temperatures. Down-temperature and up-temperature fluid circulation within the surrounding meta-sediments explains these features.

4. Furthermore stable isotope evidence from fluid inclusions and minerals indicates that these fluids were metamorphic fluids equilibrated with the crystalline basement, without large changes in H and O compositions among subsequent fluid inclusion populations. Un-equilibrated surface-derived fluids did not play a role in the observed vein mineralisation.

Chapter 6

Conclusions

6.1 General conclusions

The integrated structural, analytical and theoretical approach of this thesis leeds to the following conclusions:

The study of veining and mineralisation in the Fibbia area (chapter 3) resulted in distinguishing five different vein types. The first formed prior to peak metamorphic Alpine conditions ($V_{1a,1b}$). The second vein generation formed at or slightly after peak metamorphic conditions, after the development of the S_1 foliation. V_3 to V_5 formed during retrograde stages and continuous exhumation of the Gotthard massif. The early retrograde V_2 veins formed during SE-NW compression and near-vertical extension (≥ 20 Ma), while later V_3 to V_5 veins formed during near horizontal SW-NE extension (~ 17–14 Ma). The fluid inclusions show that the fluid chemistry and PT-conditions of mineralising fluids changed markedly from peak metamorphic to late retrograde conditions, which can be related to changes in style of mineralisation and the fluid sources. Fluids compositions changed from early CO_2-bearing inclusions (V_{1b} and V_2) to later CO_2-free aqueous saline fluids (V_3 and V_4) and ultimately to salt-depleted fluids (V_5). All fluids contain cations typical of granitic rocks (e.g. Na, K, Li, Ca), which indicates that these cations were equilibrated with the host rocks. Predicting the fluid compositions of the Fibbia granite at the conditions of vein formation shows that with decreasing PT-conditions certain minerals will precipitate after one anothers as is indicated by changes in K and Na concentrations in fluids and yields information on the equilibrium concentrations of Fe and Mg for different salinities. The following minerals precipitated together in V_2 veins: bt+ab+qtz, qtz+ad+ap. These formed between 420 and 350 °C and 3 to 2 kbar. phg+hm+rt±qtz and chl±qtz precipitated between 350 and 300 °C and 2 to 1.5 kbar in V_3 and V_4 veins. In all cases vein mineralisation was related to the host rock, at approximate equilibrium conditions with low fluid-rock ratios. In contrast, V_5 vein mineralisation of needle and split-growth quartz formed during dis-equilibrium conditions and is related to external fluid flow between 300 and 150 °C and at 0.9 to 0.7 kbar fluid pressure.

The study of fluid origins and flow-paths (chapter 4) has shown that there was a marked change in fluid origin from pre-Alpine, prograde Alpine veins (V_{1a} and V_{1b}) and early retrograde Alpine veins (V_2) to late retrograde veins (V_5). Fluids trapped in pre-Alpine and prograde Alpine veins have a similar composition to the earliest V_2 fluids, as fluid inclusions in V_1 veins were continuously re-equilibrated during prograde heating with pore fluids. The earliest V_2 fluids represent the metamorphic fluids present in rocks during and immediately after maximum temperature conditions and were related to a thermodynamically closed system. During intermediate retrograde stages fluids with a possible external

metamorphic origin could have penetrated the Fibbia granite, while during late retrograde stages heated meteoric fluids originating from a high altitude catchment area precipitated the silica. This evolution marks an increase in the scale of fluid flow from cm to $>$ km scale and shows that meteoric fluids penetrated relatively deep in the internal parts of the cooling and exhuming Alpine orogen, even during ongoing SE-NW compression.

Fissure opening and mineral precipitation occurred in the Amsteg area at lower *PT*-conditions than in the Fibbia area. Three stages of brittle fracturing and dilation-controlled fissure opening, enlargement and the distinct fissure mineralisation. Brittle en-echelon veins were formed and extended by continuous fracturing, which is however related to a similar stress regime as for the V_2 veins from the Fibbia area. These veins formed during or slightly after peak Alpine (low-grade) metamorphic conditions at T $\geq$ 350 °C and $\geq$ 3.5 kbar (11 km depth) and remained fluid filled until T $\sim$ 250 °C and 2.5 kbar (8 km) depth. Vein formation is related to late Alpine exhumation stages of the Aar massif between 18 to 13 Ma. The main mineralisation was dominated by quartz and different alumino-silicates which is similar as in the Fibbia area, but also traces of sulphides were found which are related to organic rich layers in the host sediments. The fluid inclusion characteristics of the three fluid inclusion populations show slight salinity decreases upon cooling, without large changes of the Na/K or Na/Li ratios as obtained from crush-leach analyses. In contrast Cl/Br and Na/Br ratios of fluid inclusion populations are highly variable, which suggests that variable fluid compositions were present in the veins. The amount of material leached from the host rock is small and the veins are nearly completely mineralised. Short intervals of albite precipitation after K-feldspar precipitation can be explained by short periods of fluid flow from lower temperatures. This is confirmed by slight variations in δD of the mineralising fluids and the small decrease in salinity. However, the mineralising fluids had a metamorphic signature, which excludes obvious input of meteoric waters during late stages of mineralisation.

6.2   Suggestions for further research

1. A more regional geochemical and stable isotope study of late V_3 and V_4 fractures could provide more information on the the origin of mineralising fluids in these fracture systems and could elucidate the question of whether meteoric fluids did infiltrate along these fracture systems and if they did what the scale is of the affected area. Additionally, when muscovite or other datable minerals are present in these types of veins, dating them could place better constraints on the timing of their formation.

2. Fluid thermometry based on relations between certain aqueous species and minerals could be an interesting tool to determine the temperature of fluid inclusion fluids during trapping. Systematic experiments from Orville (1963); Lagache and Weisbrod (1977) and recently Hauzenberger et al. (2001); Pak et al. (2003) and analyses from hydrothermal systems have shown that that relations between Na, K and Ca could be used to determine temperature at low to medium temperature conditions. However, additional experiments in which minerals completely equilibrate with the fluid are necessary to completely constrain the equilibrium compositions of the fluids. It is important to study the Na, K, Ca concentration differences with respect to changes in stable mineral assemblage. In addition, the Cl concentrations in the fluids should be varied to determine the dependency of cations on chlorinity. Such experiments however may prove difficult because of the low rate at which samples equilibrate at low temperatures.

3. Chapter 4 and 5 have shown that it is useful to analyse the hydrogen isotopic compositions of hydrous minerals together with fluid inclusions in order to unravel the origin of orogenic fluids. This requires exact knowledge of the hydrogen equilibrium isotopic fractionation coefficients between minerals and fluids at the approximate PT-conditions of mineral formation. As this coefficient has not yet been accurately determined further research is necessary to constrain it better.

4. As the dataset for Alpine formed veins from the surface is relatively large, this can be used in addition to fluids derived from veins from tunnel projects like the NEAT, to gain additional knowledge and to compare with fluids derived from the same area but from a greater depth.

5. Further refinement and better integration of the SUPCRT database with the Berman and/or Holland and Powell thermodynamic databases is essential to gain further understanding of hydrothermal processes. In addition, it is important for under-

standing of high temperature hydrothermal systems to extend the usability of The-riak/Domino, so that it can also be used as a tool to determine reaction-paths, similar to EQ3/6 (Wolery, 1992). The advantage would be that complex solid so-lutions or even melts could be integrated in such modelling. This is necessary to understand complex mineralisations. However, this requires further development of the numerical codes. Veins formed at higher metamorphic grade could prove more useful then veins from this study to exactly compare mineralisation in a constrained PT-range with mineralisation predicted from thermodynamic models and data, as the thermodynamic data for metamorphic minerals are mostly calibrated for medium to high-grade metamorphic conditions.

Appendix A

Deep-percolating meteoric waters in the Central Alps.[*]

Abstract

In order to investigate the origin of mineralising fluids that have precipitated quartz in Alpine fissures and fractures of the northern Pennines and the southern Gotthard Massif, the quartz and their included fluids were examined for their stable isotope and fluid inclusion geochemistry. Distinct groups of quartz could be differentiated on the basis of their occurrence, textural appearance, and composition of included fluids: 1) Tessin-habit quartz formed from a CO_2-enriched fluid in small SE-NW striking Alpine fissures at 450 to 410 °C and 3.5 to 2.2 kbars, 2) needle-like quartz precipitated from aqueous fluids with little to no CO_2 at about 320 to $\leq$ 250 °C and 1.8 to $\leq$ 0.8 kbar in large SE-NW striking, nearly vertically dipping fracture systems, 3) split-growth quartz precipitated ind the same fractures at between 250 to 180 °C and $\leq$ 1.2 to 0.5 kbar. Wall rock alteration is well developed in early-formed Alpine fissures, but not observed in the younger large fracture systems. The early CO_2-bearing fluids in Tessin-habit quartz have δD values of +7 to –70 ‰ (relative to VSMOW), measured by thermal decrepitation and isotopic analyses of the included water, and δ^{18}O values of +6 to +23 ‰, calculated from measurements of the isotopic composition of the quartz and approximated fluid inclusion filling temperatures. δ^{13}C values (relative to VPDB) of included CO_2 range between –1 to –15 ‰. These isotopic compositions support the notion that a metamorphic fluid likely to have been generated by dehydration and decarbonation reactions in the enclosing metasedimentary rocks. In contrast to the CO_2-rich fluids in Tessin-habit quartz, stable isotope compositions of water-rich fluids in needle quartz have δD values between –58 and –113 ‰ and δ^{18}O values between –2 and –6 ‰. In split-growth quartz, δD values of the fluids are between –78 and –143 ‰ and δ^{18}O values between –7 and –16 ‰, indicating increasing dominance of meteoric water for the later quartz growth. To allow for precipitation of the large amounts of young fracture-filling quartz from fluids dominated by meteoric water, a topographic high is postulated as a high-altitude catchment for the meteoric water. According to the tectonic evolution of the Central Alps, the necessary conditions were given during the Mid-Miocene in the Pennine area and adjacent Gotthard Massif, as the southern part of the Penninic nappes experienced greater uplift during the Mid-Miocene compared to the frontal part of the Penninic nappes. The southern Penninic part could, therefore, have served as a hydraulic head. Infiltrating meteoric waters must have moved through permeable North-dipping rocks or fracture systems. At temperatures above 320 °C and depths exceeding 10 km silica was dissolved. Stable isotope compositions and trapping conditions of fluids at 320 to 180 °C and 1.8 to 0.5 kbar indicate precipitation of needle and split-growth quartz from ascending meteoric fluids within extensional fracture systems.
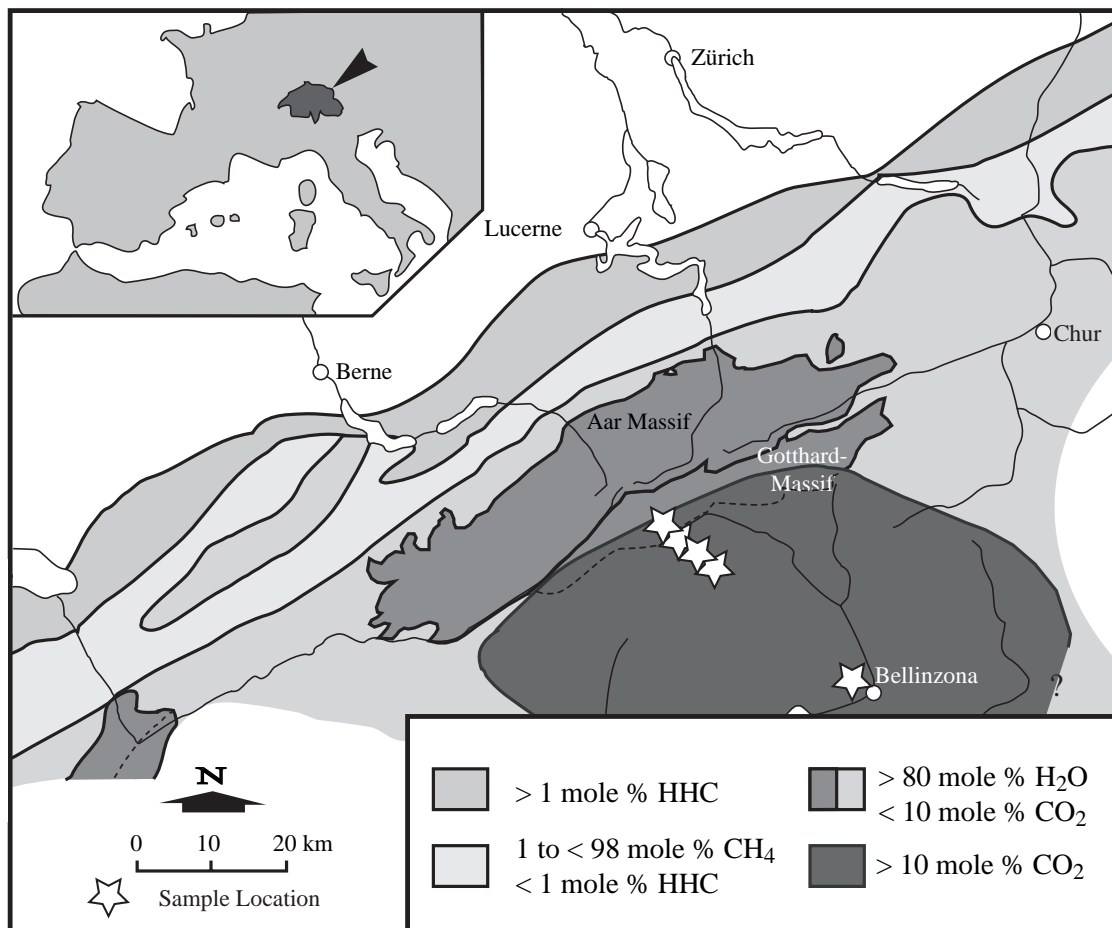
A.1   Introduction

Fig. A.1: Fluid map of Mullis (1995) for the Central Alps with the nine sampled localities (four overlapping one of the shown localities). HHC = higher hydrocarbon zone.

Twenty years ago stable isotope investigations on vein-quartz and fluid inclusions from the Northern Tessin area indicated mineralising fluids with a meteoric origin. These data were difficult to interpret at the time, and more detailed studies to investigate the nature of mineralising fluids responsible for the precipitation of fissure and vein quartz in the northern Penninic Alps and the southern Gotthard Massif was initiated. Field-observations of the veins and fissures were made at nine localities (Fig. A.1) and the quartz crystals and their fluids were the subject of further stable isotope and fluid inclusion geochemical investigation.

A.2   Stable isotope analyses methods

The oxygen isotope composition of the quartz was measured at the Universities of Tübingen and Lausanne, using either conventional extraction of oxygen and BrF_5 reagent, according to a method adopted after Clayton and Mayeda (1963), or a laser-based extraction method similar to that described by Sharp (1990) and Rumble and Hoering (1986). For the conventional analyses about 10 mg of the sample was used and the extracted oxygen was converted to CO_2. For the laser-based method about 0.5 to 2 mg of the sample was used and the isotopic composition was analysed on the extracted oxygen, collected on a molcular sieve (13X). Isotopic measurements were all made using a isotope ratio mass spectrometer (Finnigan MAT 252). Oxygen isotope compositions are given in the standard δ-notation, expressed relative to VSMOW in permil (‰). (Standard Mean Ocean Water whose isotopic composition was defined by an International Advisory Group Meeting in Vienna). Replicate oxygen isotope analyses of the standards used (NBS-28 quartz (n = 10 and UWG-2 garnet (n = 6); Valley et. al., 1995) had an average accuracy of $\pm$ 0.07‰ for $\delta^{18}O$. The precision of $\delta^{18}O$ values was better than 0.2‰ compared to accepted $\delta^{18}O$ values for NBS-28 of 9.64‰ and UWG-2 of 5.8‰.

D/H and $^{13}C/^{12}C$ analyses of fluid inclusion H_2O and CO_2: Inclusion fluids for stable isotope analyses were released by thermal decrepitation at temperatures of up to but not exceeding 550°C. Fluid inclusion water was separated from CO_2 by standard cryogenic means. Fluid inclusion water was reduced with zinc for hydrogen isotope and volume determination according to the method of Vennemann and O'Neil (1993) using a mass spectrometer. δD values are reported in the conventional δ-notation in permil (‰) relative to VSMOW. The isotopic composition of CO_2 was also measured on a mass spectrometer and the $\delta^{13}C$ values are also reported in conventional δ-notation but are reported relative to VPDB (Vienna Pee Dee belemnite). The oxygen isotope composition of the fluid was calculated from $\delta^{18}O$ values measured for quartz and using the quartz-water fractionation curve of Matsuhisa et al. (1979) at temperatures estimated from fluid inclusion homogenization temperatures.

A.3   Results

Vein structure

Early small Alpine fissures can clearly be distinguished from younger, larger vein systems. The Alpine fissures are characterized by a SE-NW strike, a near vertical orientation, and

display a distinct alteration zone. The younger vein systems outcrop over several tens to hundreds of metres, strike SE-NW and dip steeply to the ENE and WSW. The vein systems are dominated by quartz (>99.9%) but display practically no alteration zone.
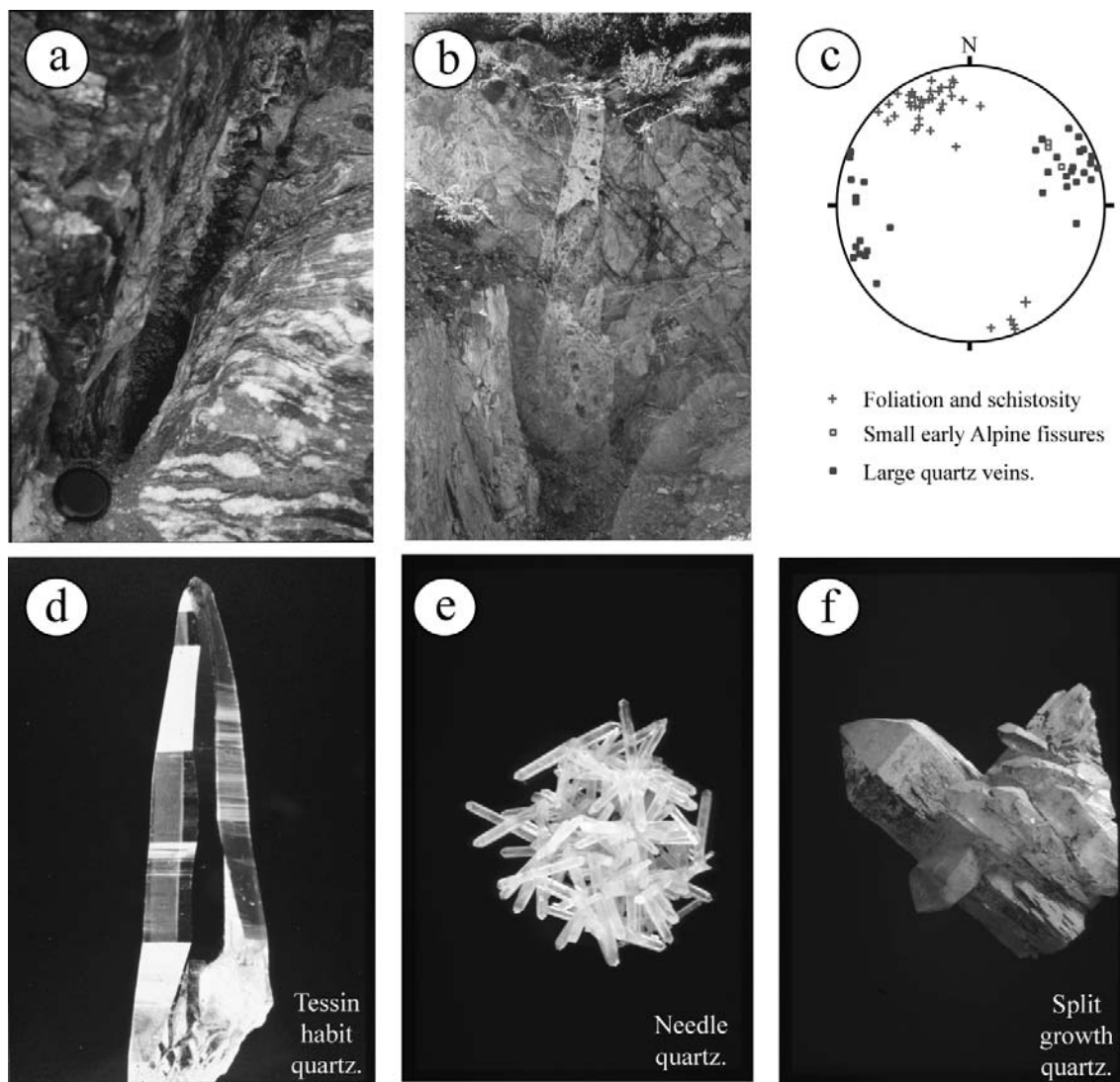

Fig. A.2: a) Open needle quartz vein striking SE-NW, b) needle and split growth quartz vein, incorporating host rock breccia, striking SE-NW, c) stereographic plot (lower hemisphere) of vein and foliation poles (planes), d) Tessin habit quartz habit, e) needle quartz habit, f) split-growth quartz.

Quartz morphology

Three types of quartz are found in the investigated fissure and vein systems (Fig. A.2). Tessin-habit quartz, associated with albite, rutile, muscovite and tourmaline represents a characteristic mineralisation assemblage for the small early fissure systems. In the younger vein systems two types of quartz morphology, with a distinct relative age succession are recognized: Needle-like quartz with a width to length ratio of between 1:10 and 1:100, and split-growth quartz with numerous smaller quartz crystals formed subparallel to the prism and rhombohedral faces. Needle quartz is often cut by a tectonic shearing and overgrown by younger quartz material. Brecciated host-rock is often found in the needle quartz veins, which in turn, are often brecciated themselves and overgrown by split-growth quartz. Both needle and split-growth quartz have well a developed growth zonation.

Fluid Inclusions

Fluid inclusion investigations were performed with a Chaixmeca heating and freezing stage designed to work in the range -80 to $+600°C$ Poty et al. (1976). Fluid inclusion compositions in the different types of quartz crystals are distinct (Fig. A.3). A CO_2-content of 10 to ≥ 50 mol% is characteristic for the Tessin-habit quartz, whereas needle and split-
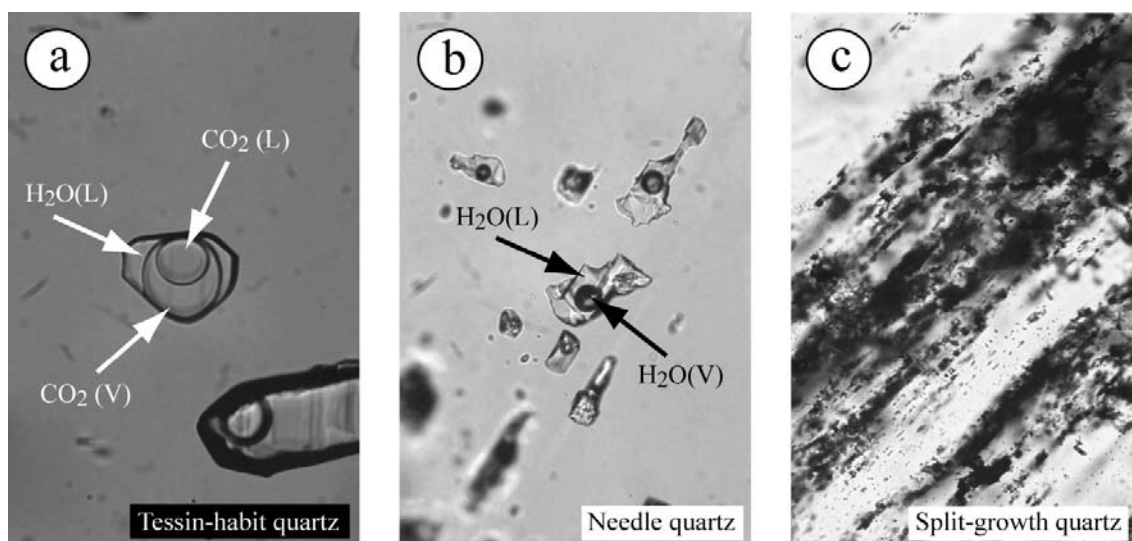

Fig. A.3: a) CO_2-enriched fluid inclusions within the Tessin-habit quartz, b) Water-rich fluid inclusions without CO_2 within the needle quartz, c) Water-rich fluid inclusions without CO_2 within the split-growth quartz.
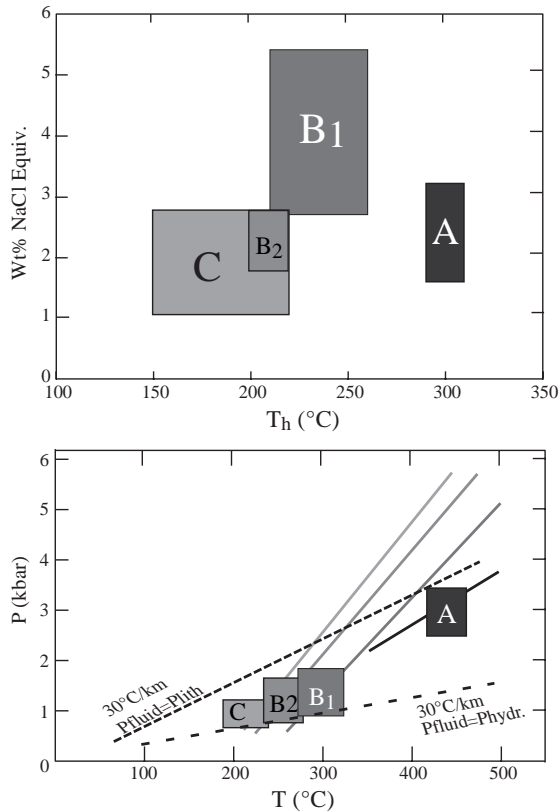
Figure A.4: a) Homogenisation temperatures (T_h °C) and salinity (wt.%. NaCl equiv.) of the investigated fluid inclusion populations derived from microthermometric investigation of nine localities. b) Approximate *PT*-path constructed from isochores of fluid inclusion trapping and crystal growth.

growth quartz contain less than 2 mol%. Salinity, in NaCl equiv., is small ($\leq$ 1mol% in the Tessin-habit and split growth quartz fluids) and shows a slight increase to 1.6 mol% in the needle quartz fluids (Fig. A.4a).

The earliest CO_2-enriched fluid inclusion populations in the Tessin-habit quartz were trapped between 450 and 410°C at fluid pressures between 3.5 and 2.5 kbar. Trapping temperatures of water-rich fluids in needle quartz range between 320 and 270°C and between 240 and $\leq$200°C for the split-growth quartz. Trapping pressures of both quartz types are between 1.5 and $\leq$ 0.7 kbar, closer to hydrostatic than lithostatic conditions (Fig. A.4b).

Stable Isotope Investigations

The hydrogen and oxygen isotope composition of the mineralising fluids shows a marked decrease from typical metamorphic fluids in the Tessin-habit quartz, to fluids approaching the meteoric water line (MWL) in the needle and split-growth quartz. The isotopic composition of the fluid in equilibrium with the Tessin-habit quartz is rock-buffered. That is
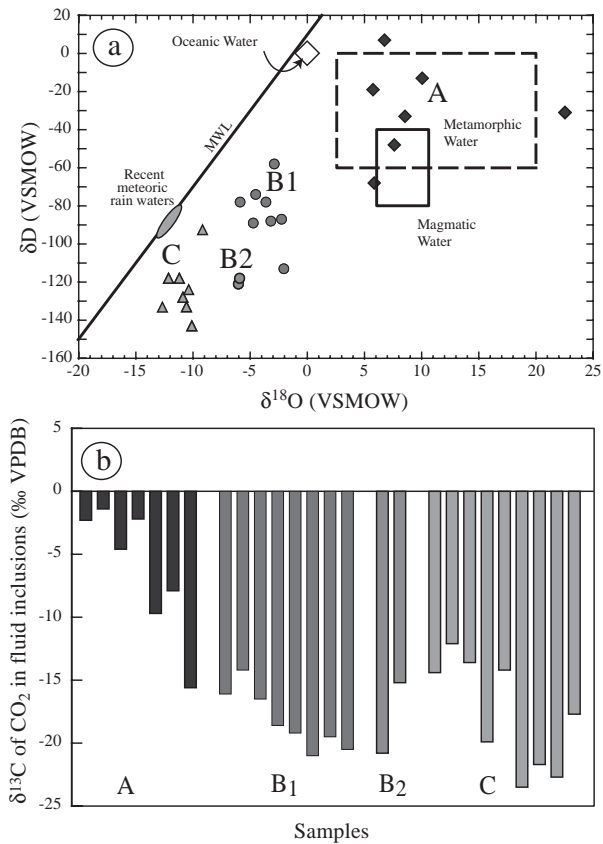
Figure A.5: a) δD vs δ^{18}O(VSMOW) distribution of the inclusion fluids from nine localities. δ^{18}O of the inclusion fluids is derived from δ^{18}O of the corresponding host quartz and corrected using the approximate formation temperature. b) Evolution of δ^{13}C of CO_2 from fluid inclusions from early to late fluid inclusions

compatible with visible wall-rock alteration adjacent to the Alpine fissure containing the Tessin-habit quartz. A trend towards strongly decreasing δD and δ^{18}O values is clearly recognisable (Fig. A.5a) and implies an increasing dominance of meteoric water. Very low δ^{18}O values measured for quartz (e.g., values down to –3.0‰), low δ^{18}O values calculated for the fluids (as low as –14 to –16‰) as well as the low δD values (–120 to –140‰) measured for the fluid inclusions require a high-altitude catchment for the meteoric water component that clearly precipitated such quartz. δ^{13}C values (relative to VPDB) of included CO_2 range between –1 to –15 ‰. These isotopic compositions support a metamorphic fluid likely to have been generated by dehydration and decarbonation reactions in the enclosing meta-sedimentary rocks (Fig. A.5b). Later CO_2 seems to be more derived from lithologies en-riched in organic matter, with values between –12 to –23 ‰.

A.4   Conclusions

1. During continued continent-continent collision of the European and Apulian plates, early brittle SE-NW striking Alpine fissures formed under conditions favouring non-ductile deformation in early Miocene times.

2. Early exhumation and cooling of the crystalline massifs, caused Tessin-habit quartz precipitation in these fissures. Precipitation took place in a closed system from a CO_2-enriched fluid, which originated from fluids derived by de-carbonatization reactions and oxidation of organic matter.

3. As a consequence of continued exhumation and up-doming of the Southern and Central Penninic realm, large SE-NW striking extensional veins formed during Mid-Miocene times.

4. These veins are filled with an enormous amount of needle- and split-growth quartz, which is indicative of the large fluid-fluxes necessary precipitate them.

5. The isotopic signature of the needle- and split-growth quartz requires an episodically open system for large-scale flow of meteoric fluids, while their relatively high homogenisation temperatures require that these fluids were heated during downward flow.

6. The presence of a topographic high can be inferred from the very low δD values either by applying recalculation methods similar to Mulch et al. (2004) or a more simple approach by Sharp et al. (2005). At least parts of the Central Alps must have been approximately 2000 m higher then the average height of the Alps today.

7. Infiltration of these meteoric fluids probably occurred along fractures of similar fracture systems. The presence of the topographic high can partially explain downward movement of meteoric fluids along such fractures as it can cause a significant hydraulic head in the upper parts of the crust. However, other mechanisms must be invoked to allow fluids to move towards deeper levels in the crust.

8. The heated meteoric fluids must subsequently have moved upwards through fractures of the same system. In the upper levels of the fracture system topographically lower sites could have played a role in creating a hydraulic head. At deeper levels permeability was provided by repeated extensional fracturing.

9. During this large-scale fluid flow, quartz was dissolved, transported and precipitated during upward movement of the fluids. This occurred between 320 and 200°C, at a depth of ∼7 to 10 km.

Appendix B

Raman-spectra

Figures showing Raman data from the Fibbia (B.1 to B.3) and Amsteg areas (B.4):
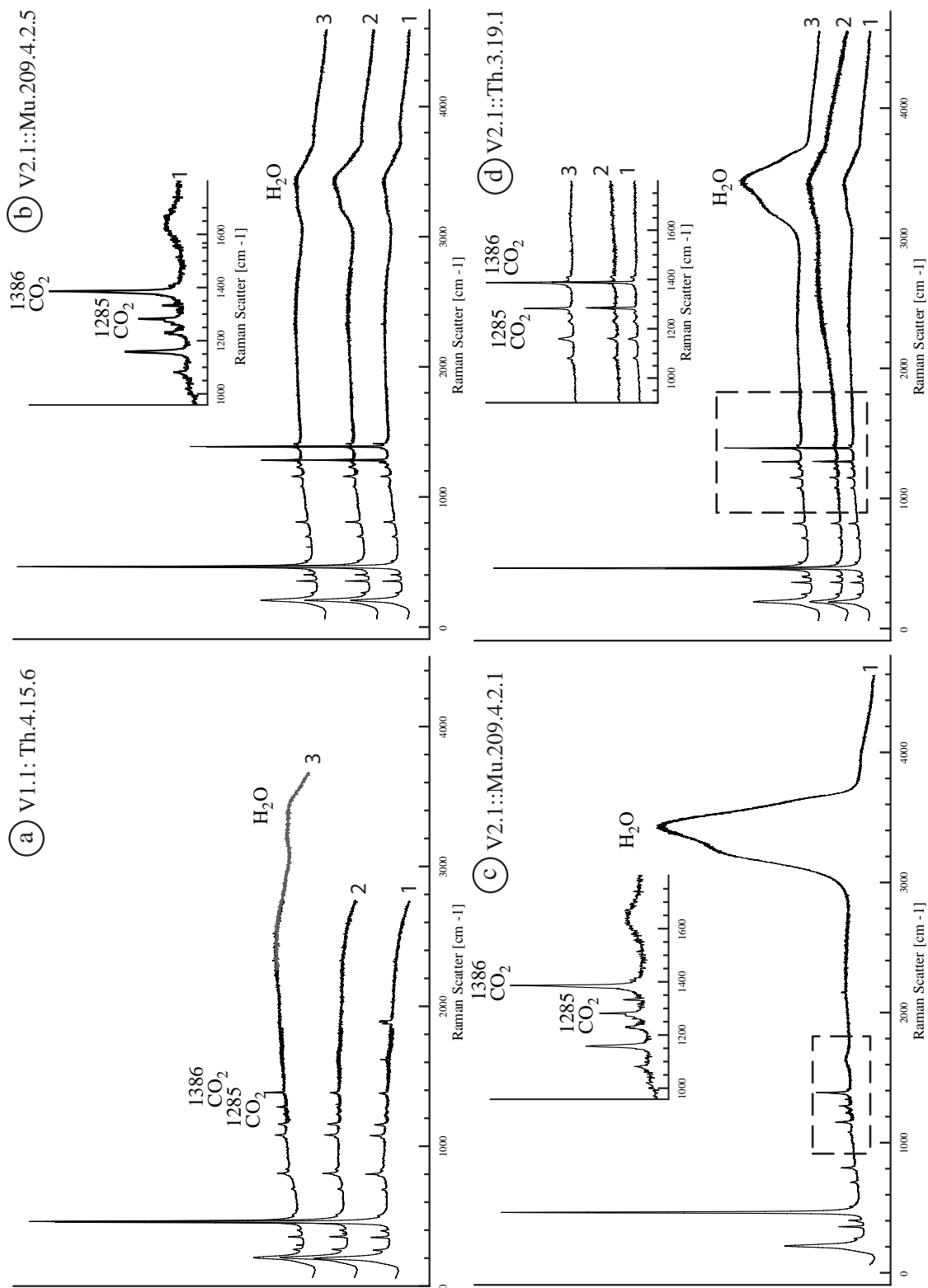
Fig. B.1: a-d) Raman spectra of vapour bubbles from fluid inclusions. a) $V_{1.2}$ fluid inclusion population, b) to d) $V_{2.1}$ fluid inclusion population.
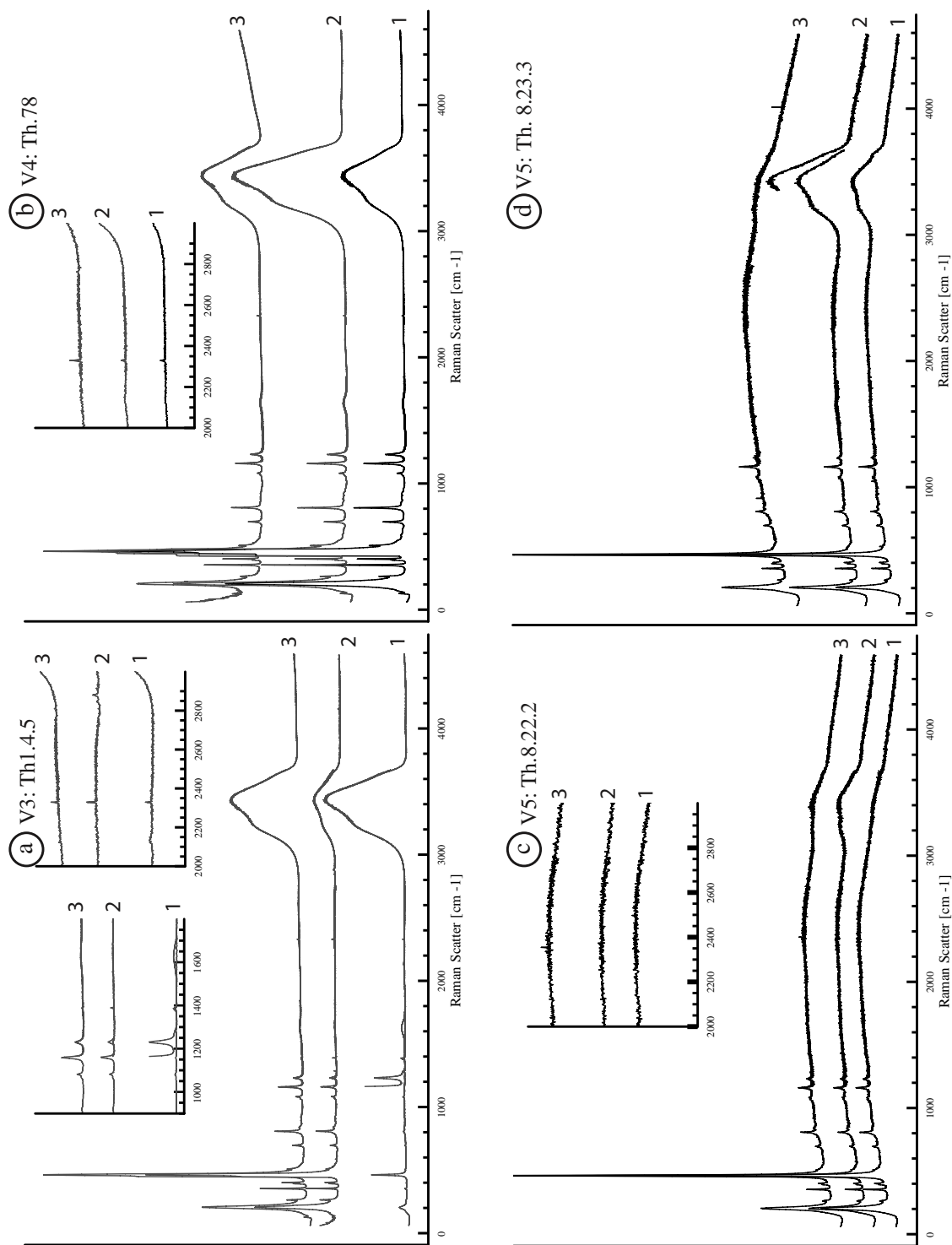
Fig. B.2: a-d) Raman spectra of vapour bubbles from fluid inclusions. a) V_3, b) $V_{4.1}$, c) $V_{5.2}$ and d) $V_{5.2}$ fluid inclusion populations.
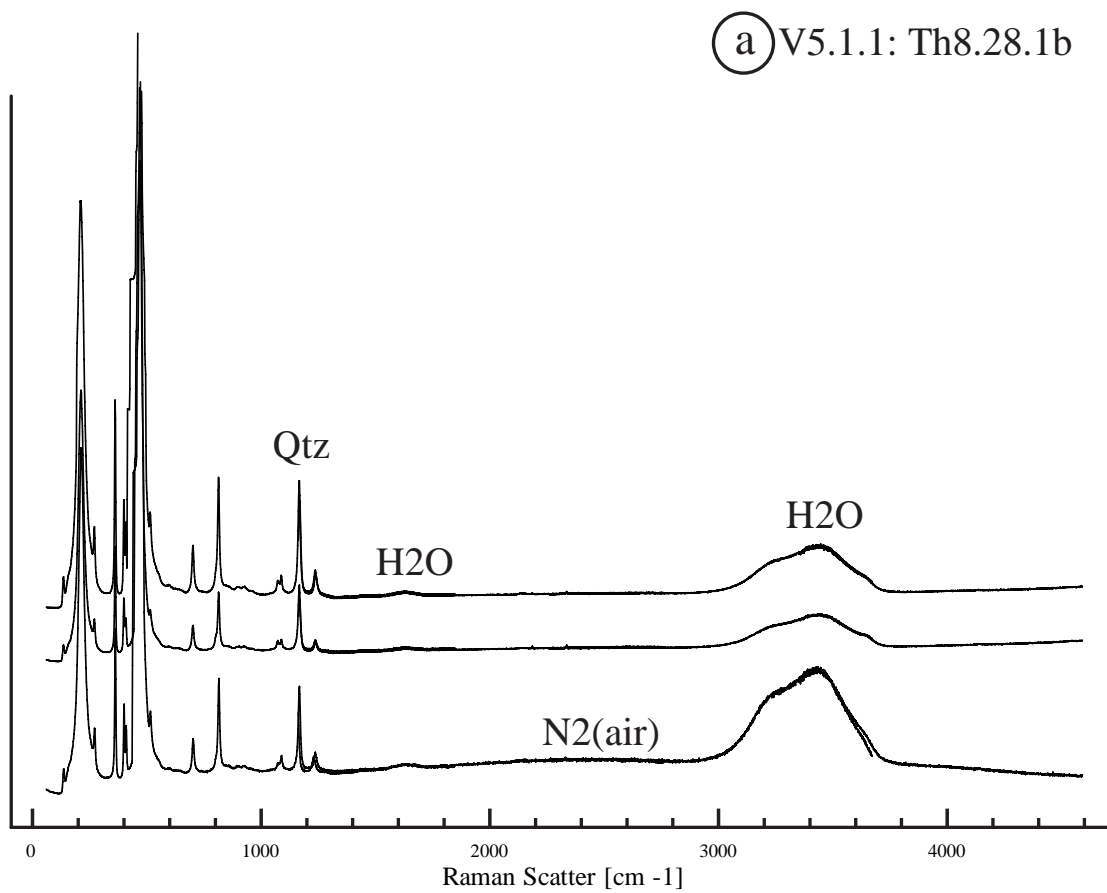
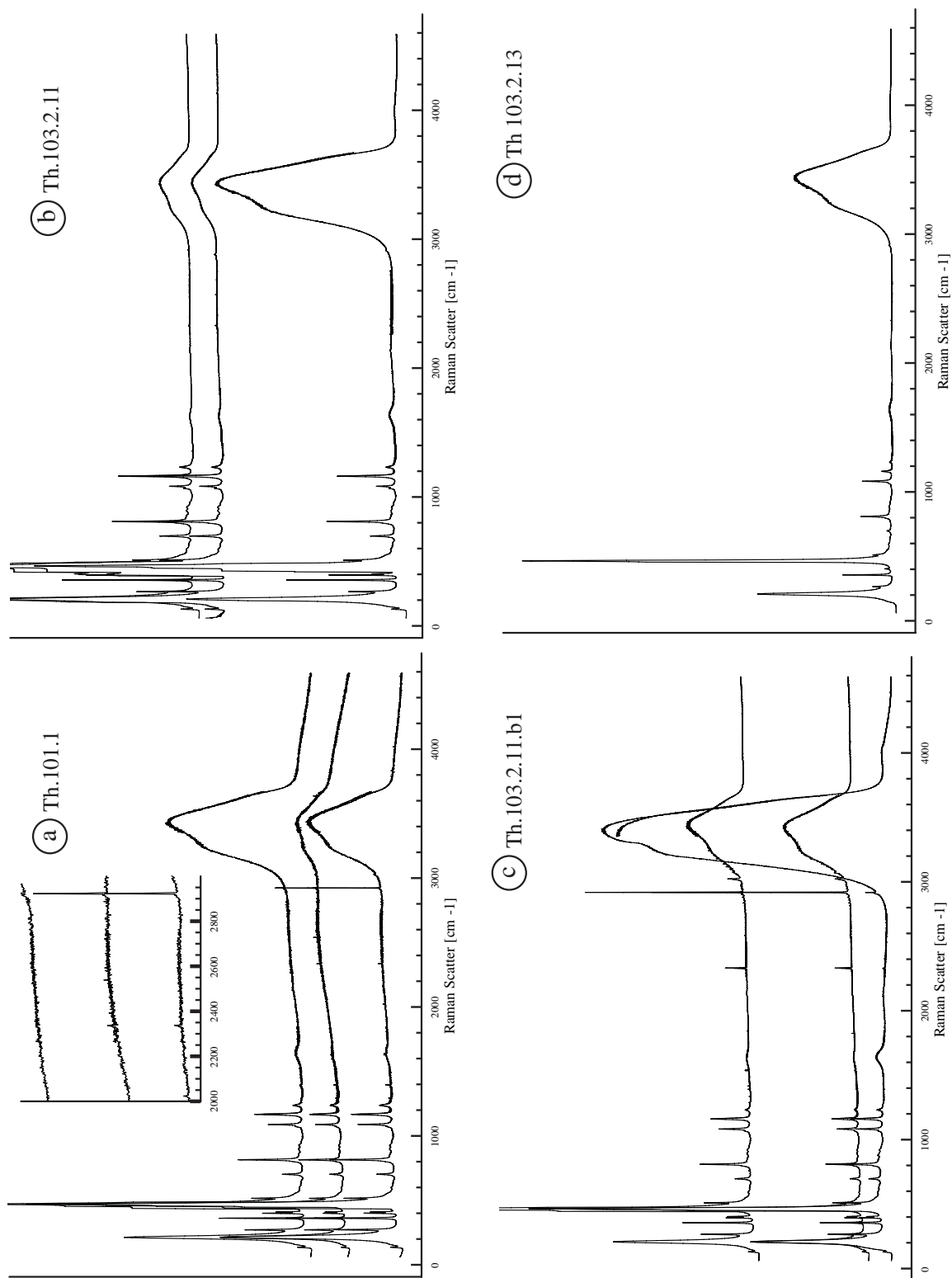**Fig. B.3:** a) Raman spectrum of vapour bubbles from fluid inclusions from $V_{5.1}$

Fig. B.4: a-d) Raman spectra of vapour bubbles from fluid inclusions.

Appendix C

Calibration for multi-element analysis using LA-ICPMS

Following is the methodology for calculation of fluid inclusion compositions from laser-ablation ICPMS employed by Heinrich et al. (2003). RSD is the relative standard deviation.

$$\frac{C_i^{Sample}}{C_{ref}^{Sample}} = \frac{C_i^{Std}}{C_{ref}^{Std}}\left(\frac{I_i^{Sample}I_r^{Std}}{I_{ref}^{Sample}I_i^{Std}}\right)\left(\frac{S_i^{Sample}S_r^{Std}}{S_{ref}^{Sample}S_i^{Std}}\right) \tag{C.1}$$

Where C is the concentration of the measured element, I is the intensity of the time integrated measurement and S is the sensitivity. i is the measured element and ref is the reference concentration of a reference element, Sample connotates the unknown sample measured and Std indicates the standard material. According to Heinrich et al. (2003) when no element fractionation takes place in the ICPMS the S ratios cancel out leaving only the concentration and intensity rations in equation C.1. It is assumed that this is the case. The limit of detection (LOD) for element i can then be expressed as:

$$LOD = C_{ref}^{Sample}\frac{C_i^{Std}}{C_{ref}^{Std}}\left(\frac{3\sigma_i^{BG}I_r^{Std}}{I_{ref}^{Sample}I_i^{Std}}\right) \tag{C.2}$$

Host mineral corrected intensities:

$$I_i^{Incl} = I_i^{Mix} - I_{Si}^{Mix} \cdot \frac{I_i^{Host}}{I_{Si}^{Host}} \tag{C.3}$$

Incl is the signal of the inclusion, *mix* is the whole measured signal, *Host* is the host signal Expressing concentration gradients to an internal standard (Na) is as follows using equation C.1:

$$\frac{C_i^{Incl}}{C_{Na}^{Incl}} = \frac{C_i^{Std}}{C_{Na}^{Std}}\left(\frac{I_i^{Incl}I_{Na}^{Std}}{I_{Na}^{Incl}I_i^{Std}}\right) \tag{C.4}$$

Combining the measured concentrations with the NaCl wt% measured from microthermometry can be done as follows:

$$NaCl(wt\%) = C_{NaCl} + 0.5 \cdot (C_{KCl} + C_{FeCl2} + C_{CaCl2} + ...) \tag{C.5}$$

Equations C.4 and C.5 need to be solved simultaneously to get the unknown concentrations for all the measured elements. Using an equation for Cl in stead of Na yields similar results.

To recalculate the fluid concentrations from ppm to molal (mol/kg H_2O) concentrations the following equation is applied for all fluid species:

$$C_{i,molal} = \frac{C_{i,ppm} - (C_{i,ppm} \cdot \sum_i C_{i,ppm})/10^6}{M_i \cdot 1000} \tag{C.6}$$

where $C_{i,molal}$ is the concentration of the species in molal, $C_{i,ppm}$ is the concentration of species i in ppm and M_i is the molar mass.

Appendix D

Raw data of Crush-Leach and LA-ICPMS analyses for chapter 1

Sample characteristics

Vein type	V1	V2	V3	V4	V5	V5	V5
Mineral Type	RQ	THQ	THQ	THQ	NQ	NQ	SGQ
Sample	Th.4.19	Mu.209.4.2.5	Th.1.4.5	Th.78.3	Th. 8.34	Th. 8.35	Th.8.23.3
Fluid type	CO_2	CO_2	H_2O	H_2O	H_2O	H_2O	H_2O
Fluid pop	V1.1	V2.1	V3.1	V4.1	V5.1.1 V5.1.2	V5.1.1 V5.1.2	V5.2
Amount(gr)	0.77	1.218	2	1.14	0.39	0.65	1
wt% NaCl	5.4	4.4	8.3	6.5	2.5	2.5	1.6

Analysed concentrations in ppb

Li	b.d.	b.d.	b.d.	1.2	b.d.	b.d.	b.d.
Mg	14.9	15	17	69	b.d.	9.9	21.9
Na	242	126	81.25	602	45	58.3	331.3
K	68.5	39	31	157	12	10	102.5
Ca	54	84	16	42	b.d.	7	62
Mn	b.d.	1.8	2.8	2.4	b.d.	b.d.	b.d.
Fe	10	12	177	134	b.d.	9	23
Cu	b.d.	6	b.d.	1.8	b.d.	b.d.	b.d.
Rb	b.d.	b.d.	2	1.8	b.d.	b.d.	b.d.
Sr	b.d.	b.d.	b.d.	2.1	b.d.	b.d.	3
Cl	496	350	192	1194	80	79	523
Br	4.6	1.9	1.4	1.5	b.d.	b.d.	0.8
SO4	108	55	71	28	b.d.	47	228
Sum of charges	1.0	1.1	0.9	1.1	1.0	1.2	1.1

Table D.1: Raw results of crush leach analyses on samples from the five vein types with concentrations in ppb. Indicated are the salinity of the different fluids and the charge balance. b.d.: analysed values were below detection limits.

Analytical results: Table D.1 shows the composition of the fluids as analysed by crush leach analysis, including both the cation and anion concentrations of the fluids. Table D.2 displays the average cation compositions of fluid inclusion populations calculated, which were measured by laser ablation. The differences between the laser ablation and crush leach data sets are the following: Be, Ti, Zn, As, Cs, Ba, Pb were analysed by

Sample Characteristics

Vein type	V1	V2	V2	V2	V2	V4	V5
Sample number	Th.4.15.3/4	Mu.209.4.2.5	Th.3.19.1	Mu.209.4.1.2	Mu. 209.4.1.3	Th.78.3	Th.8.23.3
Mineral Type	RQ	THQ	THQ	PQ	PQ	PQ	SQ
Fluid population	V1.1	V2.1	V2.1	V2.2	V2.3	V4	V5.2.1
Fluid type	CO_2	CO_2	CO_2	H_2O	H_2O	H_2O	H_2O
Nr. Inclusions	2	15	8	5	5	13	6
Quality	G	G-E	G-E	A-G	A-G	A	B-A
wt% NaCl	4.5	4.5	4.5	5.5	8.0	6.6	1.0

Analysed concentrations

Element	Average	St. dev	Average	St. dev	Average	St. Dev	Average	St. Dev	Average	St. Dev	Average	St. Dev	Average	St. Dev
Li 7	63.7	7.4	239.3	54.7	124.0	10.0	207.3	51,6	245.0	23.0	328.5	116.4	n.d.	-
Be 9	n.d.	-	n.d	-	15.6	-	7.9	-	n.d.	-	n.d.	-	n.d.	-
Na 23	16885.3	139.3	15747.3	93.9	15752.3	701.9	20358.5	145.3	28518.4	692.1	21267.3	1360.7	6003.8	503.1
Mg 25	n.d.	-	97.4	139.9	205.7	196.4	277.6	401.2	0.0	-	137.1	112.3	105.0	-
K 39	5327.3	371.4	5214.7	250.5	5856.9	129.2	5507.0	387.3	7875.6	1845.4	6056.0	495.6	n.d.	-
Ca 42	n.d.	-	n.d.	-	423.3	-	n.d.	-	n.d.	-	3132.4	1940.1	n.d.	-
Ti 49	n.d.	-	30.1	13.2	2.6	-	n.d.	-	n.d.	-	38.8	17.2	n.d.	-
Mn 55	n.d.	-	0.2	-	0.3	0.1	n.d.	-	n.d.	-	n.d.	-	n.d.	-
Fe 57	n.d.	-	n.d.	-	2.1	1.1	n.d.	-	n.d.	-	n.d.	-	n.d.	-
Zn 66	0.9	-	0.2	0.1	0.2	0.1	0.6	-	1.3	-	3.4	-	2.4	3.1
As 75	4.9	0.4	5.0	0.6	1.6	0.2	6.4	0.6	7.6	1.2	5.0	0.9	1.1	-
Rb 85	0.8	0.1	0.5	-	0.8	-	1.6	0.2	1.8	0.4	3.2	0.2	n.d.	-
Sr 88	0.5	0.5	0.3	-	0.2	-	0.5	-	0.6	0.3	2.6	0.3	0.1	-
Cs 133	0.3	0.1	0.2	-	0.2	-	0.7	0.1	0.7	0.1	3.2	0.4	0.0	-
Ba 137	0.2	0.0	0.2	0.1	0.1	-	0.1	-	n.d.	-	0.1	0.2	n.d.	-
Pb 208	44.7	-	23.0	3.5	27.6	3.7	n.d.	-	18.2	-	24.2	-	13.1	13.8

Table D.2: The mean concentrations (in ppm calculated for the respective salinity of the fluid inclusion population) and standard deviations of cation concentrations in the fluid inclusions from the different vein types that were measured by laser ablation-ICPMS. Quality of the analysis, which is related to how well the ablation proceeded and the quality of the spectrum is indicated by: E = excellent, G = good, A = average, B = bad, n.d. = not detected. "–" not more than one inclusion measured, therefore no standard deviation calculated.

laser ablation, but not by crush leach methods. Cu and Cl, Br and SO_4 were analysed by crush leach methods, but not by laser ablation. All other elements were analysed by both methods. In the case of the crush leach analyses, the total yield of the samples was low due to small sample size and the relatively low salinities of the fluids involved. Nevertheless, the calculated charge balances indicate that most of the elements in the fluids were analysed and that there are no strong contaminations of the cations. Both Th.8.34 and Th.8.35 have a very low yield and so are more prone to contaminations. In the case of laser ablation analyses, steady signals were found for Li, Na, K, As, Rb, Sr, Cs, and Ba while Pb, Be, Mg, Ti, Mn, Fe, and Zn were only occasionally measured and their signal

was not stable over different fluid inclusions of the same fluid inclusion population. This implies that these elements were present in the fluid at concentrations near the detection limit.

Bibliography

Abrecht, J., 1994. Geologic units of the Aar massif and their pre-Alpine rock associations: a critical review. Schweizerische Mineralogische und Petrographische Mitteillungen 74, 5–27.

Adams, S., 1920. A microscopic study of vein quartz. Economic Geology 15, 623–664.

Ague, J., 1997. Crustal mass transfer and index mineral growth in Barrow's garnet zone, northeast Scotland. Geology 25, 73–76.

Ague, J., 2004. Ch. 3.06 Fluid flow in the deep crust. In: Rudnick, R. (Ed.), Treatise on geochemistry: The Crust. Vol. 3. Elsevier, Amsterdam, pp. 195–222.

Bakker, R., 2003. Package FLUIDS 1. New computer programs for the analysis of fluid inclusion data and for modelling bulk fluid properties. Chemical Geology 194, 3–23.

Banks, D., Boyce, A., Samson, I., 2002. Constraints on the origins of fluids forming Irish Zn-Pb-Ba deposits: Evidence from the composition of fluid inclusions. Economic Geology 56 (97), 471–480.

Banks, D., Davies, G., Yardley, B., McCaig, A., Grant, N., 1991. The chemistry of brines from an Alpine thrust system in the Central Pyrenees: An application of fluid inclusion analyses to the study of fluid behaviour in orogenesis. Geochimica et Cosmochimica Acta 55, 1021–1030.

Banks, D., Yardley, B., 1992. Crush-leach analyses of fluid inclusions in small natural and synthetic samples. Geochimica et Cosmochimica Acta 56 (1), 245–248.

Barnes, H., 1979. Geochemistry of hydrothermal ore deposits: 2nd edn. Wiley, New York.

Berman, R., 1988. Internally-consistent thermodynamic data for minerals in the system Na_2O-K_2O-CaO-MgO-FeO-Fe_2O_3-Al_2O_3-SiO_2-TiO_2-H_2O-CO_2. Journal of Petrology 29 (2), 445–522.

Bons, P., 2000. The formation of veins and their microstructures. In: Jessell, M., Urai, J. (Eds.), Stress, Strain and Structure: A volume in honour of W D Means. Vol. 2 of Journal of the Virtual Explorer. http://www.virtualexplorer.com.au/2000/volume2/www/contribs/bons/, pp. 279–290.

Bons, P., 2001. The formation of large quartz veins by rapid ascent of fluids in mobile hydrofractures. Tectonophysics 336, 1–17.

Bottrell, S., Yardley, B., Buckley, F., 1988. A modified crush leach method for analysis of fluid inclusion electrolytes. Bulletin de Minéralogie 111, 279–290.

Burkhard, M., Kerrich, R., 1988. Fluid regimes in the deformation of the Helvetic nappes, Switzerland, as inferred from stable isotope data. Contributions to Mineralogy and Petrology 99, 416–429.

Burkhard, M., Kerrich, R., 1990. Fluid-rock interactions during thrusting of the Glarus nappe - evidence from geochemical and stable isotope data. Schweizerische Mineralogische und Petrographische Mitteilungen 70, 77–82.

Carpenter, A., 1978. Origin and chemical evolution of brines in sedimentary basins. Oklahoma Geological Survey Circular 79, 60–77.

Carpenter, A., Trout, M., Picket, E., 1974. Preliminiary report on the origin and chemical evolution of lead and zinc rich oil field brines in Central Mississippi. Economic Geology 69, 1191–1206.

Cathles, L., 1990. Scales and effects of fluid flow in the upper crust. Science 248, 323–329.

Cesare, B., Poletti, E., Boiron, M.-C., Cathelineau, M., 2001. Alpine metamorphism and veining in the Zentralgneiss Complex of the SW Tauern Window: a model of fluid-rock interactions based on fluid inclusions. Tectonophysics 336, 121–136.

Chacko, T., Cole, D., Horita, J., 2001. Equilibrium oxygen, hydrogen and carbon isotope fractionation factors applicable to geologic systems. In: Valley, J., Cole, D. (Eds.), Reviews in Mineralogy and Geochemistry Vol 43: Stable isotope geochemistry. Mineralogical Society of America, Chelsea, pp. 1–82.

Clark, S., Jäger, E., 1969. Denundation rate in the Alps from geochronologic and heat flow data. American Journal of Science 267, 1143–1160.

Clayton, R., Mayeda, T., 1963. The use of bromine pentafluoride in the extraction of oxygen from oxides and silicates for isotopic data. Geochimica et Cosmochimica Acta 27, 43–52.

Connolly, J., Podladchikov, Y., 2004. Fluid flow in compressive tectonic settings: Implications for midcrustal seismic reflectors and downward fluid migration. Journal of Geophysical Research 109 (B-04201), 1–12.

Craw, D., Koons, P., Zeitler, P., Kidd, W., 2005. Fluid evolution and thermal structure in the rapidly exhuming gneiss complex of Namche Barwa-Gyala Peri, eastern Himalaya syntax. Journal of Metamorphic Geology 23, 829–845.

de Capitani, C., Brown, H., 1987. The computation of chemical equilibrium in complex systems containing non-ideal solutions. Geochimica et Cosmochimica Acta 51, 2639–2652.

Deutsch, A., Steiger, R., 1985. Hornblende K-Ar ages and the climax of Tertiary metamorphism in the Lepontine Alps (South-Central Switzerland); an old problem reassessed. Earth and Planetary Science Letters 72 (2-3), 175–189.

Diamond, L., 1990. Fluid inclusion evidence for P-V-T-X evolution of hydrothermal solutions in Late-Alpine gold-quartz veins at Brusson, Val d'Ayas, NW Italian Alps. American Journal of Science 290, 912–958.

Diamond, L., 1992. Stability of CO_2 clathrate hydrate + CO_2 liquid + CO_2 vapour + aqeous KCl-NaCl solutions: Experimental determination and application to salinity estimates of fluid inclusions. Geochimica et Cosmochimica Acta 56 (1), 273–280.

Dong, G., Morrison, G., Jaireth, S., 1993. Quartz textures in epithermal veins, Queensland - classification, origin and implications. Economic Geology 90, 1841–1856.

Driesner, T., 1997. The effect of pressure on deuterium-hydrogen fractionation in high-temperature water. Science 277, 791–794.

Etheridge, M., Wall, V., Vernon, R., 1983. The role of the fluid phase during regional deformation and metamorphism. Journal of Metamorphic Geology 1, 205–226.

Fabre, C., 2000. Reconstruction chimique des paléofluides par spectrométrie d'émission optique couplée à l'ablation laser: Applications aux fluides alpins et aux fluides de bassins. Ph.D. thesis, Université Henry Poincaré, Nancy.

Fabre, C., Boiron, M., Dubessy, J., Cathelineau, M., Banks, D., 2002. Paleofluid chemistry of a single fluid event: A bulk and in-situ multi technique analysis (LIBS, Raman Spectroscopy) of an Alpine fluid (Mont-Blanc). Chemical Geology 182 (2-4), 249–264.

Faure, K., 2003. δD values of fluid inclusion water in quartz and calcite ejecta from active geothermal systems: Do values reflect those of original hydrothermal water? Economic Geology 98, 657–660.

Fischer, R., Kreitler, C., 1987. Geochemistry and hydrodynamics of deep-basin brines, Palo Duro Basin, Texas, USA. Applied Geochemistry 2, 459–476.

Fisher, D., Brantley, S., 1992. Models of quartz overgrowth and vein formation: Deformation and episodic fluid flow in an ancient subduction zone. Journal of Geophysical Research 97, 20.043–20.061.

Fouillac, C., Michard, G., 1981. Sodium/Lithium ratio in water applied to geothermometry of geothermal reservoirs. Geothermics 10, 55–70.

Fournier, R., 1979. A revised equation for the Na/K geothermometer. Geothermics Resource Council Transactions 3, 221–224.

Frey, M., Bucher, K., Frank, E., Mullis, J., 1980. Alpine metamorphism along the geotraverse Basel-Chiasso - a review. Eclogae Geologicae Helvetica 73 (2), 527–546.

Frey, M., Ferreiro-Mählmann, R., 1999. Alpine metamorphism of the Central Alps. Schweizerische Mineralogische und Petrographische Mitteillungen 79, 135–154.

Fricke, H. C., Wickham, S. M., O'Neil, J. R., 1992. Oxygen and hydrogen isotope evidence for meteoric water infiltration during mylonitization and uplift in the Ruby Mountains-East Humboldt Range core complex, Nevada. Contributions to Mineralogy and Petrology 111 (2), 203–221.

Fuhrman, M., Lindsley, D., 1988. Ternary-feldspar modeling and thermometry. American Mineralogist 73, 201–215.

Fyfe, W., Price, N., Thompson, A., 1978. Fluids in the Earth's crust: Their significance in metamorphic, tectonic and chemical transport processes. Developments in geochemistry: Vol. 1. Elsevier, Amsterdam.

Gleeson, S., 2003. Bulk analyses of electrolytes in fluid inclusions. In: Samson, I., Anderson, A., Marshall, D. (Eds.), Fluid inclusions: Analyses and interpretation. Vol. 32 of Short Courses. Mineralogical Association of Canada, Vancouver, pp. 233–247.

Gleeson, S., Grant, K., Roberts, S., 2000. Fluid inclusion δD in quartz does not always indicate the source of palaeo-hydrothermal fluids. In: Journal of Conference Abstracts. Vol. 5. p. 445.

Gleeson, S., Wilkinson, J., Boyce, A., Fallick, A., Stuart, F., 1999. On the occurrence and wider implications of anomalously low δD fluids in quartz veins, South Cornwall, England. Chemical Geology 160, 161173.

Graham, C., Viglino, J., Harmon, R., 1987. Experimental study of hydrogen-isotope exchange between aluminous chlorite and water and of hydrogen diffusion in chlorite. American Mineralogist 72, 566–579.

Grant, J., 1986. The Isocon diagram - A simple solution to Gresens equation for metasomatic alteration. Economic Geology 81, 1976–1982.

Grasemann, B., Mancktelow, N., 1993. Two-dimensional thermal modelling of normal faulting: the Simplon Fault Zone, Central Alps, Switzerland. Tectonophysics 225, 155–165.

Grigorev, D., 1965. Ontogeny of Minerals. Israel Program for Scientific translations, Jerusalem.

Grosjean, G., Sue, C., Burkhard, M., 2004. Late Neogene extension in the vicinity of the Simplon fault zone (Central Alps, Switzerland). Eclogae Geologicae Helveticae 97, 33–46.

Grujic, D., Mancktelow, N., 1996. Structure of the northern Maggia and Lebendun Nappes, Central Alps, Switzerland. Eclogae geologicae Helveticae 89, 461 504.

Günther, D., Audetat, A., Frischknecht, R., Heinrich, C., 1998. Quantitative analysis of major, minor and trace elements in fluid inclusions using laser ablation inductively coupled plasma mass spectrometry. Journal of Analytical Atomic Spectrometry 13, 263–270.

Hafner, S., 1958. Petrography des südwestlichen Gotthardmassivs. Schweizerische Mineralogische und Petrographische Mitteillungen 38, 256–362.

Hafner, S., Günthert, A., Burckhardt, C., Steiger, R., Jensen, J., Niggli, C., 1975. Geologischer Atlas der Schweiz 1251: Val Bedretto.

Hauzenberger, C., Baumgartner, L., Pak, T., 2001. Experimental study on the solubility of the "model"-pelite mineral assemblage albite+ K-feldspar + andalusite + quartz in supercritical chloride-rich aqueous solutions at 0.2 GPa and 600 °C. Geochimica et Cosmochimica Acta 65 (24), 4493–4507.

Heinrich, C. A., Pettke, T., Halter, W., Igner-Torres, M., Audetat, A., Günther, D., Hattendorf, B., Bleiner, D., Guillong, M., Horn, I., 2003. Quantitative multi-element analysis of minerals, fluid and melt inclusions by laser-ablation inductively-coupled-plasma mass-spectrometry. Geochimica et Cosmochimica Acta 67 (18), 3473–3496.

Helgeson, H., Lichtner, P., 1987. Fluid flow and mineral reaction at high temperatures and pressures. Journal of the Geological Society, London 144, 313–326.

Henley, R., Truesdell, A., Barton, P., 1984. Fluid mineral equilibria in hydrothermal systems. Reviews in Economic Geology, 267.

Henry, C., Burkhard, M., Goffé, B., 1996. Evolution of synmetamorphic veins and their wallrocks through a Western Alps transect: no evidence for large-scale fluid flow. Stable isotope, major-and trace element systematics. Chemical Geology 127, 81–109.

Hoefs, J., 1997. Stable isotope geochemistry, 4th Edition. Springer, Berlin.

Hoefs, J., Stalder, H., 1977. Die C-Isotopenzusammensetzung von CO_2-haltigen Flüssigkeitseinschlussen in Kluftquartzen der Zentralalpen. Schweizerische Mineralogische und Petrographische Mitteillungen 57, 329–347.

Hoernes, S., Friedrichsen, H., 1980. Oxygen and hydrogen isotopic composition of Alpine and pre-Alpine minerals of the Swiss Central Alps. Contributions to Mineralogy and Petrology 72, 19–32.

Horita, J., Wesolowski, D., Cole, D., 1993. The activity-composition relationship of oxygen and hydrogen isotopes in aqueous salt solutions: I. Vapour-liquid water equilibration of single salt solutions from 50 to 100°C. Geochimica et Cosmochimica Acta 57, 2797–2817.

Hunziker, P., 2003. The stability of tri-octahedral Fe^{2+}-Mg-Al chlorite. A combined experimental and theoretical study. Ph.D. thesis, University of Basel.

Hurford, A., 1986. Cooling and uplift patterns in the Lepontine Alps South Central Switzerland and an age of vertical movement on the Insubric fault line. Contributions to Mineralogy and Petrology 92, 413–427.

Jenkin, G., Craw, D., Fallick, A., 1994. Stable isotopic and fluid inclusion evidence for meteoric fluid penetration into an active mountain belt, Alpine Schist, New Zealand. Journal of Metamorphic Geology 12, 429–444.

Johnson, J., Oelkers, E., Helgeson, H., 1992. SUPCRT92: A software package for calculating the standard molal thermodynamic properties of minerals, gases, aqueous species, and reactions from 1 to 5000 bar and 0 to 1000°C. Computers and Geosciences 18 (7), 899–947.

Kasemann, S., Meixner, A., Rocholl, A., Vennemann, T., Schmitt, A., Wiedenbeck, M., 2001. Boron and oxygen isotope composition of certified reference materials NIST SRM 610/612 and reference materials JB-2 and JR-2. Geostandards Newsletter 25, 405–416.

Keller, L., 2004. Relationships between metamorphism and deformation: Examples on the micro- to macro scale from the western Alps (Camughera-moncucco unit and Monte Rosa nappe, Northern Italy. Ph.D. thesis, University of Basel.

Keller, L., de Capitani, C., Abart, R., 2005. A quaternary solution model for white micas based on natural coexisting phengite-paragonite pairs. Journal of Petrology 46 (10), 2129–2144.

Kesler, S., Vennemann, T., Frederickson, C., Breithaupt, A., Vazquez, R., Furman, F., 1997. Hydrogen and oxygen isotope evidence for origin of MVT-forming brines, Southern Appalachians. . Geochimica Cosmochimica Acta 61, 1513–1523.

Kharaka, Y., Meast, A., Carothers, W., Law, L., Lamothe, P., Fries, T., 1987. Geochemistry of metal-brines from Central Mississippi Salt Dome basin (USA). Applied Geochemistry 2, 543–561.

Koenigsberger, J., 1917. Über alpine Minerallagerstätten. Abhandelungen der der Könlich Bayerischen Akademie der Wissenschaften 10, 108.

Köhler, H., 1997. Mineralienaufsicht kraftwerk Amsteg: Mineralienlisten der Baulose 3,4,5 und 6.

Koonz, P., 1991. Evolution of fluid driving forces and composition within collisional orogens. Geophysical Research Letters 18, 935–938.

Kretz, R., 1983. Symbols for rock-forming minerals. American Mineralogist 68, 277–279.

Lagache, M., Weisbrod, A., 1977. The system: Two alkali feldspars-KCl-NaCl-H_2O at moderate to high temperatures and low pressures. Contributions to Mineralogy and Petrology 62, 77–101.

Lucchini, R., 2002. Étude tectonique et géochimique des fissures post-metamorphiques des Alpes Centrales. Ph.D. thesis, University of Lausanne.

Luckscheiter, B., Morteani, G., 1980. Microthermometrical and chemical studies of fluid inclusions in minerals from Alpine veins from the Penninic rocks of the central and western Tauern Window (Austria/Italy). Lithos 13, 61–77.

Mancktelow, S., 1990. The Simplon fault zone. Beitrage zur Geologische Karte der Schweiz 163, 74.

Marquer, D., 1990. Structures et déformation alpine dans les granites hercyniens du massif du Gotthard (Alpes Centrales Suisses). Eclogae Geologicae Helvetica 83 (1), 77–97.

Marquer, D., Burkhard, M., 1992. Fluid circulation, progressive deformation and mass transfer processes in the upper crust: the example of basement cover relationships in the external crystalline massifs, Switserland. Journal of Structural Geology 14 (8-9), 1047–1057.

Marshall, D., Pfeiffer, H., Hunziker, J., Kirschner, D., 1998. A pressure-temperature path for the NE Mont-Blanc massif: Fluid-inclusion, isotopic and thermobarometric evidence. European Journal of Mineralogy 10, 1227–1240.

Matsuhisa, Y., Goldsmith, J., Clayton, R., 1979. Oxygen isotopic fractionation in the system quartz-albite-anorthite-water. Geochimica et Cosmochimica Acta 43, 1131–1140.

Mavrogenes, J., Bodnar, R., 1994. Hydrogen movement into and out of fluid inclusions in quartz: Experimental evidence and geological implications. Geochimica et Cosmochimica Acta 58, 141–148.

Maxelon, M., 2004. Developing a three-dimensional structural model of the lower Lepontine nappes - Central Alps, Switzerland and Northern Italy. Ph.D. thesis, ETH-Zürich.

Maxelon, M., Mancktelow, N., 2005. Three-dimensional geometry and tectonostratigraphy of the Pennine Zone, Central Alps, Switzerland and northern Italy. Earth-Science Reviews 71, 171–227.

Mazurek, M., 1999. Evolution of gas and aqueous fluid in low-permeability argillaceous rocks during uplift and exhumation of the central Swiss Alps. Applied Geochemistry 15, 223–246.

McCaig, A., 1988. Deep fluid circulation in fault zones. Geology 16, 867–870.

Mercolli, I., 1979. Le inclusioni fluide vei noduli di quarzo dei marmi dolomitici della regione del Campolungo (Ticino). Ph.D. thesis, ETH Zürich.

Mercolli, I., Biino, G., Abrecht, J., 1994. The lithostratigraphy of the pre-Mesozoic basement of the Gotthard massif: a review. Schweizerische Mineralogische und Petrographische Mitteillungen 74, 29–40.

Mercolli, I., Schenker, F., Stalder, H., 1984. Geochemie der Veränderungen von Granit durch hydrothermale Lösungen. Schweizerische Mineralogische und Petrographische Mitteillungen 64, 67–82.

Mercolli, I., Skippen, G., Tromsdorff, V., 1987. The tremolite veins of Campolungo and their genesis. Schweizerische Mineralogische und Petrographische Mitteillungen 67, 74–85.

Michalski, I., Soom, M., 1990. The Alpine thermo-tectonic evolution of the Aar and Gotthard massifs, Central Switserland: Fission track ages on zircon and apatite and K-Ar mica ages. Schweizerische Mineralogische und Petrographische Mitteillungen 70, 373–387.

Michard, G., 1990. Behaviour of major elements and some trace elements (Li, Rb, Cs, Sr, Fe, Mn, W, F) in deep hot waters from granitic areas. Chemical Geology 89, 117–133.

Milnes, A., 1974. Structure of the Pennine zone (Central Alps): a new working hypothesis. Bulletin of the Geological Society of America 85, 1727–1732.

Mulch, A., Teyssier, C., Cosca, M., Vanderhaege, O., Vennemann, T., 2004. Reconstructing paleoelevation in eroded orogens. Geology 32, 525–528.

Mullis, J., 1976. Das Wachstumsmilieu der Quarzkristalle im Val d'Illiez (Wallis, Schweiz). Schweizerische Mineralogische und Petrographische Mitteilungen 56, 219–268.

Mullis, J., 1995. Genesis of Alpine Fissure minerals. Scientific and Technical Information 11 (2), 54–64.

Mullis, J., 1996. P-T-t path of quarz formation in extensional veins of the Central Alps. Schweizerische Mineralogische und Petrographische Mitteilungen 76, 159–164.

Mullis, J., Dubessy, J., Poty, B., O'Neil, J., 1994. Fluid regimes during late stages of a continental collision: physical, chemical, and stable isotope measurements of fluid inclusions in fissure quartz from a geotraverse through the Central Alps, Switzerland. Geochimica et Cosmochimica Acta 58 (10), 2239–2267.

Mullis, J., Ramseyer, K., 1999. Growth related Al-uptake in fissure quartz, Central alps, Switzerland. In: Lüders, V., Schmidt-Mumm, A., Thomas, R. (Eds.), ECROFI XV European Current Research On Fluid Inclusions. Vol. Abstracts and Program. Potsdam, pp. 163–164.

Mullis, J., Vennemann, T., Heijboer, T., O'Neil, J., in prep. Deep-percolating meteoric fluids in the Central Alps.

Mullis, J., Vennemann, T., O'Neil, J., 2001. Deep percolating meteoric fluids in the Central Alps. In: Noronha, F., Dória, A., Guedes, A. (Eds.), Ecrofi XVI. Vol. 7. Faculdade de Ciências do Porto, Departamento de Geologia, Memória, Porto, pp. 327–328.

Munz, I., Yardley, B., Banks, D., Wayne, D., 1995. Deep penetration of sedimentary fluids into basement rocks from southern Norway: evidence for hydrocarbon and brine inclusions in vein quartz. Geochimica et Cosmochimica Acta 59, 239–254.

Nesbitt, B., Muehlenbachs, K., 1989. Origins and movements of fluids during deformation and metamorphism in the Canadian Cordillera. Science 245, 733–736.

Nesbitt, B., Muehlenbachs, K., 1995. Geochemical studies of the origins and effects of synorogenic fluids in the southern Omineca Belt of British Columbia, Canada. Geological Society of America Bulletin 107, 1033–1050.

Niggli, P., Koenigsberger, J., Parker, R., 1940. Die mineralien der Schweizeralpen. Wepf & Co, Basel.

Oliver, N., 1996. Review and classification of structural controls on fluid flow during regional metamorphism. Journal of Metamorphic Geology 14, 477–492.

Oliver, N., Bons, P., 2001. Mechanisms of fluid flow and fluid-rock interaction in fossil metamorphic hydrothermal systems inferred from vein-wallrock patterns, geometry and microstructure. Geofluids 1, 137–162.

Ord, A., Oliver, N., 1997. Mechanical controls on fluid flow during regional metamorphism: some numerical models. Journal of Metamorphic Geology 15, 345–359.

Orville, P., 1963. Alkali ion exchange between vapor and feldspar phases. American Journal of Science 261, 201–239.

Pak, T., Hauzenberger, C., Baumgartner, L., 2003. Solubility of the assemblage albite + K-feldspar + andalusite + quartz in supercritical aqueous chloride solutions at 650 °C and 2 kbar. Chemical Geology 200, 377–393.

Parker, R., 1973. Die Mineralfunde der Schweiz. Wepf & Co, Basel.

Pauwels, H., Fouillac, C., Fouillac, A. M., 1993. Chemistry and isotopes of deep geothermal saline fluids in the Upper Rhine Graben: origin of compounds and water-rock interactions. Geochimica et Cosmochimica Acta 57, 2737–2749.

Pennacchioni, G., 2005. Control of the geometry of precursor brittle structures on the type of ductile shear zone in the Adamello tonalites, Southern Alps (Italy). Journal of Structural Geology 27, 627–644.

Peretti, A., Bucher, I., Steiger, R., 1981. Rb-Sr Alter von Kluftmineralien im südlichen Gotthard massiv. Schweizerische Mineralogische und Petrographische Mitteilungen 61, 360–361.

Pfiffner, O., Lehner, P., Heizmann, P., Mueller, S., Steck, A., 1997. Deep Structure of the Swiss Alps: Results From NRP 20. Birkhäuser Verlag, Basel-Boston-Berlin.

Potter, R., Clynne, M., 1978. Solubility of highly soluble salts in aqueous media–part 1, NaCl, KCl, CaCl$_2$, Na$_2$SO$_4$, and K$_2$SO$_4$ solubilities to 100 °C. Journal of Resources U.S. Geological Survey 6, 701–705.

Poty, B., 1969. La croissance des cristaux de quartz dans les filons sur l'example du filon de la Gardette (Bourg d'Oisans) et des filons du massif de Mont Blanc. Memoires des Sciences de la Terre 17.

Poty, B., Leroy, J., Jachimowicz, L., 1976. A new device for measuring temperatures under the microscope; the Chaixmeca microthermometry apparatus. In: Roedder, E., Kozlowski, A. (Eds.), Current research on fluid inclusions and on mineral deposits. Vol. 9 of Fluid Inclusion Research. University of Michigan Press, Ann Arbor, MI, United States, pp. 173–178.

Poty, B., Stalder, H., Weisbrod, A., 1974. Fluid inclusions studies in quartz from fissures of Western and Central Alps. Schweizerische Mineralogische und Petrographische Mitteilungen 54, 717–752.

Pürdy, J., Stalder, H., 1973. K-Ar ages of fissure minerals from the Swiss Alps. Schweizerische Mineralogische und Petrographische Mitteillungen 53 (1), 79–98.

Ramsay, J., 1980. The crack-seal mechanism of rock deformation. Nature 284, 135–139.

Ramsey, J., Huber, M., 1987. Modern structural geology: Folds and fractures. Vol. 2. Academic Press, London.

Rumble, D., Hoering, T., 1986. Carbon isotope geochemistry of graphite vein deposits. Geochimica et Cosmochimica Acta 50, 1239–1247.

Rumble, D., Hoering, T., 1994. Analysis of oxygen and sulfur isotope ratios in oxide and sulfide minerals by spot heating with carbon dioxide laser in a fluorine atmosphere. Accounts of Chemical Research 27, 237–241.

Schaer, J., Reimer, G., Wagner, G., 1975. Actual and ancient uplift rate in the Gotthard Region, Swiss Alps: A comparison between precise levelling and fission-track apatite age. Tectonophysics 29, 293–300.

Schenker, F., 1986. Spätpaläozischer saurer Magmatismus und Beckenbildung im Aar massif unter kompressiver Tektonik. Ph.D. thesis, University of Bern.

Schenker, F., Abrecht, J., 1987. Prä-Aargranitische Anatexis, variszische Kontaktmetamorphose und alpidische Regional metamorphose im Oberhasli (zentrales Aarmassiv, Schweiz). Schweizerische Mineralogische und Petrographische Mitteillungen 67, 13–26.

Schlunegger, F., Willett, S., 1999. Spatial and temporal variations in exhumation of the central Swiss Alps and implications for exhumation mechanisms. In: Ring, U., Brandon, M., Lister, G., Willett, S. (Eds.), Exhumation processes: Normal Faulting, Ductile Flow and Erosion. Vol. Special. Geological Society, London, pp. 157–179.

Schmid, S., Pfifner, O., Froitzheim, N., Schönborn, G., Kissling, E., 1996. Geophysical-geological transect and tectonic evolution of the Swiss-Italian Alps. Tectonics 15 (5), 1036–1064.

Schmid, S. M., Fügenshuh, B., Kissling, E., Schuster, R., 2004. Tectonic map and overall architecture of the Alpine orogen. Eclogae Geologicae Helvetica 97, 93–117.

Schmidt, C., Bodnar, R., 2000. Synthetic fluid inclusions: XVI. PVTX properties in the system H$_2$O-NaCl-CO$_2$ at elevated temperatures, pressures and salinities. Geochimica et Cosmochimica Acta 22, 3853–3869.

Sharp, Z., 1990. A laser based microanalytical method for the in situ determination of oxygen isotopes of silicates and oxides. Geochimica et Cosmochimica Acta 54, 1353–1357.

Sharp, Z., Atudorei, V., Durakiewicz, T., 2001. A rapid method for determination of hydrogen and oxygen isotope ratios from water and hydrous minerals. Chemical Geology 178, 197–210.

Sharp, Z., Masson, H., Lucchini, R., 2005. Stable isotope geochemistry and formation mechanisms of quartz veins; extreme paleoaltitudes of the Central Alps in the Neogene. American Journal of Science 305, 187–219.

Sheppard, S., 1986. Characterization and isotopic variations in natural waters. In: Valley, J., Taylor, H., O'Neil, J. (Eds.), Stable isotopes in high temperature geological processes. Vol. 16 of Mineralogical Society of America: Reviews in Mineralogy. Blacksbug, Virginia, pp. 165–181.

Sibson, R., 1981. Controls on low-stress hydrofracture dilatancy in thrust, wrench and normal fault terrains. Nature 289, 655–667.

Sibson, R., 1996. Structural permeability of fluid driven fault fracture meshes. Journal of Structural Geology 18, 1031 –1043.

Sibson, R., 2000. Tectonic controls on maximum sustainable overpressure: fluid redistribution from stress transitions. Journal of Geochemical Exploration 69-70, 471–475.

Simon, K., 2001. Does δD from fluid inclusions in quartz reflect the orginal hydrothermal fluid? Chemical Geology 177, 483–495.

Smith, J., 1995. True and apparent geometric variability of en-échelon vein arrays. Journal of Structural Geology 17 (11), 1621–1626.

Smith, J., 1996. Geometry and kinematics of convergent conjugate vein array systems. Journal of Structural Geology 18 (11), 1291 – 1300.

Spicher, A., 1980. Tectonic map of Switzerland 1:500.000.

Spötl, C., Vennemann, T., 2003. Continuous-flow IRMS analysis of carbonate minerals. Rapid Communications in Mass Spectrometry 17, 1004–1006.

Stalder, H., 1964. Petrographische und mineralogische Untersuchungen im Grimselgebiet BE. Schweizerische Mineralogische und Petrographische Mitteilungen 44, 188–398.

Stalder, H., Touray, J., 1970. Fensterquarze mit Methan-Einschlüssen aus dem westlichen Teil der schweizerischen Kalkalpen. Schweizerische Mineralogische und Petrographische Mitteilungen 50, 109–130.

Stipp, M., Stünitz, H., Heilbronner, R., Schmid, S., 2002. The eastern Tonale fault zone: a "natural laboratory" for crystal plastic deformation of quartz over a temperature range from $250 - 700\,^\circ$C. Journal Structural Geology 24, 1861–1884.

Suzuoki, T., Epstein, S., 1976. Hydrogen isotope fractionation between OH-bearing minerals and water. Geochimica et Cosmochimica Acta 40, 1229–1240.

Tarantola, A., 2005. Redox mechanisms controlling carbon chemistry in anchimetamorphic fluids: paleofluids composition, isotopic geochemistry and phyllosilicate crystallochemistry in the external part of the Central Alps (Switzerland). Ph.D. thesis, Universität Basel & Université Henri Poincaré Nancy.

Thompson, A., Connolly, J., 1992. Migration of metamorphic fluid: some aspects of mass and heat transfer. Earth Science Reviews 32, 107–121.

Trümpy, R., 1980. Geology of Switzerland, a guide book, Part A: An outline of the geology of Switzerland.

Upton, P., Koons, P., Chamberlain, C. P., 1995. Penetration of deformation-driven meteoric water into ductile rocks: isotopic and model observations from the Southern Alps, New Zealand. New Zealand Journal of Geology and Geophysics 38 (38), 535–543.

Vazquez, R., Vennemann, T., Kesler, S., Russell, N., 1998. Carbon and oxygen isotope halos in the host limestone, El Mochito Zn, Pb (Ag) skarn massive sulfide/oxide deposit, Honduras. Economic Geology 93, 15–31.

Vennemann, T., O'Neil, J., 1993. A simple and inexpensive method of hydrogen isotope and water analyses of minerals and rocks based on zinc reagent. Chemical Geology (Isotope Geoscience Section) 103, 227–234.

Verma, S. P., Santoyo, E., 1997. New improved equations for Na/K, Na/Li and SiO_2, geothermometers by outlier detection and rejection. Journal of Volcanology and Geothermal Research 79, 9–23.

Wagner, G., Reimer, G., Jäger, E., 1977. Cooling ages derived by apatite fission-track, mica Rb-Sr and K-Ar dating: the uplift and cooling history of the Central Alps. Mem. Ist. Geol. Padova 30, 1–28.

Walter, L., Steuber, A., Huston, T., 1990. Br-Cl-Na systematics in Illinois basin fluids: Constraints on fluid origin and evolution. Geology 18, 315–318.

Walther, J., Wood, B., 1986. Ch. 4: Fluid flow during metamorphism and its implications for fluid-rock ratios. In: Walther, J., Wood, B. (Eds.), Advances in Physical Geochemistry: Volume 5: Fluid-Rock interactions during Metamorphism. Springer Verlag, New York, pp. 89–108.

Wangen, M., Munz, I., 2004. Formation of quartz veins by local dissolution and transport of silica. Chemical Geology 209, 179–192.

Wickham, W., Taylor, H., 1985. Stable isotopic evidence for large scale seawater infiltration into a regional metamorphic terrane; the Trois Seigneurs Massif, Pyrenees, France. Contributions to Mineralogy and Petrology 91, 122–137.

Wolery, T., 1992. EQ3NR, a computer program for geochemical aqueous speciation-solubility calculations: theoretical manual, user's guide and related documentation. Laurence Livermore National Laboratory, Livermore.

Yardley, B., 1997. Ch. 6: The evolution of fluids through the metamorphic cycle. In: Jamtveit, B., Yardley, B. (Eds.), Fluid flow and transport in rocks. Chapman and Hall, London, pp. 99–137.

Yardley, B., Banks, D., Bottrell, S., Diamond, L., 1993. Post-metamorphic gold-quartz veins from N.W. Italy: the composition and origin of the ore fluid. Mineralogical Magazine 57, 407–422.

Yardley, B., Bottrell, S., 1992. Silica mobility and fluid movement during metamorphism of the Connemara schists, Ireland. Journal of Metamorphic Geology 10, 453–464.

Zhang, Y., Frantz, J., 1987. Determination of the homogenization temperatures and densities of supercritical fluids in the system $NaCl$-KCl-$CaCl_2$-H_2O using synthetic fluid inclusions. Chemical Geology 64, 335–350.

Zheng, Y., 1991. Calculation of oxygen isotope fractionation in metal oxides. Geochimica et Cosmochimica Acta 55, 2299–2307.

Zheng, Y., 1993. Calculation of oxygen isotope fractionation in hydroxyl-bearing silicates. Earth and Planetary Science Letters 120, 247–263.

Curriculum Vitae

Tjerk Cornelis Heijboer is Dutch, was born in Zwolle (The Netherlands) at the 28th of December 1977. He went to the "Dr. Algra school", a primary school in Leeuwarden between 1983 and 1990 and went on to the "Christelijk Gymnasium", a secondary school, in Leeuwarden between 1990 and 1996. Afterwards he studied Earth-Sciences in Utrecht (The Netherlands) between 1996 and 2001. In the year 2000 he participated in an Erasmus exchange-program with the University of Oslo (Norway) for half a year. In 2001 he finished his Master Thesis with as topic "A structural and chemical analysis of Otrøy garnet-peridotites, pyroxenites and websterites from the Western Gneiss Region, Norway", which was supervised by Dr. M. Drury and Dr. H. van Roermund. Since then he has been working on his doctoral thesis supervised by Prof. J. Mullis and Prof. C. de Capitani at the University of Basel, Switzerland.